Reconstructing sea surface temperatures in the Caribbean during the early-mid Holocene from a reef exposure in Cañada Honda, Enriquillo Valley, Dominican Republic

by:

Jose A. Morales Collazo

Thesis submitted in partial fulfillment of the requirements for the degree of

MASTER OF SCIENCE

in

GEOLOGY

UNIVERSITY OF PUERTO RICO

MAYAGÜEZ CAMPUS

2015

____________________________	________________
Félix R. Román Velázquez, Ph.D. Member of the Graduate Committee	Date
____________________________	________________
Amos Winter, Ph.D. Member of the Graduate Committee	Date
____________________________	________________
Hernán Santos Mercado, Ph.D. Member of the Graduate Committee	Date
____________________________	________________
Wilson R. Ramírez Martínez, Ph.D. President of the Graduate Committee	Date
____________________________	________________
Julio M. Morell Rodríguez, M.S. Representative of Graduate Studies	Date
____________________________	________________
Lizzette A. Rodríguez Iglesias, Ph.D. Chairperson of the Department of Geology	Date

Abstract

Temperatures during the Holocene are driven by seasonal changes in insolation; however, a better understanding of insolation mechanisms and how it affects tropical climate is still necessary. This study presents annual growth rates seasonally resolved oxygen and carbon isotopic and Sr/Ca trace elemental variations from five fossils *Montastraea sp.* corals from Cañada Honda Enriquillo Valley, Dominican Republic. U/Th dates obtained from fossil corals in M1 facies indicate early-mid Holocene dates ranging from 8.0-8.9 ka B.P. The aragonite skeleton composition was confirmed by X-ray diffraction. Growth rates in *Montastraea sp.* corals, with a record of 30-80 years, collected at this site, range from 2.07 ± 0.14 to 3.55 ± 0.37 mm/yr (n=5). High sedimentation rates in the reef were estimated to range from 1.53 ± 0.18 to 2.48 ± 0.45 mm/yr (n=8). $\delta^{18}O$ measurements range from -0.69 to -2.41 (n=430) values that are heavier relative to modern corals from the tropics by ~2‰. Sr/Ca measurements range from 9.07 to 9.70 mmol/mol (n=430), values higher than modern corals from the tropics. Both proxies suggest colder environments during this time period. Calculated SST for each variable suggest temperature variations of 6°-7°C values never reported by any proxy from the Early Holocene, but may be explained by periods of freshwater influx. A low correlation index (R) estimated (0.26-0.85) suggests that both paleothermomethers are reacting to different variables.

Resúmen

Las temperaturas durante el Holocene son impulsadas por cambios estacionales en insolación, sin embargo, un mejor entendimiento de los mecanismos de insolación y como estos afectan el clima en los trópicos es aun necesario. Este estudio presenta tasas de crecimientos anual resuelto estacionalmente por variaciones isotópicas de oxígeno y carbono, y elementos traza Sr/Ca en cinco corales fósiles de la especie *Montastraea sp.* en Cañada Honda, Valle Enriquillo, Republica Dominicana. Dataciones de U/Th obtenidas de corales fósiles en facies M-1 indican edades del Holoceno temprano-tardío que oscilan entre 8.0-8.9 kya A.P. La composición del esqueleto aragonítico fueron confirmados en un análisis de XRD. La tasa de crecimiento en corales *Monstrastraea sp.,* en un récord de 30-80 años, colectados en esta zona, varían entre 2.07 ± 0.14 to 3.55 ± 0.37 mm/yr (n=5). Las altas tasas de sedimentación en el arrecife fueron estimadas y varían entre 1.53 ± 0.18 to 2.48 ± 0.45 mm/yr (n=8). Medidas de $\delta^{18}O$ varían entre -0.69 to -2.41 (n=430), valores pesados relativo a corales modernos en el trópico por ~2‰. Medidas de Sr/Ca varían entre 9.07 to 9.62 mmol/mol (n=430) , valores más altos, que corales modernos en el trópico. Las TSM calculadas para cada variable sugieren variaciones en temperatura de 6°-7°C. Valores como estos no han sido reportados por ningún proxy durante el Holoceno temprano. El bajo índice de correlación (R) estimado (0.02-0.85) sugiere que ambos paleotermometros estan reaccionando a diferentes variables.

Acknowledgments

I would like to use this space to express my appreciation and thank those who made this research possible and guided me through it. My highest gratitude is extended to my advisor Dr. Wilson Ramirez for his continuous support and believing in me and my skills, and always trusting my judgment. I will also like to thank those members of my committee; Dr. Hernan Santos was always available for counseling and word of truth, Dr. Amos Winter shared his knowledge and provided me with the tools required to pursue this research and Dr. Felix Roman for his input and disposition. I want to offer extended gratitude Dr. James Joyce, Dr. Lysa Chizmadia, Dr. Rebeca Orama for their insights and efforts to help me during this process.

I have to honor those whose contribution was essential and vital for this research. Starting with Exxon Mobil-UPRM Diversity Award, who partially funded the field work required for this project and Sociedad Geológica de República Dominicana and its president Santiago Muñoz for providing the permissions required for this investigation. Also it is important to mention Dr. Kim Cobb's Lab at Georgia Institute of Technology with special recognition to Hussein Sayani and Pamela Grothe since they were the ones taking from their time to work with me in the analytical analyses. Additional acknowledgment goes to Dr. Larry Edwards and his collaborators, Angela Min and Hai Cheng, from University of Minnesota and Dr. Ivette Roche and her staff form the San Antonio Hospital in Mayagüez, as their work was crucial for the fulfillment of this project. Thanks to Marianela Mercado for helping me obtain funding to conduct the analytical analyses.

I want to say that I am very grateful to my colleagues from the Geology Department in UPRM especially to Leila Joyce, Kevian Pérez and Rolf Vieten (Marine Sciences) for their unconditional support and insights in this work, Elson Core for working with me in the field and Jennifer Toledo and Edgardo Quiñones for their back up and teamwork. I also appreciate the work and assistance of the students Mariangely Gonzalez and Katherine Velez. Nonetheless it is important to mention the staff of the UPRM-Geology Department, the administrative secretaries and the laboratory technicians because their aid and hard work were part of my success and the Department of Chemistry at UPRM, especially Prof. Sara Delgado, for giving me the opportunity and means of funding. Last but not least, thanks to Gabriel Cedeño because none of this would have been possible without him being by my side this entire time. I deeply appreciate everyone for showing their support and extending their hand to me whenever possible.

Table of contents:

List of Tables

List of Figures

List of Appendixes

1. Introduction

During the last few decades several initiatives have raised awareness of drastic changes in climate suggesting that anthropogenic forcing was superimposed on climate variability at centennial scales (Saenger et al., 2008). Since 1980's anthropogenic impact has been reported to become more severe with time (Hughes, 1994). The role of human activity on climate variability is barely understood and is one of the most important questions facing scientists today (Pandolfi, 2002).

A direct and reasonable way to obtain adequate information to answer this question is to study seasonal records of temperature using fossil corals as proxies. Fossil corals are means to study past climate (Grottoli, 2001) at seasonal resolution, however, studies using corals as a proxy for paleoclimate reconstruction and climate variability in the Caribbean region have shown significant discrepancies (Saenger et al., 2008). One of the problems is that fossil coral skeletons are commonly altered early in their diagenetic history by recrystallization, micritization and neomorphism among others processes. These processes alter the original character, texture, and geochemistry of the corals and can produce chronological errors in radiocarbon and U/Th dating and isotopic and trace elemental changes in the coral skeletons (Sayani et al., 2011; Saenger et al., 2008). Due to the unstable nature of the aragonite mineral, it is quite difficult to find adequate fossil corals that provide accurate geochemical information during the early-mid Holocene. The Holocene fossil corals present at the gully called Cañada Honda in the Enriquillo Valley, Dominican Republic, have been very well preserved retaining their geochemical nature and provide a unique opportunity to study paleoclimate as well as coral reef changes since the early Holocene (Cuevas et al. 2005; Greer and Swart, 2006).

1.1 Objective statement

Banded corals can serve as a paleoclimatic archives to reconstruct past climate in the pre-industrial periods (Felis and Pätzold, 2004). The geochemical composition of the coral skeleton can be used as proxy record for climate variations, because within the chronology of the coral growth, information about the environment when they were calcified in is stored (Greer and Swart, 2006). $\delta^{18}O$ isotopic values and trace element ratios (Sr/Ca) can reflect specific marine environment characteristics of the coral as it precipitated its skeleton (Felis and Pätzold, 2004; Greer and Swart, 2006).

This study attempts to reconstruct sea surface temperature (SST) variations using Sr/Ca ratios and $\delta^{18}O$ isotopic values from coral skeletons. The SST records obtained from the coral skeletons were used to assess climate change and explore seasonality during the early Holocene. A decadal to multi-decadal SST record (approximately from 8.0-8.4ka B.P.) from corals present at a reef exposure in Enriquillo, Dominican Republic is reported here.

The length of the records obtained are in the same timeframe as climate cycles such as El Niño Southern Oscillation (ENSO) or North Atlantic Oscillation (NAO) (Giannini et al., 2001a; Greer et al., 2006), and solar sunspot cycles that have been found to have constant 11-year cyclicity (Haigh, 2011). The results obtained will provide information to develop climate interpretations of natural climate variability during the early Holocene in the northern Caribbean and the interaction between natural vs. anthropogenic factors producing climate change.

1.2 Background

1.2.1 The Holocene climate

The Holocene epoch (11,700yr – present) (Walker et al., 2009) is an interglacial period that has experienced substantial changes in climate variability. A study by Wanner et al. (2008) used selected proxy reconstructions of different climate variables from models such as General Circulation Models (GCMs) and Earth Models of Intermediate Complexity (EMIC) to study global climate change since the Mid-Holocene. Other studies looked at the microfauna, pollen and vegetation distribution during this epoch. These studies provide evidence of the impact of orbital variations in climate and explored events of rapid climate change (Mayewski et al., 2004; Wanner et al. 2008). These studies have shown millennial-scale climate variations of polar cooling, tropical acidity and major atmospheric oscillations and have attributed them to super-imposed changes in insolation and solar variability (Mayewski et al., 2004; Greer and Swart, 2006).

The early Holocene, defined as 11,700-8.200yr (Walker et al., 2012) is a stage of continued deglaciation in the Northern Hemisphere as a consequence of the lagged response of the ice sheet and insolation forcing before the Holocene (Mayewski et al., 2004). From the Pleistocene, the early Holocene resulted in a global change from dry and cool to warmer and more humid climate conditions that still persists (Greer and Swart, 2006). Climate during the early Holocene is characterized by an amplification of $30Wm^{-2}$ in insolation during boreal summer in phase with precessional insolation leading to warmer summers and colder winters (Luan et al., 2012). Concentrations of CO_2 have increased from 270ppm at 11ka (Indermuhle et al, 1999) to over 400ppm today (Tans and Keeling, 2015) and it is still debatable what is causing this major increase (Ruddiman et al., 2011). A predominant anomaly has been identified during the early Holocene at the interval of 9-8ka before present called the Glacial Aftermath by Mayewski et al. (2004). It was a unique event that occurred in the Northern Hemisphere when large ice sheets form the Pleistocene was still present. There is evidence at this time of a cool Northern Hemisphere in which a lot of ice rafting and stronger atmospheric circulation took place (Mayewski et al., 2004).

1.2.2 The 8.2kya event

Within the early Holocene, there is a brief abrupt near-global cooling event ~8.2ka named the "8.2ka event" in which climate became much dryer and windy, for about 150 years (Kobashi et al., 2007; Wiersma, 2008) than the Glacial Aftermath itself. The exact timing of this event remains ambiguous, but precise characterization of methane and nitrogen isotopes from air bubbles trapped in Greenland ice cores suggests the event started approximately at 8175 ± 30 years ago with temperatures that dropped by 3.3-7.4° (Kobashi et al., 2007). The most accepted hypothesis for this phenomenon establishes that this event took place due to the massive flow of freshwater running from proglacial lakes Agassiz and Ojibway due to the ongoing deglaciation (Kobashi et al., 2007; Wiersma, 2008; Morril et al., 2013). Consequently, the Atlantic Meridional Overturning Circulation (AMOC) slowed drastically due to a decrease in the sea surface salinity enabling a dryer and cooler near-global environment as shown by anomalies in proxies such as ice cores and speleothems (Morril et al., 2013). Other hypothesis suggest that this happened as a consequence of a repeating pattern of long-term anomalies as manifestation of solar output influences due to atmospheric circulation (Rohling and Pälike, 2005) or that a solar minimum triggered the cooling (Kobashi et al., 2007).

The 8.2ka event has been characterized in-near the Caribbean region using speleothems (Lachniet et al., 2004; Cheng et al., 2009; Winter et al., 2013) and sediment stratigraphy (Sallun et al., 2012). Cheng et al. (2009) and Sallun et al. (2012) determined that the South American Monsoon intensified during this time period and that it correlates to climate variations of North Atlantic climate events. Winter et al. (2013) interpreted that this event was associated with increased precipitation in the Eastern Caribbean and that stalagmite growth rates were much faster than any other growth period except for modern. So far, records in the Caribbean that address this event using proxies in the marine setting are scarce. Some of the reasons are the lack of time resolution from proxies such as foraminifera, or the poor preservation of skeletal organisms such as scleractinean corals in the geologic record. The coral samples used for this project have been dated to be 8.0 to 8.9 ka B.P. and are pristinely preserved. These corals existed during this interval providing the opportunity to study the 8.2kya event anomalies.

1.2.3 Climate change and the Caribbean.

As means to study the past to predict the future, scientists have developed procedures to study past climate using proxies. Paleoclimate is the study of climate through time across Earth's history by looking at changes in weather conditions known as climate change (Dinse, 2009). The idea of climate change in the past was brought up when evidence of glacial deposits was found in places were no a glacier are present today (Riebeek, 2005). These findings motivated the study of ice cores, speleothems, scleractinian corals and other proxies providing valuable information of climate variability (Felis and Pätzold, 2004; Riebeek, 2005). Climate reconstruction methods can be done by measuring the concentration of oxygen isotopes archived in these proxies. Other means of understanding climate change, is to document changes in sea surface temperatures (SST) through time using trace elemental concentrations such as Sr/Ca and Mg/Ca present in calcareous marine organisms (Swart et al., 2002; Rosenthal and Linsley., 2006).

El Niño Southern Oscillation (ENSO) and the North Atlantic Oscillation (NAO) are the major components of climate variability such as SST at an interannual timescale (Giannini et al., 2001a). SST is partially responsible of both precipitation and temperature changes that have a major impact in ecosystem dynamics and therefore human development (Giannini et al., 2001a; Cobb et al., 2013. Coral records from Bonaire indicate that southern Caribbean Sea was dominated by cooler conditions during the Holocene compared to today (Giry et al., 2012).

ENSO is a phenomenon that occurs in the equatorial Pacific (Donders, 2005). El Niño, or the oceanic component, is seen as the irregular warming in SST while Southern Oscillation, or the atmospheric component, is the variation in surface air pressure from Central Pacific to the South American coasts (Donders, 2005; Birgmark, 2014). It is known that the effects of this climate variability extends globally via the atmospheric bridge including the Caribbean (Alexander et al., 2002), but its strength is yet to be understood. Sediments record from a lake in Equador showed that ENSO frequencies were larger (~15 years) during the early Holocene, suggesting a weaker ENSO during this time period (Rodbell et al., 1999). In addition, NAO is known to be a major climate variability pattern in the North Atlantic. It is widely affected by the strength of the Icelandic Low and the Azores High pressure systems during winter climate variability (Charlery et al., 2006, Birgmark, 2014). NAO has positive and negative oscillation depending on the atmospheric pressure generated. When the pressure gradient between the Azores and Iceland is lower than normal then it is a negative phase and positive when they are higher. These variations will have different climatic effects in the mid and high-latitutes by controlling the strength of the subpolar winds from the west (Felis et al., 2004). The relationship between NAO and SST has been studied and it influences with amount of ice in the Polar Regions (Birgmark, 2014).

Several studies have looked over the effects of ENSO and NAO in the Caribbean and have found that their combined forcing is one of the factors responsible for climate variability in the region. After a winter season of positive NAO, sea level pressure (SLP) is responsible for dry weather in the subtropical regions and is augments the dryness associated with a warm ENSO during the summer. Otherwise, after a winter season of negative NAO, a wet climate following a warm ENSO increases due to the wetness associated with the warmer SST in the tropical North Atlantic during spring (Giannini et al., 2001a). ENSO also seems to be a primary driver in the development of hurricane activity in the Caribbean because it alters the vertical wind shear (Klotzbach, 2011). Overall, ENSO effects in the Caribbean are augmented by the NAO, which is negatively correlated to the amount of rainfall in the region (Birgmark, 2014) and it has been found to have increased with time (Giannini et al., 2001b; Giry et al., 2012). Foraminiferal and phytoplankton Mg/Ca SST reconstructions in the Caribbean during the Holocene, suggests that warming of the western Atlantic and Caribbean region is due to a trend in the NAO mean state from a positive phase in the early Holocene towards a negative phase in the late Holocene due to insolation (Giry et al., 2012). Both ENSO and NAO seem to have an impact in the strength of the trade winds in the Caribbean which influences the SST because of cooling due to evaporation. However, the strength of these two patterns is hard to assess as they are affected by locally driven phenomena such as upwelling and advection and also the seasonal changes (Birgmark, 2014).

During the last few decades, air climate in the Caribbean has become warmer at an average rate of 0.27°C/decade (Chollett et al., 2012) with temperature seasonality of 2.8 ± 0.2°C within periods of 3-6 years (Giry et al., 2012). This warming rate is drastic compared to the preindustrial period as it took approximately 2000 years to raise the temperature 0.6°C during the early Holocene (Marcott et al., 2013). Seasonality has decreased since the mid-late Holocene and periodicity is associated with ENSO-NAO cycles at present. It has been predicted that by 2100, temperatures will exceed the Holocene temperature mean by 3°C of global warming similar to the rise in temperature since the last ice age (Hagelaars, 2013).

1.2.4 Corals as proxies

The geochemical composition of coral skeletons is one of the most accurate ways to recover past records of timescale variations in tropical climate because the environmental information in which these organism grew is stored within their skeleton chronologically. (Grottoli, 2001; Greer and Swart, 2006). Corals are aimals from the phylum *Cnidaria* that are mostly allocated roughly at 23-24° latitude where mean annual temperatures are not under 24°C or 18°C during the winter minimum and salinities range from 32-40 PSU (Felis and Pätzold, 2004). It is known, that ocean circulation can transport tropical warm waters that lead to coral colonies at higher latitutes (Felis and Pätzold, 2004). Scleractinean corals live in colonies most commonly in surface waters (can live down to 4km deep) with skeletal growth rates usually ranging from 5-25mm/yr (Grottoli, 2001; Felis and Pätzold, 2004). Basically, their body consists of a polyp overlaying a skeleton built of aragonite ($CaCO_3$) that lives in symbiosis with a unicellular photosynthetic phytoplankton known as zooxantellae.

Typically, scleractinian corals deposit a high density (HD) band and a low density (LD) band within the interval of one year. Understanding the causes of short- and long-term changes of coral populations in reefs provide valuable climate information and scleractinian corals growth bands are high-resolution archives of past climates and coral reef environments (Felis and Patzold, 2004; Brachert et al., 2006). In an optimal temperature environment, corals precipitate skeleton at a faster rate, while the opposite occurs in sub-optimal temperature conditions (Grottoli, 2001). Density bands can be measured by luminance and by coupling a LD and a HD band, a sclerochronology can be estimated. Climate information can be obtained by analyzing trace elements and isotope geochemistry which can be related to time.

Mid-late Holocene centennial paleoclimate records with sub-annual resolution have been obtained from single coral skeletons using geochemistry and Sclerochronology (Winter et al., 2003). Holocene millennial records of continuous paleoclimate data with sub-annual resolution from coral skeletons have been more difficult to obtain because of the lack of unaltered individual coral colonies. To develop Holocene millennial records of continuous paleoclimate data with sub-annual resolution from coral skeletons a pristine coral reef with aragonitic corals, oriented in growth position and located at the proper stratigraphic framework would be needed. The probability of finding such a place is extremely low not only because most Holocene reefs are submerged but also because Holocene reefs records are fragmentary with most of the corals broken and out of place (Hubbard, 1997).

The Sr/Ca ratio obtained from the coral skeleton is one of the trace element analysis used for climate reconstruction, the others being Mg/Ca and U/Ca. Calcium ion (Ca^{+2}) is substituted within the crystal structure by many divalent trace ions such as strontium (Sr^{+2}) and magnesium (Mg^{+2}) dissolved in water (Faure, 1998), which keeps the chemical identity of the environment preserved in the skeleton. This is because corals do not incorporate rubidium (Rb) in their skeleton meaning that Sr does not come from radiogenic decay but the waters the coral skeleton is precipitated. Beck et al., 1992 found an inverse relationship between the amount of Sr and SST in corals from southwest Pacific Ocean with a precision better than 0.1%, allowing precise documentation of paleotemperatures by measuring Sr/Ca ratios in the coral skeleton. Sr/Ca ratio as a paleothermometer, requires to be calibrated with modern sea water, because calculated SST-Sr/Ca are highly dependent on the location (Saenger et al. 2008). Swart et al. (2002) calibrated the relationship of Sr/Ca and temperature in the scleractinean coral *Montastraea annularis* producing a high correlation (R^2 = 0.83; Sr/Ca (mmol/mol) between the two variables. Other paleothermometers have already been tested such as Mg/Ca and U/Ca ratios. However, these ratios have shown to be affected by other variables other than temperature, leaving Sr/Ca as the most reliable proxy (Beck et al., 1997; Swart and Grottoli, 2003; Felis and Pätzold, 2004).

Oxygen isotopes ($^{18}O/1^{6}O$) are also incorporated as part of the skeleton and are directly influenced by the marine environment (Grottoli, 2001). This isotopic tool has proven to be very successful in reconstructing past climate and even pointing out climate variability and patterns (Felis et al., 2004, Cobb et al., 2013). Even though $\delta^{18}O$ shows a high correlation with temperature, it is also sensitive to salinity variations (Smith, 2006) in contrast with Sr/Ca ratio, which seems to be affected only by temperature (Swart and Grottoli, 2003) and have better temperature resolution (Swart et al., 2002). Greer and Swart (2006) conducted a study in Enriquillo using $\delta^{18}O$ and $\delta^{13}C$ isotopic compositions from coral skeletons directed to study decadal ciclicity patterns. Their data suggested the primary driver for the decadal oscillations in $\delta^{18}O$ and $\delta^{13}C$ was salinity. This study concluded that the isotopic variability was affected by local precipitation and that fresh water flooding influenced the $\delta^{18}O$ and $\delta^{13}C$ variations more significantly than the temperature fluctuations. This study reported decadal and multidecadal variations in $\delta^{18}O$ and $\delta^{13}C$ in the coral skeletons and suggested Sr/Ca as a better proxy to determine possible temperature variations, since Sr/Ca is not affected by salinity.

Proxy records require an accurate timescale based on absolute ages. Many studies have relied on radiocarbon dating for sclerochronology, however radiocarbon is significantly affected by ocean reservoir effects and variations of radiocarbon in the atmosphere. The uranium-thorium (U/Th) radiogenic dating method is more accurate because is considered to provide absolute ages compared to radiocarbon, therefore, it has better resolution (Felis and Pätzold, 2004). U/Th dating has been used in coral samples as young as a few years (Cheng et al., 2013) and as old as the last interglacial period (Felis et al., 2004). The reliability of this method is based in the fact that corals do not incorporate non-radiogenic ^{230}Th (at least its concentration is fairly negligible) and that carbonates are uranium rich. This means that the only source of ^{230}Th is radiogenic and produced from the decay of ^{238}U in-situ and in the coral skeleton (Cobb et al., 2003). The absolute age provided by the U/Th dating method is combined with the internal chronology present in the coral to provide a reliable timescale.

1.3 Study Area

1.3.1 Geologic history

Cenozoic plate tectonic history establishes that during the Late Eocene, under-thrusting and accretion took place against the Hispaniola (Fig. 1). The formation of the Peralta Belt exposed deep-water sediments that now are deposited in the Southern Hispaniola. Then in the Early Miocene, oblique movement of the oceanic plate caused a transpressional uplift and thrusting of the Peralta Belt and the converging plate sediments. Geologic structures in the region explicitly show evidence of the tectonic events during this period that led to the geomorphic features present in Southern Hispaniola.

The southernmost part of the island is dominated by very young anticlinal mountains and synclinal valleys. This geomorphology results from the active reverse and oblique-slip faulting during the Late Miocene's transpression of the North America-Caribbean boundary characterizing this region by its low topography and fault bounded Neogene basins like Enriquillo Valley (Mann and Lawrence, 1991; Mann et al., 2008). Later during the Pliocene, undergoing ramping and thrusting started in the area (Mann, 1999) surrounding the basins with The Sierra de Neiba and Sierra de Bahoruco (Fig. 2) steep mountain ranges mainly composed of faulted Paleocene-Miocene carbonates and oceanic basalts from the Late Cretaceous (Mann, 1999) that will serve as the main source of modern deposits within the basins. Sea level rise during the Holocene, after the last interglacial period, flooded the basin forming a gulf known at the time as Enriquillo Bay (Mann et al., 1999). Fringing and patch reefs developed along the marine gulf with an average elevation of the surface of the reef crest at approximately 5m below sea level (Mann et al., 1984). At this time, active tectonism has not significantly affected the basin, as uplift/subduction during the Holocene appears to be minimal (< 1m) (Mann et al., 1995).

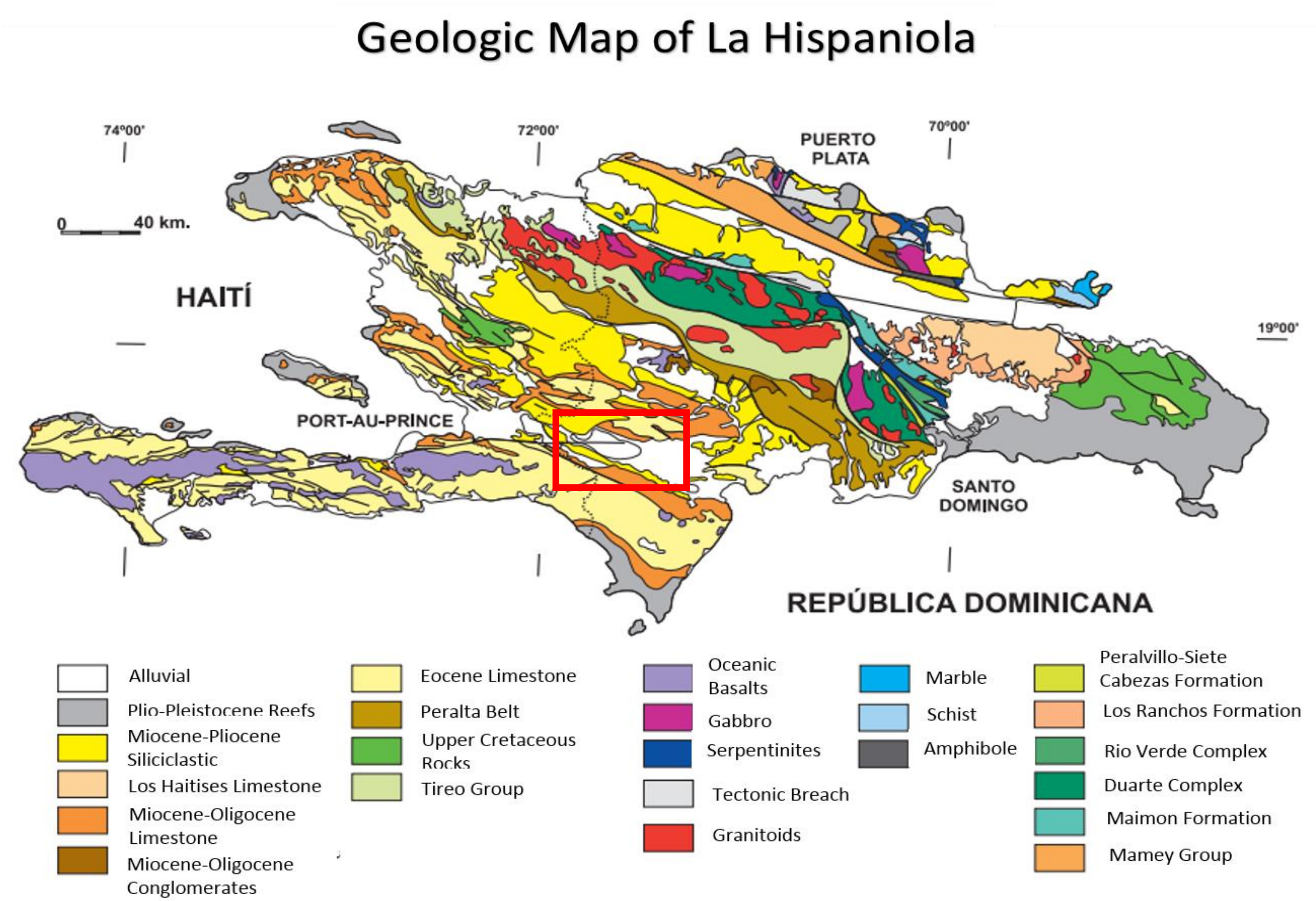

Figure 1: Geologic map of La Hispaniola. Red square indicates the location of Enriquillo Lake in southwestern, Dominican Republic (Modified from Escuder Viruete et al., 2002)

1.3.2 Location

Enriquillo Valley, located in the south-westernmost part of Southern Hispaniola (Fig. 2), is an east-west trending feature from the Caribbean Sea to the Baie de Port-au-Prince in Haiti (Greer and Swart, 2006), settled in a tropical climate with little seasonal temperature variations (25^{0}C) but affected by significant variability in precipitation produced by seasonal changes (Teneva, 2006). The valley is a Neogene marine sedimentary basin with an ideal setting for biofacies and lithofacie studies (McLaughlin and Van Den Bold., 1991). It contains fossiliferous rich reefal carbonates and thick evaporite deposits and clastic rocks, all very well preserved due to the semi-arid environment present (McLaughlin and Van Den Bold, 1991; Pierce, 2014). The valley formed as result of north-south compression subsidence (Mann et al., 1984) and contains very well preserved subaerial exposures of shallow-water reef environments dating approximately 5297 ± 41 to 7203 ± 77 years before present according to U/Th dating (Greer and Swart, 2006) at different locations in Enriquillo and 6.9-8.9ka using radiocarbon dates in Cañada Honda (Hubbard et al., 2004). During the early Holocene rapid sea level rise flooded the valley resulting on transgressive deposits that eventually formed shallowing upward sequences (Cuevas et al., 2005). Quaternary deposits from local rivers isolated the open bay separating the Caribbean Sea and forming the hypersaline Lago Enriquillo around 5ka (Cuevas et al., 2005). Drastic evaporation dominated in the lake as fluvial influxes in the region created erosional gullies, exposing the Holocene coral reefs in an arid environment. Constant sediment influx of calcareous composition (Cuevas et al., 2005) covered much of the reef creating a very well preserved exposure. The constant influx could have been responsible for low growth rates ranging from 1.3-4.5 mm/yr (Cuevas et al., 2005) in *Montastraea sp.* compared to low sedimentation growth rates that vary from 5 and 7.5 mm/yr (Dokken et al., 2003) to 8.5-10 mm/yr (Gischler and Oschmann, 2005). The chemistry of the water have also been widely influenced by seeping spring waters, some of them considered to be a source of sulfur (Buck et al., 2005). This study takes place in Cañada Honda, one of the erosional gullies that is initially described in Taylor (1985) and later described in detail by Hubbard et al. (2004) and Cuevas et al. (2005).

The Enriquillo Valley, unlike few places, has the conditions that allow the preservation of the reef structure and corals skeletons (Hubbard et al. 2004). The valley used to be a bay filled with marine water in a restricted environment with limited wave action, which resulted in the absence of *Acropora palmata* (Hubbard et al., 2004). High sediment influx from the mountains that bound the lake on the north and south affected the growth of the corals into forming columnar assemblages of platy corals as means of adapting to the environment (Hubbard et al., 2008). As a consequence these corals grew under stress conditions (Cuevas et al., 2005; Hubbard et al., 2008) and corals under stress, may be subject to alterations in Sr/Ca ratio. Even though Sr in the aragonite skeleton is mostly dependent on the water concentrations rather than inhibitors (such as KCN) or the amount of light, Ca is highly affected by the latter, generally inhibiting calcification (Marshall and Mculloch, 2002). This will result in higher Sr/Ca ratios to those crystals that precipitate.

The Holocene fringing reef exposure, generally, is highly abundant by corals in growth position of the species *Montastraea sp*. and *Siderastrea sp.* with the absence of *Acropora palmata* and *Diploria sp.* which marks a difference compared to other reefs in the Caribbean (Taylor et al., 1985; Cuevas et al., 2005; Greer and Swart, 2006; Hubbard et al., 2008). Still the coral species' diversity varies as the reef accreted suggesting changes in the ecology of the reef with time. Two major coral morphologies were surveyed: cone shaped and pancake shaped (Fig. 3), which are formed depending on the sediment influx rate of the area (Hubbard et al., 2008). Cone shaped corals are mostly formed when the coral outgrows the sediment input and pankace shaped corals when corals keep up with the sediment input (Hubbard et al., 2008). The climate and temperature conditions of the area have made possible the preservation of these rocks and most of its ecology and zonation of the fossilized reef (Greer and Swart, 2006). Stratigraphy shows little degree of faulting and erosion due to being uplifted during the Pliocene (~4Mya), prior to the reef development (Cooke 1989; Mann et al, 1999). Enriquillo reef exposures, with some exceptions, resembles modern reefs throughout the Caribbean, however, evidence from $\delta^{234}U$ suggests that this reef does not seem to have evolved in a closed system with normal seawater and that it is highly probable that these corals grew highly influenced by freshwater (Edwards, 1988).

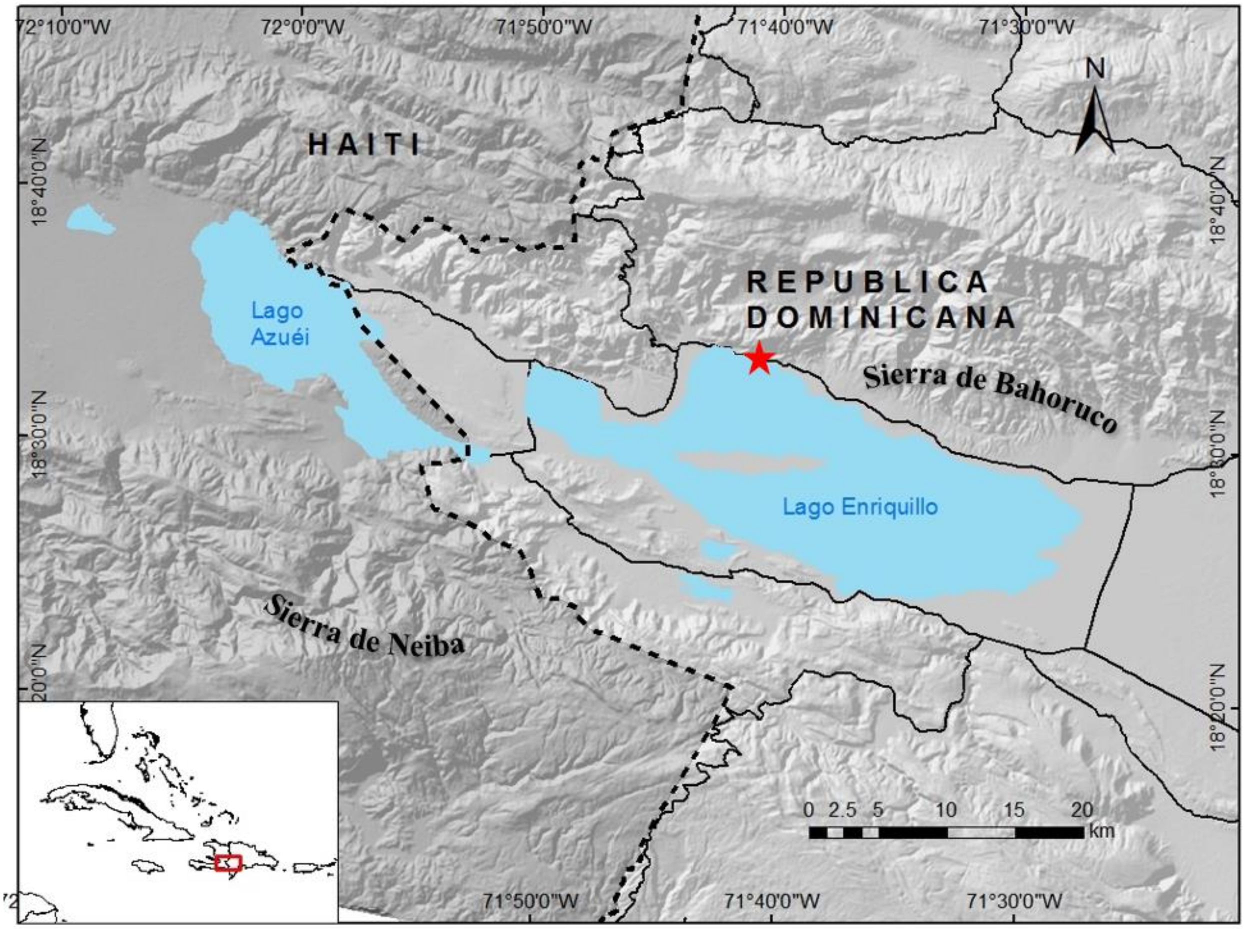

Figure 2: Map of Lago Enriquillo, Dominican Republic. Red star indicates the approximate location of Cañada Honda where this study takes place (Modified from Gonzalez et al., 2013)

Figure 3: Pancake morphology from a coral piece in Cañada Honda. Not that each layer presented may be interpreted as a sedimentation event (Hubbard et al., 2004).

2. Methodology

Five procedures were used to complete this research: 1) sampling of corals in growth position along specific stratigraphic intervals; 2) skeletal assessment to determine the degree of preservation and mineralogy of the samples; 3) measurement of changes in density (i.e. luminosity in x-rays) to determine growth rates in corals; 4) coral dating using U/Th radiogenic method; and 5) isotopic ($^{18}O/^{16}O$) and trace elemental (Sr/Ca) geochemical analysis to determine paleotemperatures related to SST. *Montastraea sp.* corals were used since many previous works have studied the skeletization in these species and have develop correlations (and equations) that establish the relationship between the isotopic and trace elemental concentrations to the temperatures, making possible to use their skeletons as paleothermometers (Greer and Swart, 2006). In this way the geochemistry in the skeleton, specifically Sr/Ca and $\delta^{18}O$ values were measured and used as proxy records of SST. Growth rates and SST variations obtained are compared with growth rates and SST variations of modern and ancient corals available in the literature (Felis et al., 2004; Greer and Swart, 2006; Smith, 2006; Giry et al., 2012; Cobb et al., 2013, Winter et al., 2003 and others) and from undergoing research in La Parguera, Puerto Rico. Measurement of the coral bands combined with radiometric dates provides timelines along the coral skeletons to study climate change including and making emphasis in rates of change and variability.

2.1 Sampling procedures

This research focuses on analyzing *Montastraea sp.* coral samples from the Massive Zone 1 (M1) shown in the Cañada Honda facies map (Fig. 4). The study area was surveyed prior to sampling, to identify major features already described on previous surveys done by Hubbard et al. (2004) and Cuevas et al. (2005) (Fig. 5). Possible samples were surveyed by looking at the taphonomy (external preservation and bioerosion) their geometry (growth position) and morphology. These characteristics are pertinent as this study relies in that the geochemistry and growth position of the corals needs to remain intact data to assess if the corals grew in situ and to obtain accurate paleoclimate data. As most corals of interest were grouped and assembled in columns, each of the columns were assigned a number seaward to landward (except M1-2 which is more seaward than M1-1 due to mislabeling) and each of the pieces an uppercase letter from bottom to top. If the same coral had to be split, each of the pieces will be assigned a lowercase letter from bottom to top. Each column and individual coral were photographed as means to document their exact position prior to sampling for future references.

Twenty four specimens were sampled and documented based on the facies map and stratigraphy; four of them were discarded due to not being the correct coral species or major diagenetic alteration leaving only 20 samples for further analysis (Fig. 6). Their position was measured both laterally and vertically using a measuring tape, using previous markings and facies boundaries described by Hubbard et al. (2004). M1-1 was the column of greater interest, because they cover the whole M1 facies from bottom to top, being a possible tool to study a continuous growth assemblage (Fig. 7). Some samples were cut in half in the field along the growth axis, using a portable Nakita Doc 7301 cutting machine for easier transportation and to reassure the degree of preservation of the coral. These samples were carefully cleaned to remove the external sediment and dust from the cutting machine, packed and sent to the Geology Department of the University of Puerto Rico, Mayagüez Campus.

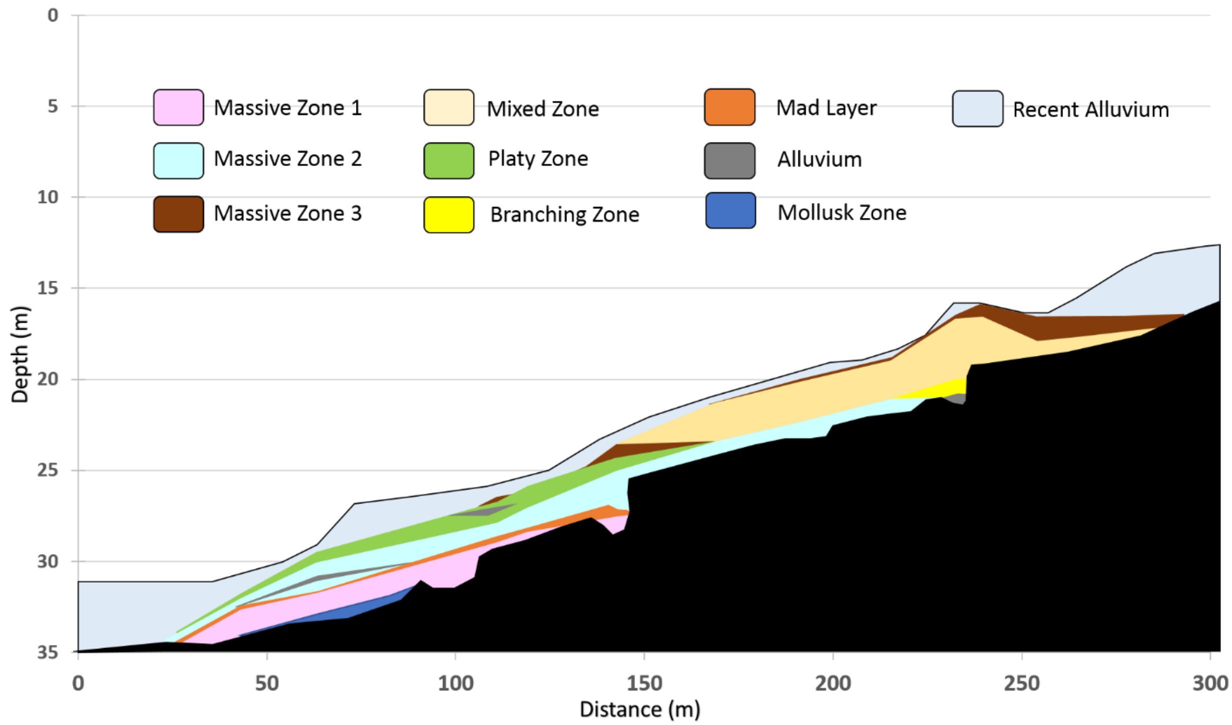

Figure 4: Facies map of Cañada Honda erosional gully. The focus of this study was to analyze coral samples within Massive Zone 1, shown in pink. (Modified from Hubbard et al., 2004; Cuevas et al., 2005).

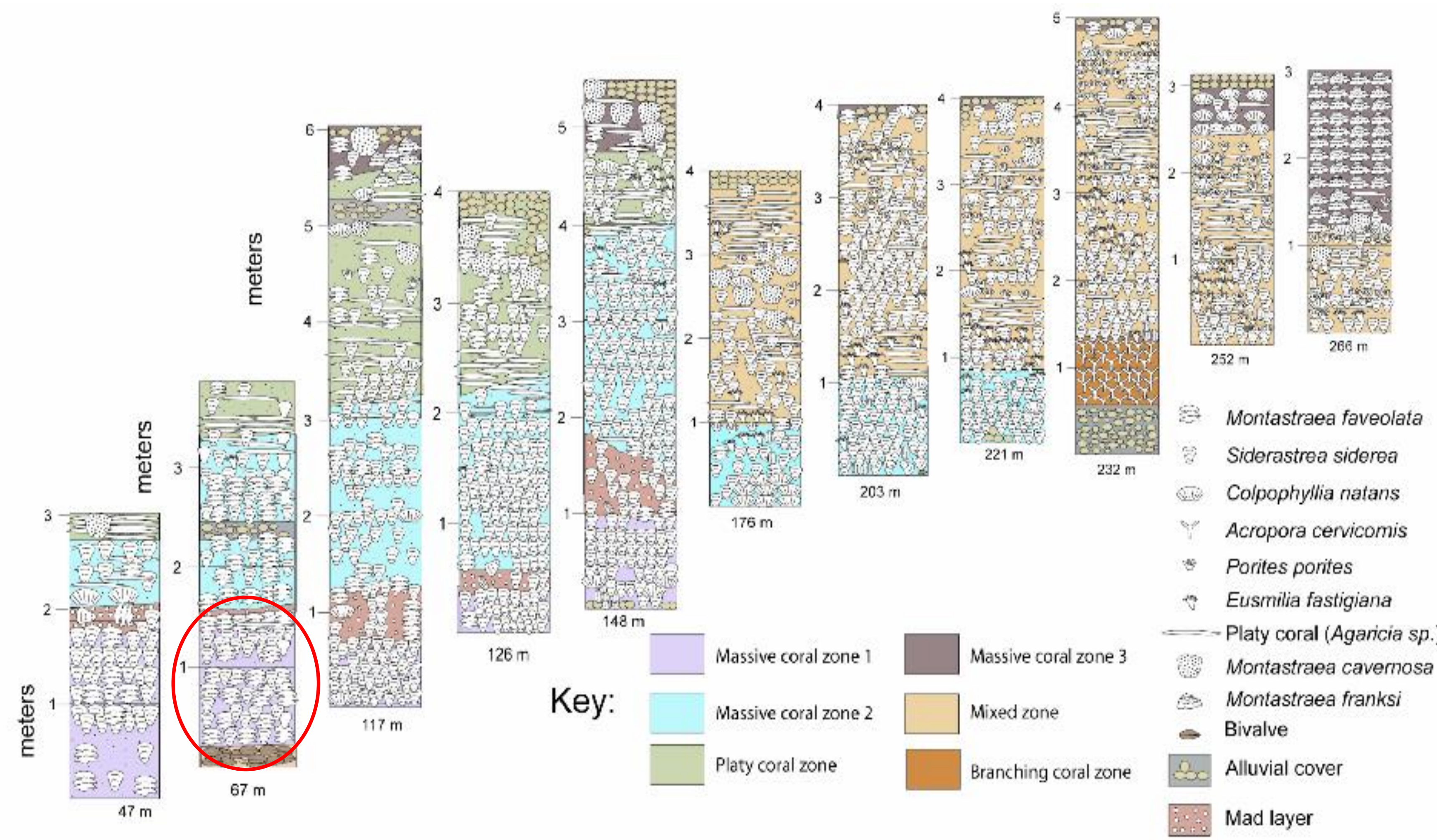

Figure 5: A portion of Cañada Honda fossil reef stratigraphy. Vertical trancects are shown in columns with the distance relative to the southern end of the outcrop on the bottom. Elevation in meters is shown on the vertical scale of each column. Location where samples were collected in this study is circled in red (Modified from Cuevas et al., 2005).

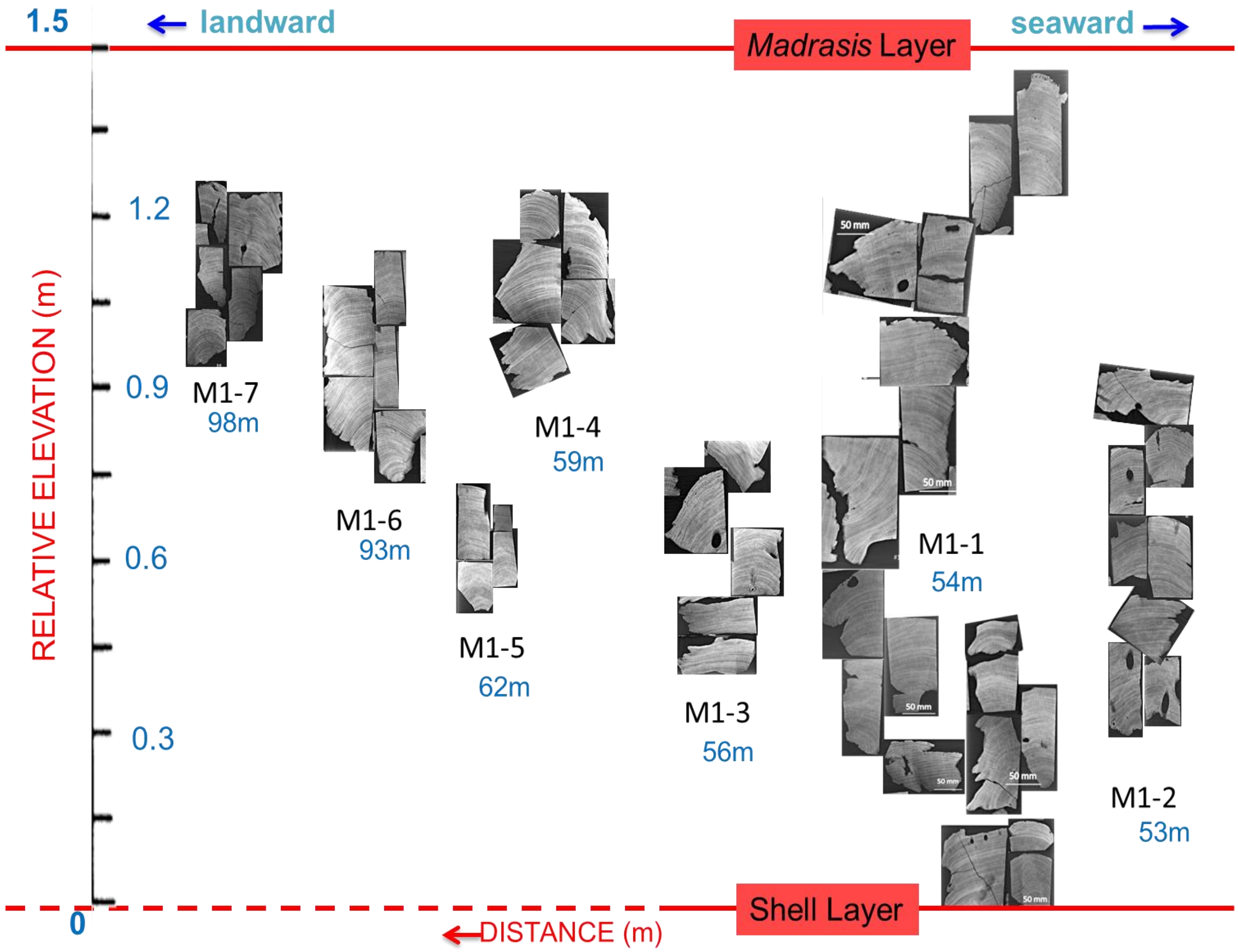

Figure 6: Samples collected from M1 facies assembled relative to their vertical position. Relative elevations were estimated based on the measurements taken from the visible layers. Horizontal position relative to the southern end of the outcrop is given for each column. Dashed lines indicate that the corresponding layer was not visible at that point.

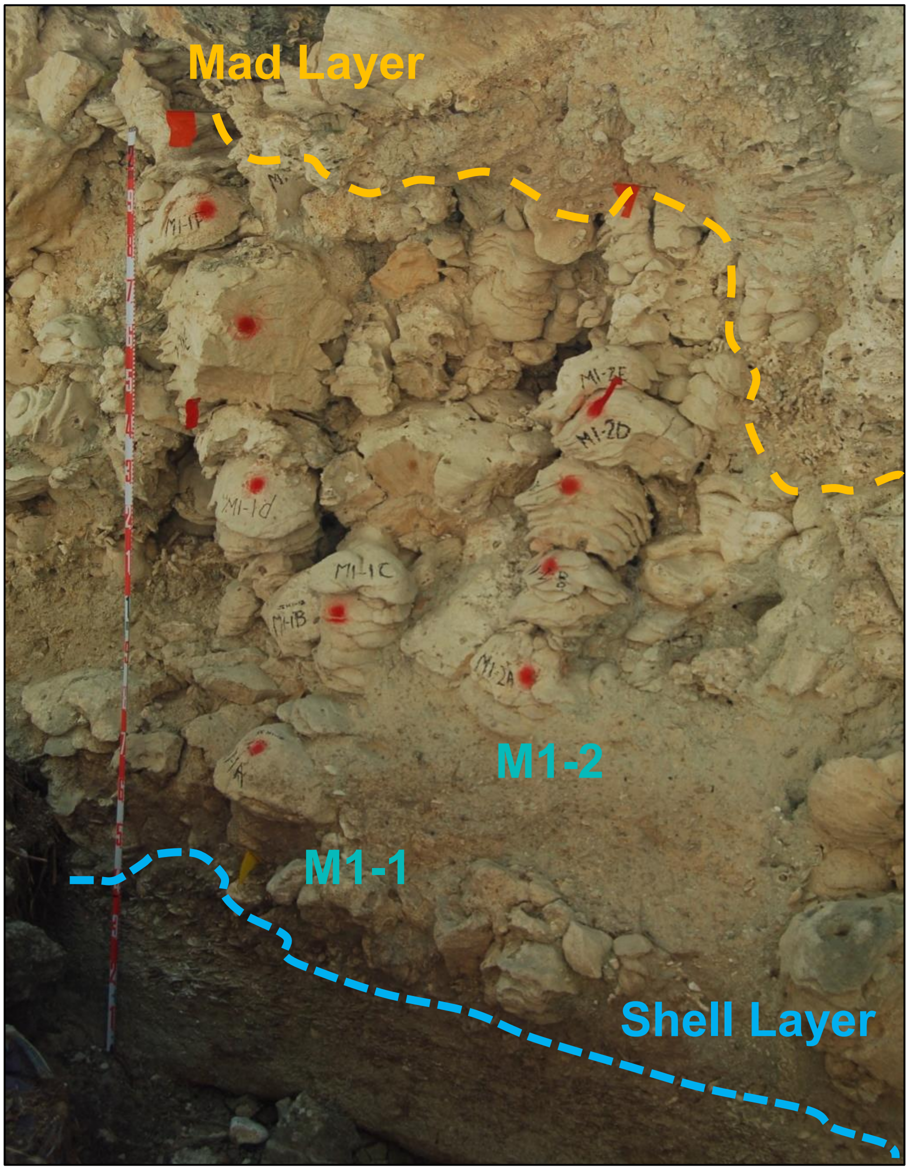

Figure 7: Photo of M1-1 and M1-2 columns with the Mad layer and Shell layer boundaries marked.

2.2 Sample preparation

The geometry of the samples was studied, to estimate the growth axis, as this is the area of interest for microsampling. Samples were cut in longitudinal slabs of 5mm thick using a SMI Fulker DiMet C/149B masonry and concrete saw. This thickness is required to be able to obtain clear x-ray images for the measurement of coral growth rates. A slab that is too thick will block the light form the x-ray machine, thus obscuring the growth bands. Each of the 24 samples was radiographed in the San Antonio Hospital at Mayagüez radiography facilities and both digital and physical copies of the radiographies were obtained.

Four samples (M1-1D_c, M1-1E_e, M1-2B_a and M1-2E) from the 24 samples collected were selected for micro-sampling based on the position, preservation and growth patterns shown in the radiography. Corals from the column 1 (M1-1) are important, because they comprise the whole M1 facies (Fig. 6 and 7). M1-1D_c, M1-1E_e were selected as they showed clear banding and the best preservation in both hand sample and radiography. Samples from column 2 (M1-2) M1-2B_a and M1-2E were chosen because they stratigraphically overlap those already chosen from column 1 as means to understand the lateral variations of the reef. One sample (M1-1G_b) identified as diagetic altered was chosen to obtain measurements of altered materials for comparisons and also because its position was at the top of the M1 facie. M1-1G_b showed bioerosion and observed variations in coloration that led to possible diagenetic alteration. This sample is associated with beds that have been interpreted as storm deposits that separate facies M1 from M2. These deposits were described in Hubbard et al. (2004) and Cuevas et al. (2005) as the *Madrasis* "Mad" layer, based on the abundant broken pieces of the *Madrasis sp.* coral (Fig. 7)

2.3 Assessment of coral skeleton integrity

Pristine coral skeleton preservation and original aragonitic composition is a major requirement for the samples used in this study. To test the integrity of the coral skeleton, samples were analyzed using a Siemens X-Ray Difractometer (XRD) D500 from the UPRM Geology Department. A section of the coral was sampled and pulverized using a mortar and pestle until a very fine powder was produced. The samples were analyzed using a step of 0.02, a time of 1 sec and range from 15-65° 2-Theta scale. Results obtained were compared to the aragonite XRD analysis done by Downs (2006) to reassure the aragonitic composition and discard any sediment contamination of the samples. Peaks for aragonite are expected to be present at 26.2° (I_1=100%), 45.86° (I_2=65%) and 27.2° (I_3=52%). From this analysis, the presence of calcite and its dominance over aragonite can be studied by looking at possible peaks at 29.4° (I_1=100%), 43.1° ($I_{2\text{-}3}$=18%) and 39.4° ($I_{2\text{-}3}$=18%). Since peaks at 43.1° and 39.4° for calcite have the same intensity percent (I), it can't be distinguished between I_2 or I_3.

2.4 Montastraea sp. Growth rate estimates

Extension rates were obtained by measuring the lineal distance of the high density (HD) and low density (LD) bands in digital images obtained from X-rays using Coral X-radiograph densitometry system (Coral-XDS) software. The software was calibrated using the radiography image scale, obtained from the digital image, both for the x and y axis. The accuracy of this scaling method was tested by measuring the dimensions of M1-1E_e and comparing it to the scale produced digitally. For each sample, a transect (Fig. 8) was drown following the growth direction using the oblique setting trying to avoid any dark spots or possible luminance errors in the image as those will give inaccurate densitometry results. The densitometry analysis was done at steps of 0.1cm following the intended microsampling intervals (see section 2.7) at an automatic scale based on the previous calibration. The software automatically builds a graph of luminance as a function of extension (Fig. 8) where maximum or LD and minimum or HD luminance points are detected. However, some of the maximums and minimums are not detected and had to be entered manually using the add maximum or add minimum feature. Once the plot was completed, it was obtained from the software through a screenshot and the data extracted as a .DAT file for further study. Using the data obtained from the software, since each couplet of LD-HD bands represents a year of skeletal growth, the chronology of the years present in the coral skeleton is developed by counting the number of couplets present in the sample (Winter et al., 2000). With this information, growth rates were calculated using equation 1 for samples M1-1D_c, M1-1E_e, M1-2B_a, M1-2E and test sample M1-1G_b

$$Growth\ rate = \frac{Coral\ growth\ extension\ (mm)}{number\ of\ couplets\ (yr)} \qquad (1)$$

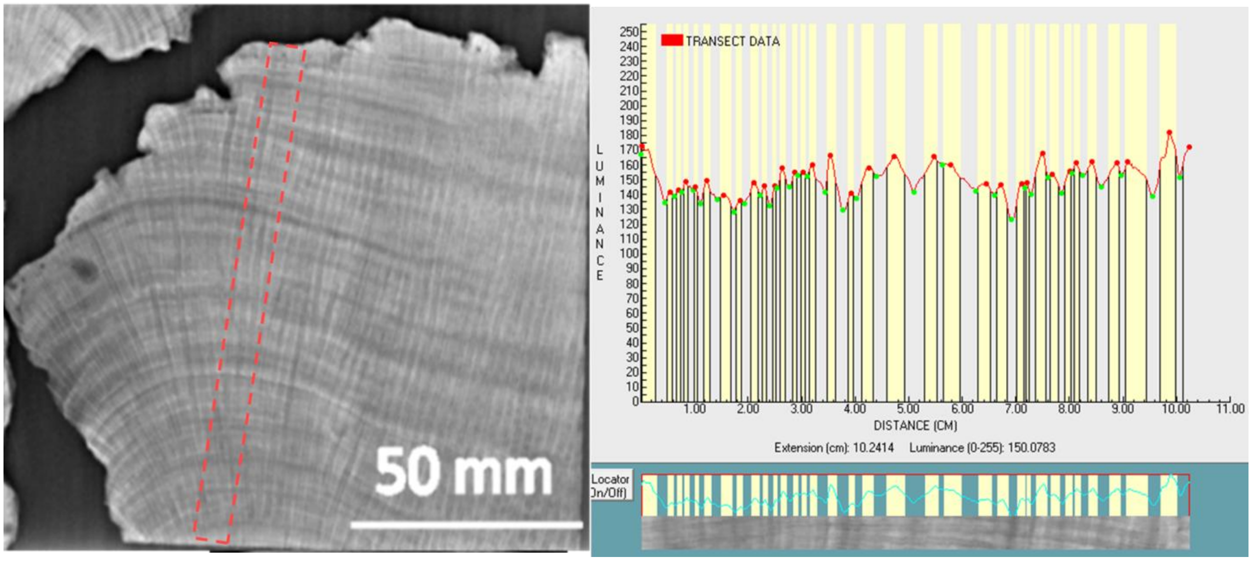

Figure 8: Example of the densitometry analysis done on M1-1E$_e$. Sample radiography with a drawn transect (red square) on the left and the output plot obtained from Coral XDS for that sample on the right.

2.5 Sedimentation rate estimates

Sedimentation rates were estimated using equation 2 by looking at the pancake morphology developed by some corals in this fossil reef. Each pancake of the coral is associated with a sedimentation event (Hubbard et al., 2008), meaning, that by measuring the extension of a pancake along the growth axis with relation to the growth bands, sedimentation rates can be estimated. Sample M1-2B_a is an example of pancake morphology where eight events, labeled from M1-2B_a-S1 to M1-2B_a-S8 from bottom to top, of sedimentation can be observed (Fig. 9). Each of the events was analyzed using the method described for growth rates (see section 2.4),

$$Sedimentation\ rate = \frac{Pancake\ growth\ extension\ (mm)}{number\ of\ couplets\ (yr)} \quad (2)$$

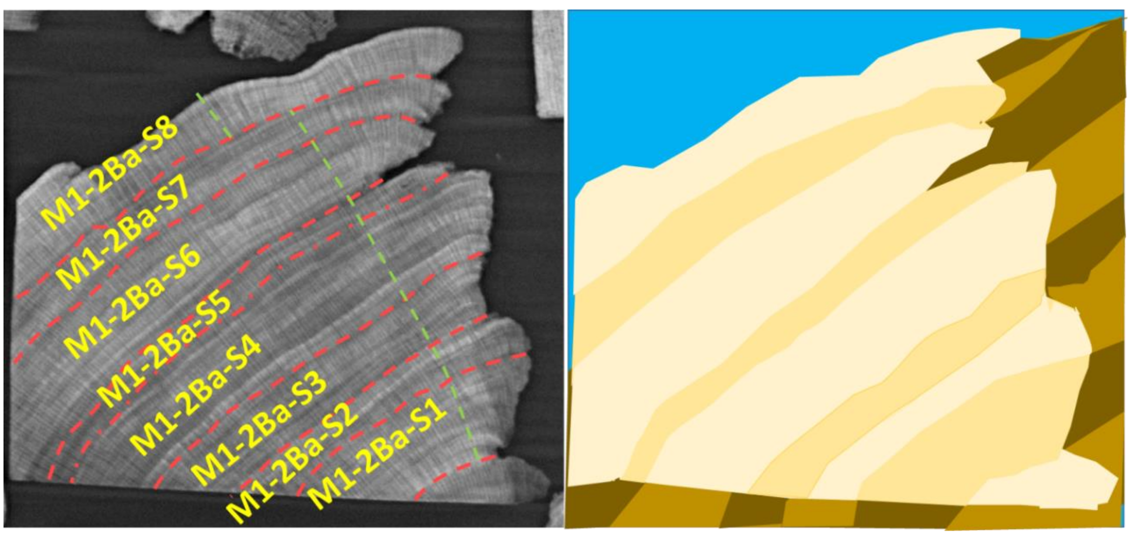

Figure 9: Pancake morphology of sample M1-2B_a. Sample radiography marked with the observed boundaries of the pancake morphology (dashed red lines) and a drawn transect (dashed green line) on the left and a sketch of the sedimentation events on the right.

2.6 Radiogenic dating

The four coral samples analyzed for isotopes and trace elements (M1-1D_c, M1-1E_e, M1-2B_a and M1-2E) were also dated using uranium thorium radiogenic dating (U/Th). In addition, sample M1-1A_a located at the base and M1-4A_e at the top of the M1 facies (Strat figure), although not analyzed for isotopes and trace elements, were dated since they are expected to be the oldest and youngest coral samples respectively. Fragments of the coral skeleton of approximately 1g were obtained from each coral skeleton sample. The sampling location along coralline structure was documented in detail and was deliberately taken close to the location that was micro-sampled for geochemical analyses (see section 2.7). The powdered samples were analyzed in a multi-collector inductive coupled plasma mass spectrometer (MC-ICP-MS) at the University of Minnesota. Decay constants were obtained and used for U as $\lambda_{238} = 1.55125x10^{-10}$ (Jaffey et al., 1971) and $\lambda_{234} = 2.82206x10^{-6}$ (Cheng et al., 2013) and for Th as $\lambda_{230} = 9.1705x10^{-6}$ (Cheng et al., 2013). Radiogenic $\delta^{234}U$ isotope was calculated using equation 3 and $\delta^{234}U_{initial}$ was calculated based on 230Th age (t) using equation 4. Corrected ^{230}Th assumes an initial $^{230}Th/^{232}Th$ ratio of $4.4 \pm 2.2 \times 10^{-6}$ a value known for secular equilibrium with the bulk earth $^{232}Th/^{238}U$ value of 3.8. Errors for this analysis are arbitrarily assumed to be 50% and present day is established as 1950 A.D. More details on the method used are described by Cobb et al., (2003) and Cheng et al. (2013). $\delta^{234}U$ obtained during U/Th dating, is studied to try and understand the nature of the waters where this corals formed as this is a tool frequently used to test diagenesis and open system behavior in marine environments (Robinson et al., 2003). Regular seawater mean $\delta^{234}U$ values for the Atlantic is 144 ± 3‰ ranging from 140 to 150‰ (Edwards et al., 1985; Edwards et al., 1987). Input of freshwater into the system is known to decrease the $\delta^{234}U$ values in in the coral skeleton (Robinson et al., 2004; Mey et al., 2005).

$$\delta^{234}U = ([^{234}U/^{238}U]_{activity} - 1) * 1000 \qquad (3)$$

$$\delta^{234}U_{initial} = \delta^{234}U_{measured} * e^{\lambda_{234} t} \qquad (4)$$

2.7 Microsampling

From the four coral samples selected for isotopes and trace elements analysis (M1-1D_c, M1-1E_e, M1-2B_a and M1-2E), 500 samples (~100-130 per coral) were micro-sampled each millimeter (1mm or 0.1cm) using a X0 Micromill with a 1mm drill bit (Fig. 10). The sampling was also performed in test sample M1-1G_b, however, only 20 micro-samples were collected as this is a test sample to asses values of altered materials (see section 2.3). The procedure was performed by following the growth axis along the thecal wall of a corallite using the naked eye and the radiography. Micro-samples were obtained at increments of 1mm approximately and each sample address a sub-monthly resolution time-series given growth rates of approximately 10mm/yr (Nurhati et al., 2009). Powders were carefully collected and weighted using a Mettler UMT2 Micro-balance consecutively for both stable isotope (80-100µg) and trace element analysis (150-200µg). Excess of powders were carefully placed in a glass vial and stored for future references. Both the micro-sampling and the geochemical analyses were done at Cobb's Lab in Georgia Intitute of Technology.

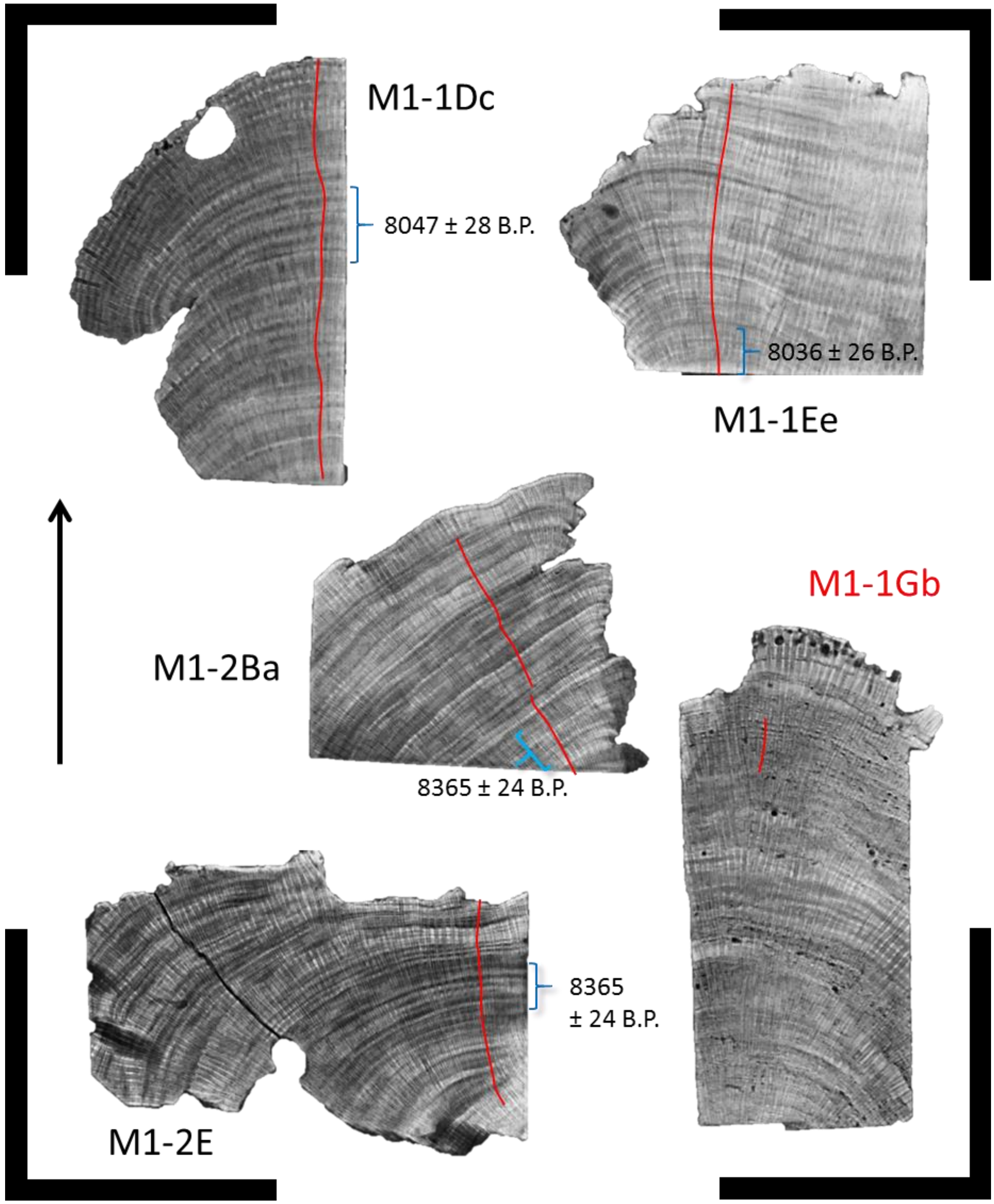

Figure 10: X-Ray radiographs and fossil *Montastraea sp.* coral samples analyzed in this study. Black bars are at a scale of 10cm both vertically and horizontally. Test sample M1-1G$_b$ is labeled in red. Red lines indicate microsampling transects at increments of 1mm along the thecal wall, blue brackets indicate the position where the dating sample was obtained and black arrow indicate growth direction.

2.8 Stable isotope analysis

$^{18}O/^{16}O$ and $^{13}C/^{12}C$ isotopic ratios were analyzed using a GV Isoprime Mass Spectrometer equipped with a Multiprep device with an analytical precision of ±0.05‰ (1σ). A *Porites* aragonite standard (PDA) converted to Pee Dee Belemnite (PDB) values was used as a standard. Weighted powders (80-100µg), including the standards, were quantitatively transferred to an acid-cleaned glass tube and documented for analysis. A quality control assessment provided by the laboratory technician (Table 1) was done to discard samples that were damaged before or during the analysis. For each analytical run, standard deviation was calculated using the standard (PDA) results obtained from the analysis. Isotopic values were corrected by adding the correction factor (Standard $^{18}O/^{16}O$ – PDA Mean $^{18}O/^{16}O$) to the raw values of $^{18}O/^{16}O$. Results obtained are compared to results obtained from similar coral samples in Enriquillo by Greer and Swart (2006) for reproducibility. Values of $\delta^{18}O$ obtained are converted to temperature using a calibration done by Leder et al. (1996) shown in equation 5, keeping the oxygen isotope values of the water constant ($\delta^{18}O_w = 0$). With this assumption, variations in $\delta^{18}O$ will be solely attributed to changes in temperature due to fractionation of the isotopes and not to variations in $^{18}O/^{16}O$ in the water (Greer and Swart, 2006).

Table 1: Quality control for the stable isotope analyses. Samples who did not meet these requirements were discarded and not taken into consideration for interpretations.

Parameter	**Expected values**
Standard Deviation $^{18}O/^{16}O$	< 0.07
Standard PDA $^{18}O/^{16}O$	~ -5.32
Standard PDA $^{13}C/^{12}C$	~ -1.32
Leak Rate	< 1000
Pno Acid	< 100
Total CO_2	~ 1000
Exp	0

$$SST = 5.33 - 4.519\ (\pm 19) * (\delta^{18}O_c - \delta^{18}O_w) \qquad (5)$$

2.9 Trace metal analysis

Sr/Ca ratios were measured using a Horiba JY Ultima-C Inductively Coupled Plasma Optical Emission Spectrometer (ICP-OES) with analytical precision of ±0.08-0.24% (1σ) using the Schrag (1999) nearest-neighbor correction method. Weighted samples (150-200μg) were quantitatively transferred into acid-washed polypropylene tubes and diluted with 2% nitric acid (HNO_3). Each sampled was centrifuged using a S1-0236 Vortex-Genie Mixer, 120V to ensure a well-mixed solution. A calibration curve was constructed using previously prepared standards with calcium concentration of 20, 30, 40 and 50 ppm as means to discard contaminated samples.

To obtain Sr/Ca-derived SST, a Sr/Ca calibration using modern corals from a reef in the region under the same marine conditions would be ideal. However, this is impossible as this reef was formed in a semi closed bay environment that no longer exists. Still, calibrations made by Swart et al. (2002) in Ball Buoy Reef, Southern Florida (Eq. 6), Felis et al. (2004) in the Gulf of Aqaba, Red Sea (Eq. 7), Flannery et al. (2013) in Dry Tortugas, Florida (Eq. 8), Giry et al (2012) in Bonaire, Southern Caribbean (Eq. 9) and Smith (2006) in Dry Tortugas, Florida (Eq. 10) were tested to obtaine possible SST estimates. The environment present in the Red Sea and Bonaire are probably the most consistent to Enriquillo. The Red Sea is a semi-closed environment similar to what Enriquillo was before the closure of the bay and a model of SST seasonality anomaly done by Giry et al. (2012) suggest that there were similar conditions in SST about 6kya between Bonaire and Southern Hispaniola.

$$Sr/Ca = 10.165 - 0.0471 * SST \quad (6)$$

$$Sr/Ca = 10.781 - 0.0597 * SST \quad (7)$$

$$Sr/Ca = 10.205 - 0.0392 * SST \quad (8)$$

$$Sr/Ca = 10.6 - 0.050 * SST \quad (9)$$

$$Sr/Ca = 9.962 - 0.0282 * SST \quad (10)$$

3. Results

3.1 Densitometry analysis

Densitometry analysis for samples M1-1D_c, M1-1E_e, M1-2B_a, M1-2E and M1-1G_b are plotted in (Fig. 11) and interpreted in (Fig. 12) with luminance intensity in the Y axis and extension in the X axis (See appendix 1-5 for individual plots). Interpretation of luminance variation in sample M1-1D_c (15.03cm) shows constant values with 1 cm intervals of thinner growth at 7cm and 12 cm. Sample M1-2E (8.36cm) shows a decreasing trend in luminance values from 0-6cm then increases from that point with variations of growth thickness approximately every 1-2cm. Sample M1-1E_e (10.24cm) shows increasing trend in luminance values with thickness variations of 3.5cm during two intervals and 1cm the following two intervals. Sample M1-2B_a (10.61cm) shows decreasing trend in luminance values from 1-6.5cm and then increases from that point. Growth thickness variations in this sample are less drastic during the first 5.5 cm (2-3cm) and then vary more rapidly (0.5-1cm) towards the end. Densitometry plots for each section of M1-2B M1-2B_a are presented in (Fig. 13). Base-M1-2B_a extends for 2.50cm followed by mid-M1-2B_a which extends for 3.54cm and then by top-M1-2B_a for the last 3.35cm. Sample M1-1G_b (17.47cm) shows variable luminance values trends within the coral. There is a decreasing trend during the first 3.8cm followed by a decrease-increase trend from 4.3-9cm. At 9.2 cm there is an increasing trend in luminance values later followed by a decrease-increase trend from 11.2-15.4 cm from where it decreases until the end of the plot. Thickness variations in this coral are not as remarkable, yet lengthy. Thinner growth occurs during the first 6.5 cm, then at 8.4-9.1cm and later at 13-15cm.

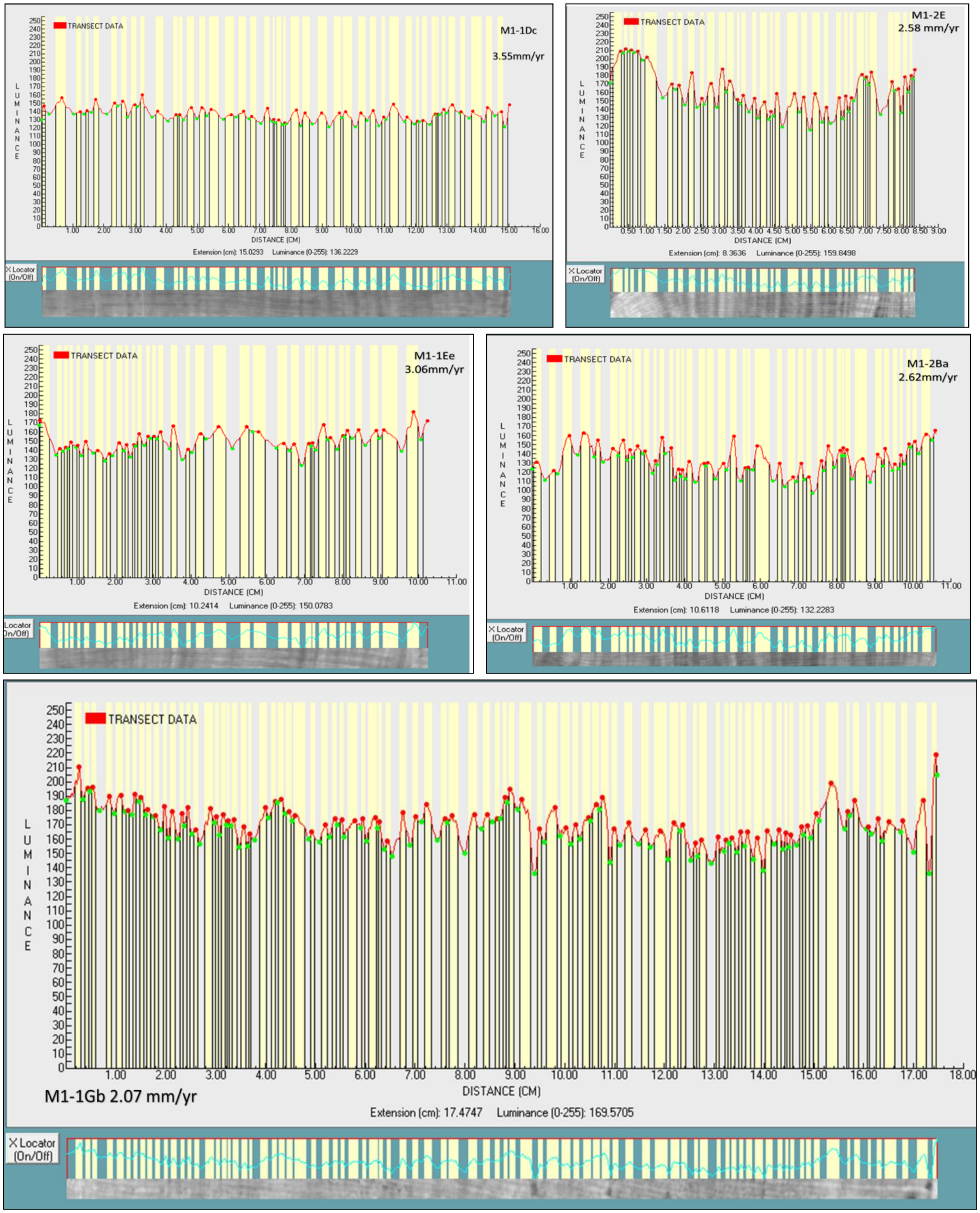

Figure 11: Densitometry analysis of samples of M1-1D_c, M1-2E, M1-1E_e, M1-2B_a, M1-2E and M1-1G_b produced by Coral-XDS. Figures include estimated growth rate and transect at the bottom of the figure for each sample. Refer to appendix 1-5 for drawn transects.

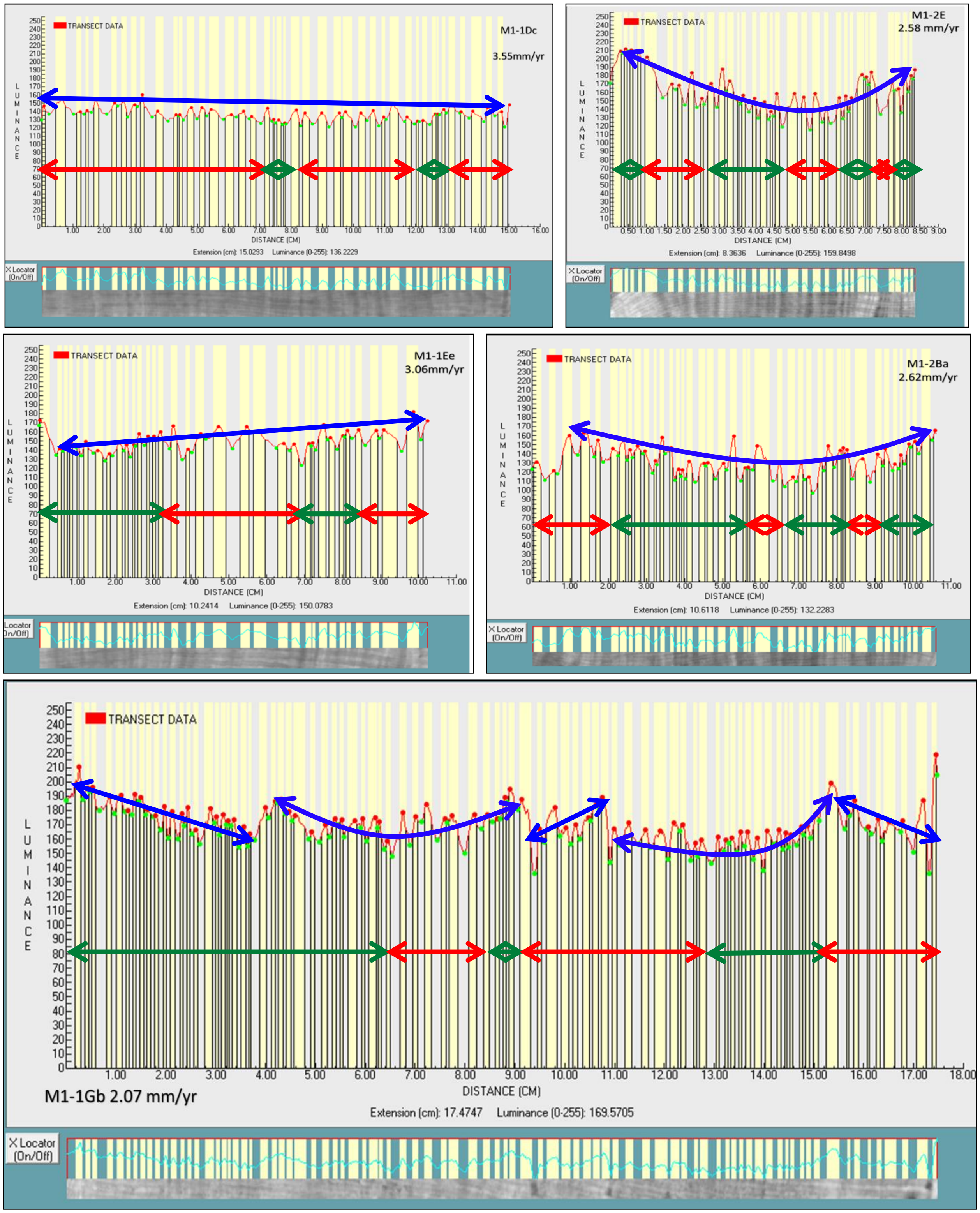

Figure 12: Interpreted densitometry analysis of samples M1-1D$_c$, M1-2E, M1-1E$_e$, M1-2B$_a$ and M1-1G$_b$ produced by Coral-XDS. Blue arrows indicate visual trends of luminance intensity; red arrows indicate intervals of relatively thicker extension and green arrows intervals of relatively thinner extensions. Refer to appendix 1-5 for drawn transects.

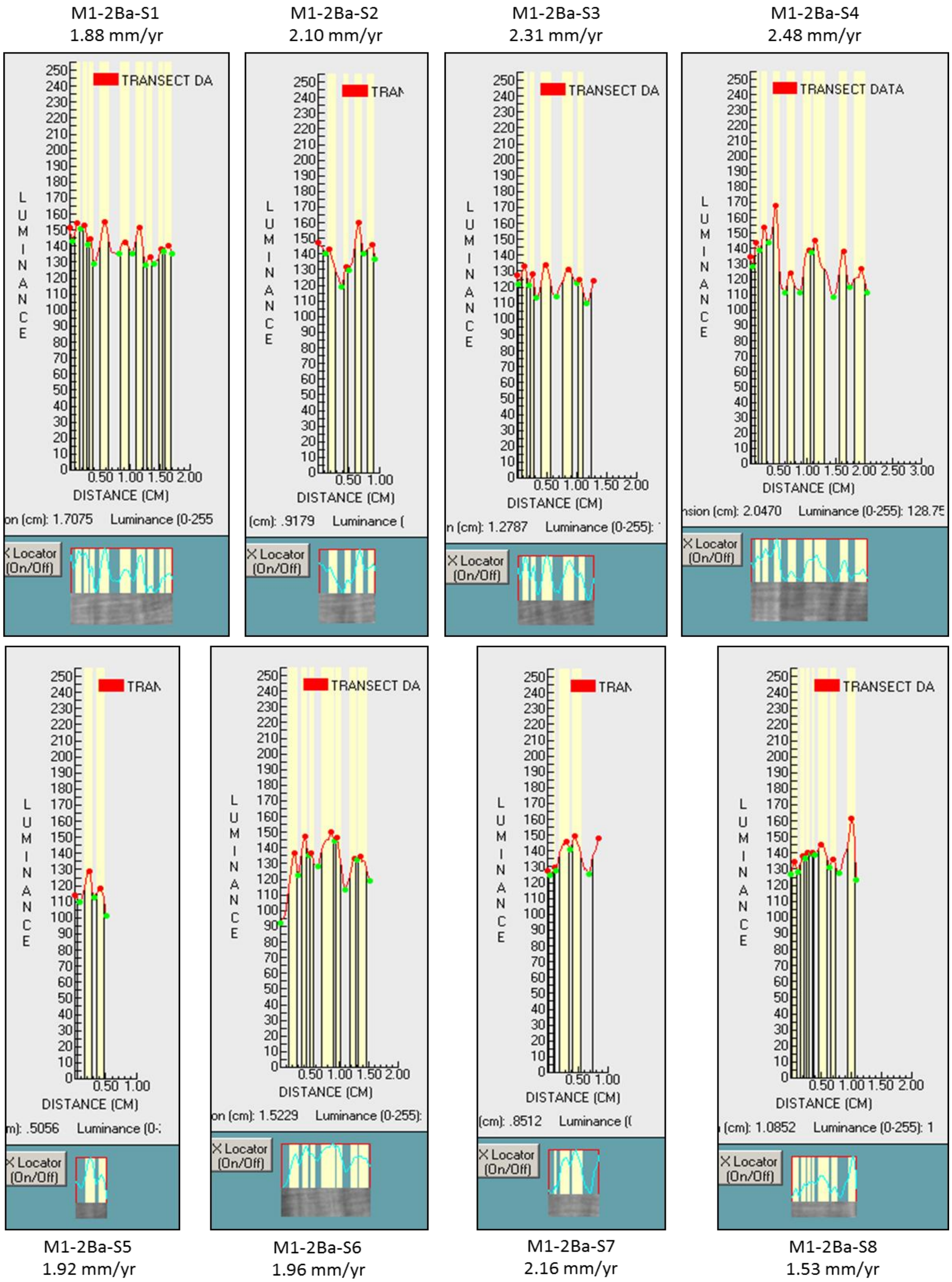

Figure 13: Densitometry analysis of the eight sedimentation events (S1-S8) interpreted from sample M1-2B_a produced by Coral-XDS. Figures include estimated growth rate and coral transect at the bottom of the figure for each section. Refer to Fig. 9 for drawn transects.

3.2 Skeletal composition

The output produced by the XRD analysis shows a graph with intensity counts in the Y axis and the 2theta in the X axis (Fig. 14, see appendix fig 6-10 for individual plots). All four samples (M1-1D_c, M1-1E_e, M1-2B_a, M1-2E) and the test sample sample (M1-1G_b) only show aragonite peaks. The spectrum shows two prominent peaks at approximately 26° (1800-2100 counts) and 27° (1000-1100 counts) matching the aragonitic peaks I_1 and I_3 respectively. There is also a separate peak at approximately 46° (1300-1600 counts) which corresponds to the I_2 peak for aragonite. The distinctive calcite peak I_1 expected at 29° is not present in any of the samples, including test sample M1-1G_b.

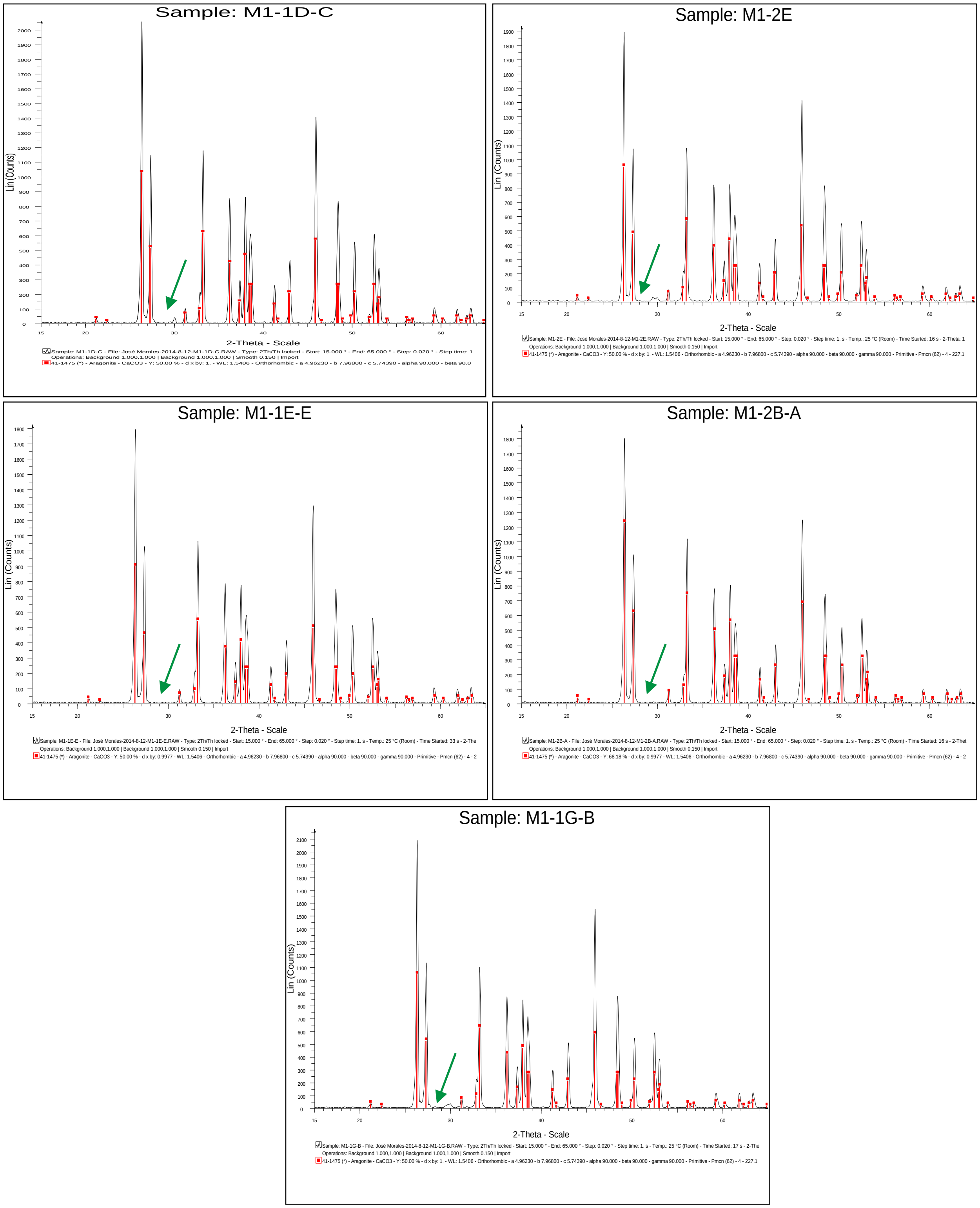

Figure 14: XRD results for samples M1-1D$_c$, M1-2E, M1-1E$_e$, M1-2B$_a$ and M1-1G$_b$. Peaks for aragonite (red) are marked for each sample. Note the absence of the calcite peak (green arrow) in each sample. Refer to appendix 6-10 for individual plots.

3.3 Growth rates estimates

Calculated growth rates for each studied samples (M1-1D_c, M1-2E, M1-1E_e, M1-2B_a and M1-1G_b) are summarized in (Table 2). The extensions based on the variations in luminosity from this table may differ from those given in the densitometry analysis because a single band at the end of the transect might have not been analyzed by the Coral XDS software. Average growth rates in stratigraphy position along the reef range from 2.07 ± 0.14 to 3.55 ± 0.37 mm/yr with an average value of 2.77 ± 0.56 mm/yr (n=5) in a time lapse of 30-80 years. Growth rates measured decrease as we move up stratigraphically in both M1-1 and M1-2. Growth rates measured increase laterally as we move landward (north) (Fig. 15).

Table 2: Summary of the densitometry analysis, growth rate and sedimentation rate estimates.

Sample ID	Years (n)	Extension (mm)	Growth Rate (mm/yr)
M1-1D_c	42	149.31	3.55 ± 0.37
M1-1E_e	33	101.04	3.06 ± 0.45
M1-2B_a	40	105.13	2.62 ± 0.48
M1-2E	32	82.66	2.58 ± 0.20
M1-1G_b	83	171.97	2.07 ± 0.14

Section ID	Years (n)	Extension (mm)	Sedimentation rate (mm/yr)
M1-2B_a-S1	8	15.04	1.88 ± 0.33
M1-2B_a-S2	3	6.32	2.10 ± 0.30
M1-2B_a-S3	5	11.57	2.31 ± 0.43
M1-2B_a-S4	7	17.40	2.48 ± 0.45
M1-2B_a-S5	2	3.84	1.92 ± 0.07
M1-2B_a-S6	6	11.78	1.96 ± 0.15
M1-2B_a-S7	3	6.49	2.16 ± 0.57
M1-2B_a-S8	6	9.21	1.53 ± 0.18

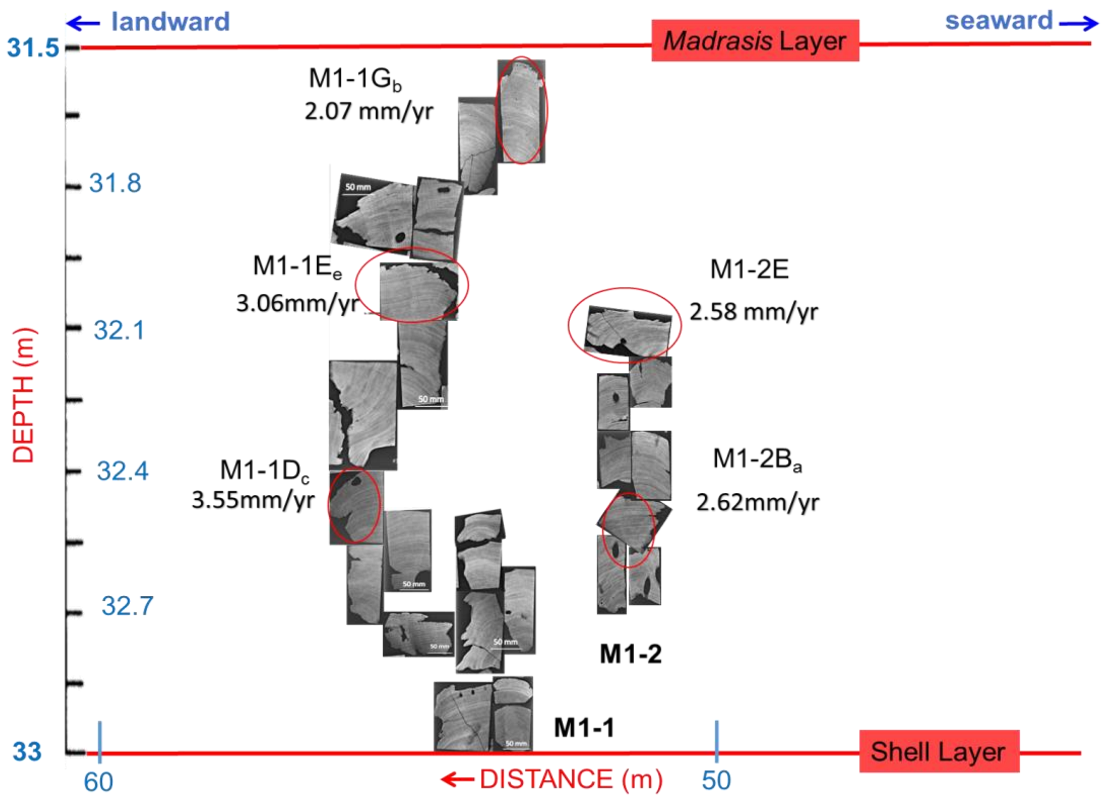

Figure 15: Growth rates of M1 facies' columns M1-1 and M1-2. Samples used for densitometry analysis are circled in red.

3.4 Sedimentation rate estimates

Estimated sedimentation rates for each section in sample M1-2B$_a$ (S1 to S8) are summarized in (Table 2). Sedimentation rates range from 1.53 ± 0.18 to 2.48 ± 0.45 mm/yr with an average value of 2.06 ± 0.30mm/yr (n=8) in time intervals of 2-8 years. The events started at a rate of 1.88mm/yr then became more rapid until the fourth sedimentation event (S4) with a maximum rate of 2.48mm/yr. Sedimentation slowed down to 1.92mm/yr then increased until the seventh sedimentation event (S7) at 2.16mm/yr where rated slowed to 1.53mm/yr (Fig. 16).

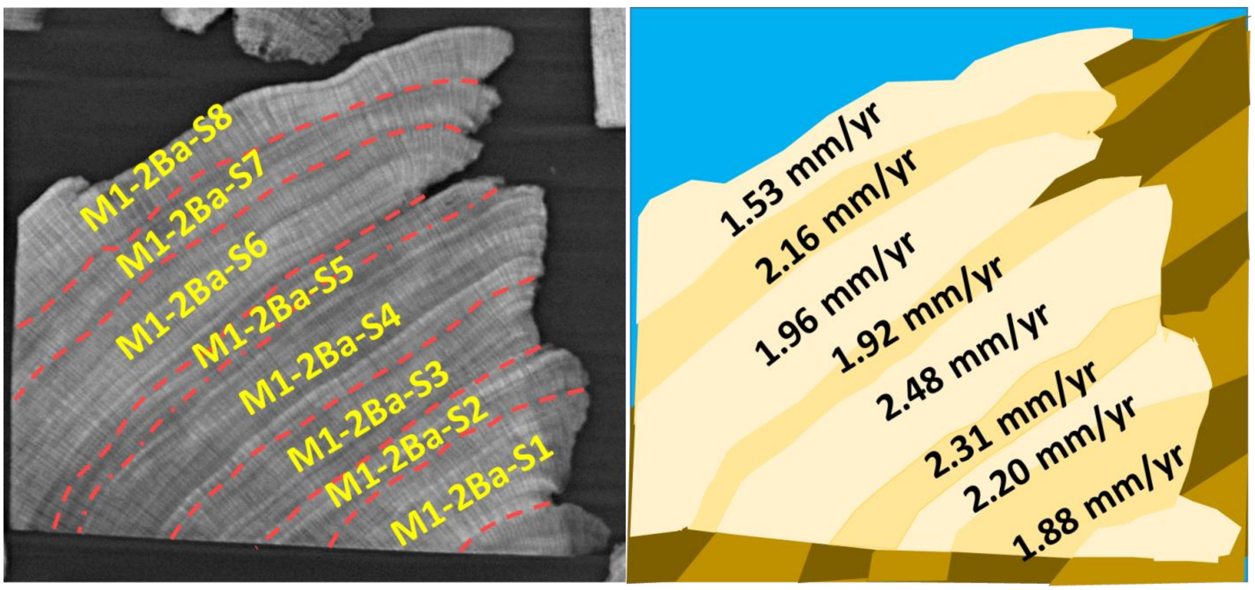

Figure 16: Sedimentation rates of each section in M1-2B$_a$ (S1-S8). Sedimentation rate boundaries are marked with red dashed lines.

3.5 U/Th Radiogenic dating

Each of the four samples ($M1\text{-}1D_c$, $M1\text{-}1E_e$, $M1\text{-}2B_a$, M1-2E) under study, including the sample at the base of the facies ($M1\text{-}1A_b$) and another at the top of the facies ($M1\text{-}4A_e$), have U/Th dates that range from 8036 ± 26 to 8910 ± 28 yr B.P. (Fig. 17). As expected, Sample $M1\text{-}1A_b$ is the oldest coral of M1-1 and corals get younger following the vertical growth of the column. Samples in M1-2 get younger following the vertical growth of the columns, however, overlapping samples on M1-2 are much older than those in M1-1. Sample M1-4Ae was the exception to this, as it dated since is older than samples from M1-1. $\delta^{234}U$ was measured as part of the dating process, and it ranges from 87.9 ± 1.4 to 113.3 ± 1.3‰ with an average value of 104.7 ± 1.4‰.

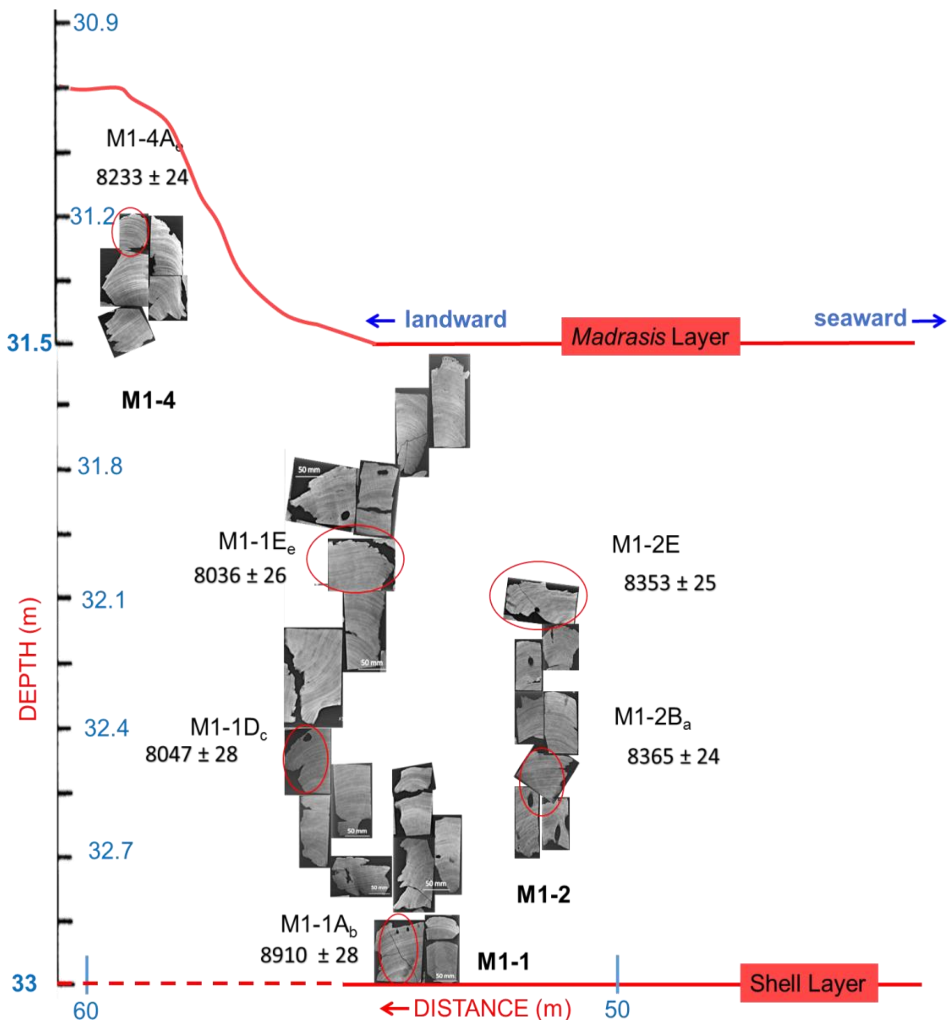

Figure 17: U/Th radiometric dates of M1 facies' columns M1-1, M1-2 and M1-4. Samples used for radiogenic dating analysis are circled in red.

3.6 Stable Isotopes analysis

The $\delta^{18}O$ and $\delta^{13}C$ values from the samples under study (M1-1D_c, M1-1E_e, M1-2B_a, and M1-2E) and test sample (M1-1G_b) are plotted with depth in Fig. 18 and isotopic ranges and variation are summarized in Table 3. $\delta^{18}O$ and $\delta^{13}C$ values are very similar in all samples. $\delta^{18}O$ variations are not large and most values are around (average) -1.56‰ with the exception of sample M1-2B_a with an average of 1.18‰. $\delta^{13}C$ variations is not large either and most samples under study average -2.06‰ with the exception of sample M1-1D_c with an average of 2.45‰. Sample M1-1G_b $\delta^{18}O$ values (-1.41 to -2.25‰) fall within the values obtained for the samples under study with a variation of 0.84‰. However, $\delta^{13}C$ values were lower (2.43 to -4.04‰) with a variation of 1.61‰.

3.7 Trace elemental analysis

Sr/Ca ratio for the samples under study (M1-1D_c, M1-1E_e, M1-2B_a, and M1-2E) and sample (M1-1G_b) are plotted along with $\delta^{18}O$ and $\delta^{13}C$ in Fig. 18 and results are summarized in Table 3. Samples M1-1D_c, M1-1E_e, M1-2B_a, and M1-2E, Sr/Ca results vary from 9.07-9.70 mmol/mol with variations that relatively similar among them. Sample M1-1G_b have lower values (8.84-9.31 mmol/mol) than the other samples. In the majority of the cases, Sr/Ca follows the expected inverse trend in variation relative to $\delta^{18}O$. Sample M1-1D_c and M1-2E have correlation indexes (R) of 0.85 and 0.72 however; calculated correlation index for samples M1-1E_e (0.02) and M1-2B_a (0.20) are considerably lower.

Table 3: Stable isotope composition range of values and variability for samples M1-1D_c, M1-1E_e, M1-2B_a, M1-2E. Sample M1-1G_b is shown in italics as this was a test sample.

Sample ID	**$\delta^{18}O$ range** (‰)	**$\delta^{18}O$ variation** (‰)	**$\delta^{13}C$ range** (‰)	**$\delta^{13}C$ variation** (‰)	**Sr/Ca range** (mmol/mol)	**Sr/Ca Variation** (mmol/mol)
M1-1D_c	-0.69 to -2.23	1.54	-3.51 to -5.96	2.45	9.30-9.66	0.36
M1-1E_e	-0.84 to -2.41	1.57	-3.37 to -5.47	2.10	9.07-9.62	0.55
M1-2B_a	-0.77 to -1.95	1.18	-3.23 to -5.28	2.05	9.30-9.70	0.40
M1-2E	-0.81 to -2.38	1.57	-3.17 to -5.21	2.04	9.24-9.67	0.43
M1-1G_b	*-1.41 to -2.25*	*0.84*	*-2.43 to -4.04*	*1.61*	*8.84-9.31*	*0.47*

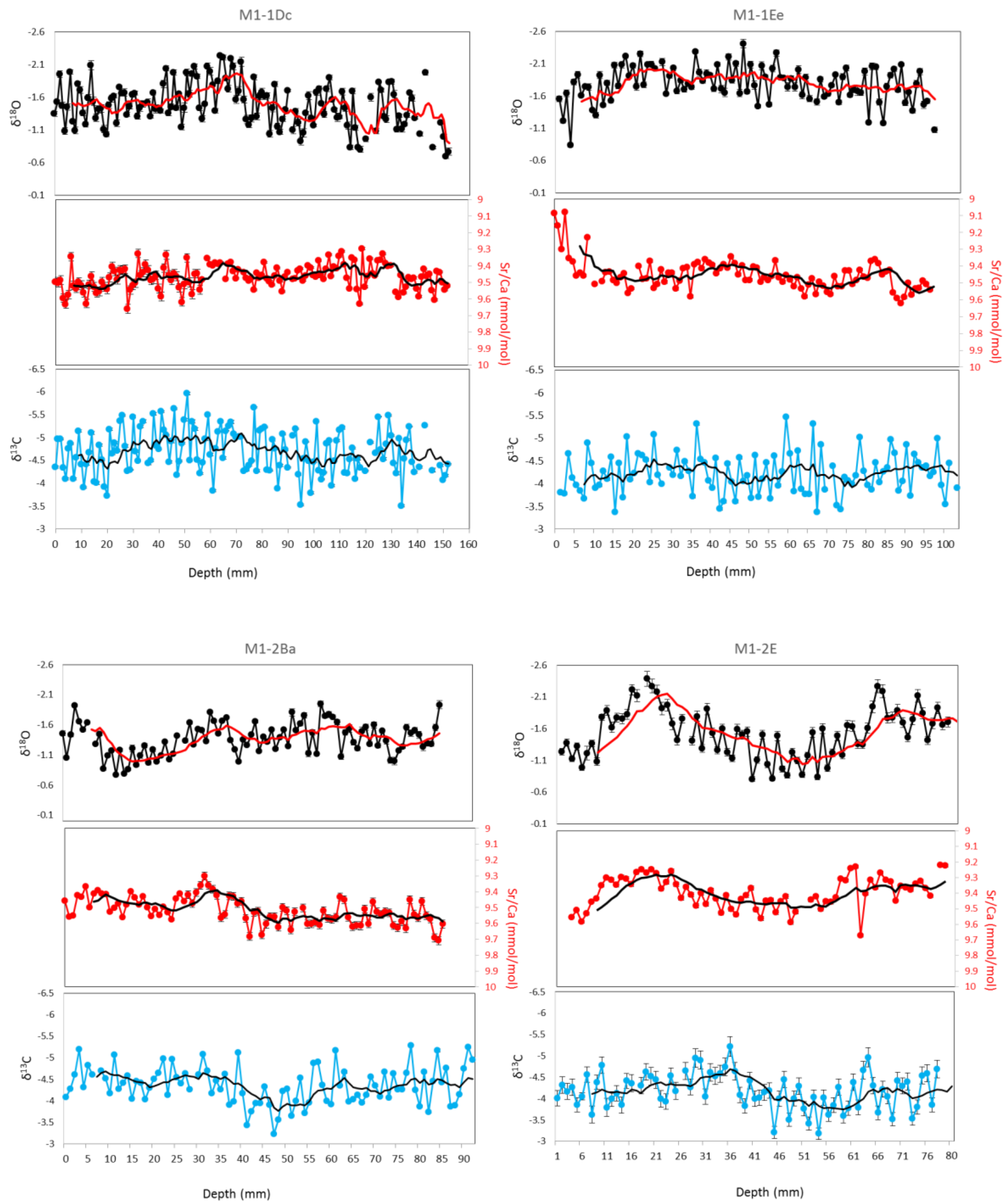

Figure 18: Geochemical $\delta^{18}O$, Sr/Ca and $\delta^{13}C$ records for samples M1-1D$_c$, M1-1E$_e$, M1-2B$_a$, M1-2E plotted with depth. Plots are ordered from older to youngest samples from left to right.

4. Discussion

4.1 Coral mineralogy composition

XRD analysis for the samples studied (M1-1D_c, M1-1E_e, M1-2B_a, and M1-2E) are similar and consistent to the spectral analysis done by Downs (2006) using a pure aragonite standard. The analysis indicates the samples studied are 100% aragonite in composition. The possibility of secondary aragonite was not tested in this study, however, secondary aragonite is expected to yield both high $\delta^{18}O$ and Sr/Ca (Sayani et al., 2011) and this was not the case for the latter. Additionally Greer and Swart (2006) already concluded the presence of secondary aragonite is negligible based on Fluorescence and SEM analyses done in coral samples from the same reef in Enriquillo Valley. The test sample (M1-1G_b) also shows 100% aragonitic composition suggesting this sample was not recrystallized but affected in other ways. The anomaly coloration may have been caused by sediments deposited in the interstices of the coral skeleton during storm events or simply by the stress the coral was subjected to.

4.2 Montastraea sp. Growth rates

The estimated average growth rates for each samples (M1-1D_c, M1-1E_e, M1-2B_a, and M1-2E), located at depths between 16.5-18.0 meters below the paleo sea level at 8.5kya, are much lower than values reported form modern corals of the species *Montastraea sp.* 6.5 mm/yr in Looe Key (Smith, 2006) and Bonaire 6.6-10.0mm/yr (Giry et al, 2011) at unknown depths. The possible difference in depth and zonation, which plays a major role in *Montastraea sp.* growth rates (Hubbard and Scaturo, 1985; Morelock et al., 2000; Hubbard et al., 2008), can account to differences in growth rate estimates between studies. At least, in this study, the effect of the depth component affecting the growth of these corals is present. It seems that at the base of the reef, growth rates were much faster and as the coral column grew up, its rates slowed. The average growth rate results obtained in this study are very similar and consistent with another study done in the same coral species (*Montastraea sp.*) of the same reef (Cañada Honda) at the same facies (M1) by Cuevas et al (2005). Cuevas et al (2005) reported average growth rates values of 2.6-3.2mm/yr while this project measured average growth rates of 2.07 ± 0.14 to 3.55 ± 0.37 mm/yr. They are also similar to a modern and fossil sample analyzed in Dry Tortugas by Smith (2006) (3.0 mm/yr) at approximately 13 m deep. The causes for these slow rates are not further explained. Sample M1-1G_b show the lowest average growth rate of the study (2.07mm/yr). Located just above sample M1-1G_b are the mud and rubble deposits named as the Mad Layer (Fig. 7). The low growth rates in the sample may be the result of massive inputs of sedimentation represented by the Mad Layer.

Another component affecting growth rates of these corals can be due the effects of high turbid waters as consequence of high sediment influx. At some point, light reaching the corals and the symbiotic photosynthetic organism *Zooxanthellae sp.* may be limited thus inhibiting photosynthesis and calcification rate respectively (Hubbard and Scaturo, 1985).

4.3 Sedimentation rate estimates

Sedimentation rates estimated from the eight sections (S1-S8) of sample M1-2B_a vary between average values of 2.06 ± 0.30mm/yr. The results in this study agree with sedimentation rates of 1.67 ± 0.05mm/yr estimated from *Montastraea sp.* corals in M2 done by Hubbard et al., (2004). To compare these sediment rates to modern sedimentation rates from other studies (Rogers, 1990), a conversion of these values to mg cm^{-2} d^{-1} can be done using equation 11, by making simple conversions and assuming all of the incoming sediments of Enriquillo are of carbonate provenance. Cuevas et al. (2005), estimated that non-carbonate material in the reef in Cañada Honda are very low (<10%), implying that the rest of it is of carbonate provenance from the surrounding mountain ranges, making this assumption not far from accurate. Converted values yield sedimentation rates of 1.53 ± 0.22 mg cm^{-2} d^{-1} which are higher than modern sedimentation rates estimated in reefs from Discovery Bay, Jamaica (0.5-1.1 mg cm^{-2} d^{-1}) and lower than modern sedimentation rates in Puerto Rico (2.5-2.6 mg cm^{-2} d^{-1}) by Rogers (1990).

Sediment rates are equal or almost equal to growth rates estimated in this study, suggesting that corals were keeping up with the upcoming sediment influx. These sedimentation events occur in episodes of 3-8 years consistent with ENSO/NAO. The consequent rainfall caused by this climate phenomena, could be responsible for the high sediment influx that led to developing the pancake morphology.

$$Sedimentation\ rate\ \left(\frac{mg}{cm^2 * d}\right) = Sedimentation\ rate\ \left(\frac{cm}{d}\right) * sediment\ density\ \left(\frac{mg}{cm^3}\right) \qquad (11)$$

4.4 Radiogenic dating and $\delta^{234}U$

U/Th dates obtained from the samples (M1-1D_c, M1-1E_e, M1-2B_a, M1-2E, M1-1A_b, M1-4A_e) show that these skeletons were precipitated early in the Holocene Epoch (8036 ± 26 to 8910 ± 28 yr B.P.). These dates are consistent to those reported by Hubbard et al. (2004) ranging from 8.400-8.900 yr B.P. (See appendix 11). As expected, pieces cut from the same colony have younger dates following the vertical growth of the columnar assemblage. Also, as expected, the ages of corals located at stratigraphic similar levels but different lateral positions have different ages and coral samples from M1-2 (southward from M1-1) are considerably older than M1-1. M1-4A_e was expected to be the youngest coral, due to its stratigraphic position (Fig. 17) but this was not the case. M1-4A_e is older than samples M1-1D_c and M1-1E_e but younger than M1-2B_a, M1-2E.

δ^{234}U values of the studied corals are lower than those expected from open seawater (Fig. 19). Similar δ^{234}U values were also obtained by Edwards (1988) in coral samples from Cañada Honda and other corals from the Enriquillo Valley. Edwards (1988) interpreted a trend in which values seems to be getting closer to seawater (saltier) composition as they become younger, similar to the samples in this study. The decrease in δ^{234}U from the samples in this study to the samples from Edwards (1988) may indicate events of freshwater influx which may be due to storm events as evident from the Mad Layer deposits.

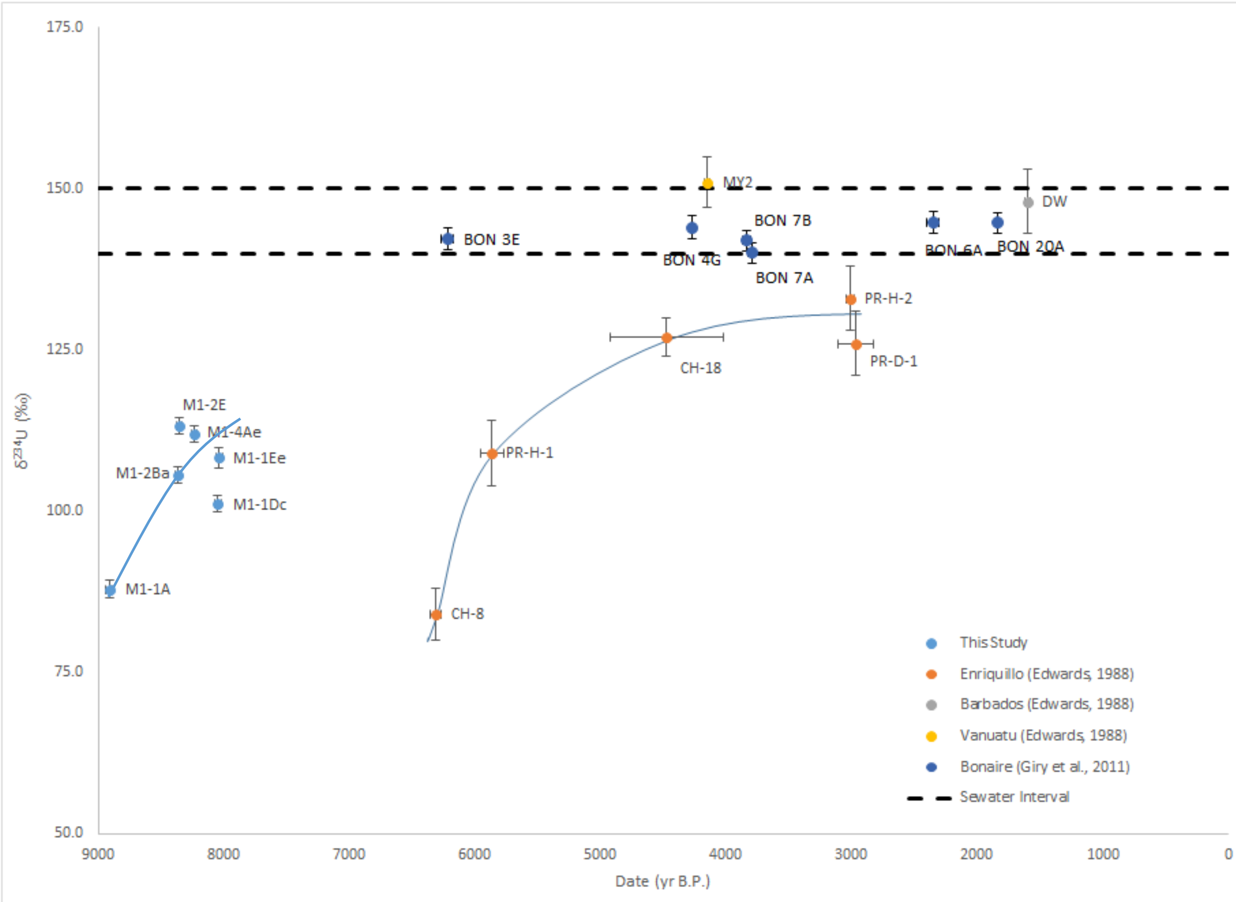

Figure 19: Plot of $\delta^{234}U$ concentration relative to time. The Enriquillo Valley fossil corals in this study (M1-1D$_c$, M1-1E$_e$, M1-2B$_a$, M1-2E, M1-1A$_b$, M1-4A$_e$) and a study from Edwards (1988) show lower $\delta^{234}U$ concentrations relative to open ocean corals from Bonaire (Giry et al.,2012). In both studies the $\delta^{234}U$ concentration in the corals follow a trend in which values seems to be getting closer to seawater composition as they become younger. In the studied samples the values show a similar trend but the data is more scattered. Range of seawater values (dashed lines) and trends (blue lines) are marked (Modified from Edwards, 1988).

4.5 Stable Isotopes

$\delta^{18}O$ and $\delta^{13}C$ values from *Monstrastraea sp.* obtained in this study are compared to values from modern marine corals (Tucker and Wright, 1990; Smith, 2006) and Enriquillo Valley fossil corals from other studies (Greer and Swart, 2006), (Fig. 20). $\delta^{18}O$ values obtained from the corals in this study (-0.69 to -2.41‰) are considerably heavier relative to values for modern corals ranging approximately from -3.0 to -6.0 (Tucker and Wright, 1990; Smith, 2006) and -1.94 to -4.94 from other studies in the Enriquillo Valley of (Greer and Swart, 2006). These results support the idea by Greer and Swart (2006) that the enrichment in $\delta^{18}O$ of the Enriquillo Holocene corals relative to modern values is probably due to the corals being exposed to a high salinity environment. However, samples from Greer and Swart (2006) were younger (5.3-7.2kya B.P) and at shallower depths (13.44 -15.57 feet below sea level). Then it is possible that samples in this study (8.0-8.9kya B.P) at depths of 31.5-33.0 feet below sea level, suffered from a more severe saline conditions. $\delta^{18}O$ and $\delta^{13}C$ patterns suggest interannual variability in a decadal and multi-decadal oscillations for samples under study in records of approximately 30-40 years. The magnitude of the variations obtained for $\delta^{18}O$ (1.18-1.57‰) are compared to other studies in Fig. 21. The values in this study are relatively lower compared to those obtained by Greer and Swart (2006) (1.51-3.00‰), Smith (2006) (~2.5‰) and Eemian sample from Winter et al. (2003). However, they are similar (~1.0-1.5‰) to fossil corals (2.9kya B.P.) studied by Felis et al. (2004) and modern corals from Cobb et al., (2013) and Winter et al., (2000). The opposite was expected, as it is known that the seasonality in the past was higher that the seasonality today (Winter et al., 2003; Giry et al., 2012).

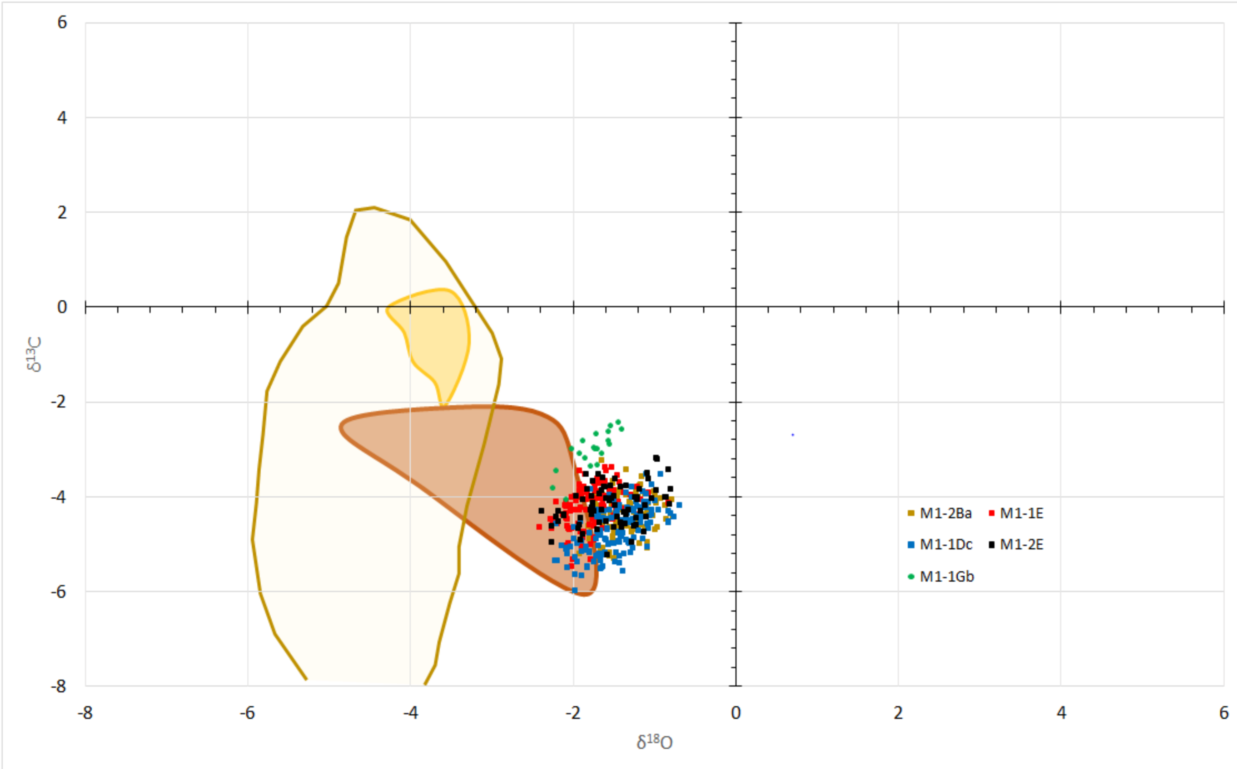

Figure 20: $\delta^{18}O$ vs. $\delta^{13}C$ values obtained for samples M1-1D$_c$, M1-1E$_e$, M1-2B$_a$, M1-2E, M1-1A$_b$ and sample M1-1G$_b$. Expected $\delta^{18}O$ vs. $\delta^{13}C$ values of modern marine corals are shown in beige (Tucker and Wright, 1990). Maximum and minimum $\delta^{18}O$ vs. $\delta^{13}C$ values from fossil corals in Dry Tortugas (4.2-5.1kya B.P.) (Smith, 2006) are shown in yellow and from Enriquillo Valley (5.3-7.2kya B.P.) (Greer, 2001; Greer and Swart, 2006) are plotted in brown.

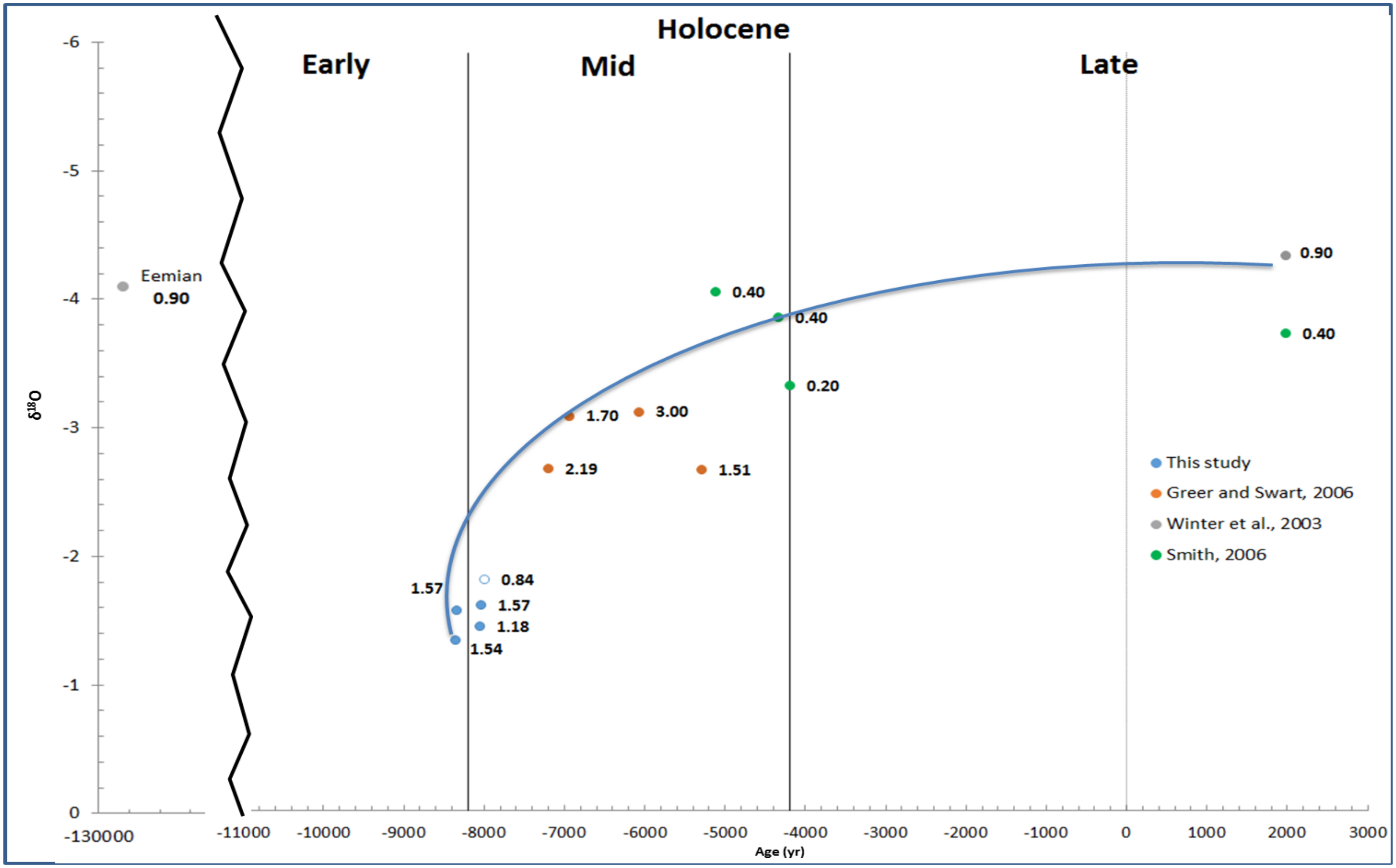

Figure 21: $\delta^{18}O$ vs. age in corals from this study and other studies in the Caribbean. Negative ages indicate age B.P.. $\delta^{18}O$ variations are given for each sample and sample M1-1G$_b$ is plotted as a hollowed icon because its age is extrapolated to have been precipitated 8000 yr B.P. Blue line represents a trend, interpreted to be the Holocene Sea Level Curve. Holocene sub-divisions were added as proposed by Walker et al. (2012).

4.6 Trace Elemental Concentrations

Analyzed Sr/Ca ratios in this study are compared to Caribbean *Diploria sp.* samples (6.2kya B.P. to modern) in Bonaire (Giry et al., 2012), *Monstrastraea sp.* samples (5.1kya B.P. to modern) in Dry Tortugas (Smith, 2006) and modern *Monstrastraea* sp. samples in Parguera, Puerto Rico (Winter et al., 2003) as seen in Fig. 22. It is understood that comparing geochemical data with corals from other genus is not optimal, however, Sr/Ca ratio records in the Caribbean on fossil corals that grew in waters that have close to similar SST (Giry et al., 2011) are very scarce. Mean Sr/Ca results in this study are relatively higher (9.40-9.50 mmol/mol) than modern samples (8.90-9.20 mmol/mol), mid Holocene samples (9.18-9.28 mmol/mol) and Eemian sample (9.35 mmol/mol) from the locations mentioned above. Although, secondary aragonite alteration causes high Sr/Ca ratios (Enmar et al., 2006; Hendy et al., 2007; Sayani et al., 2011), this is not a likely scenario for the studied corals (see section 4.1). It is possible that the high Sr/Ca ratio relative to modern corals have been produced by input of strontium from groundwater and/or high sediment influx. Discharge of sulfurous spring water associated with residual Pliocene volcanism towards the southern part of the lake (La Zurza, Borbollones and others) may have been a source of strontium (Mann and Lawrence, 1991; Buck et al, 2005). Other possibilities for higher Sr/Ca ratios are slower calcification rates estimated in these samples (Smith 2006, Inoue et al., 2007), sampling an off axis (non-corallite) section of the coral (Rosenthal and Linsley, 2006) or simple contamination during sample collection and/or processing.

Variations in Sr/Ca ratios range from 0.36 to 0.55 mmol/mol and are relatively higher than Bonaire Sr/Ca ratio variations (0.15-0.30 mmol/mol) in corals from the last 4.2kya B.P but close to mid Holocene corals from 6.2kya B.P., all reported by Giry et al. (2012). Sr/Ca variations in the studied corals are also higher than variations (0.19 mmol/mol) in modern samples from Parguera, but similar to Eemian corals (0.40 mmol/mol) of Mona Island, all reported by Winter et al. (2003). These result are consistent to seasonality variations since the Eemian (Winter et al.,2003; Felis et al., 2004).

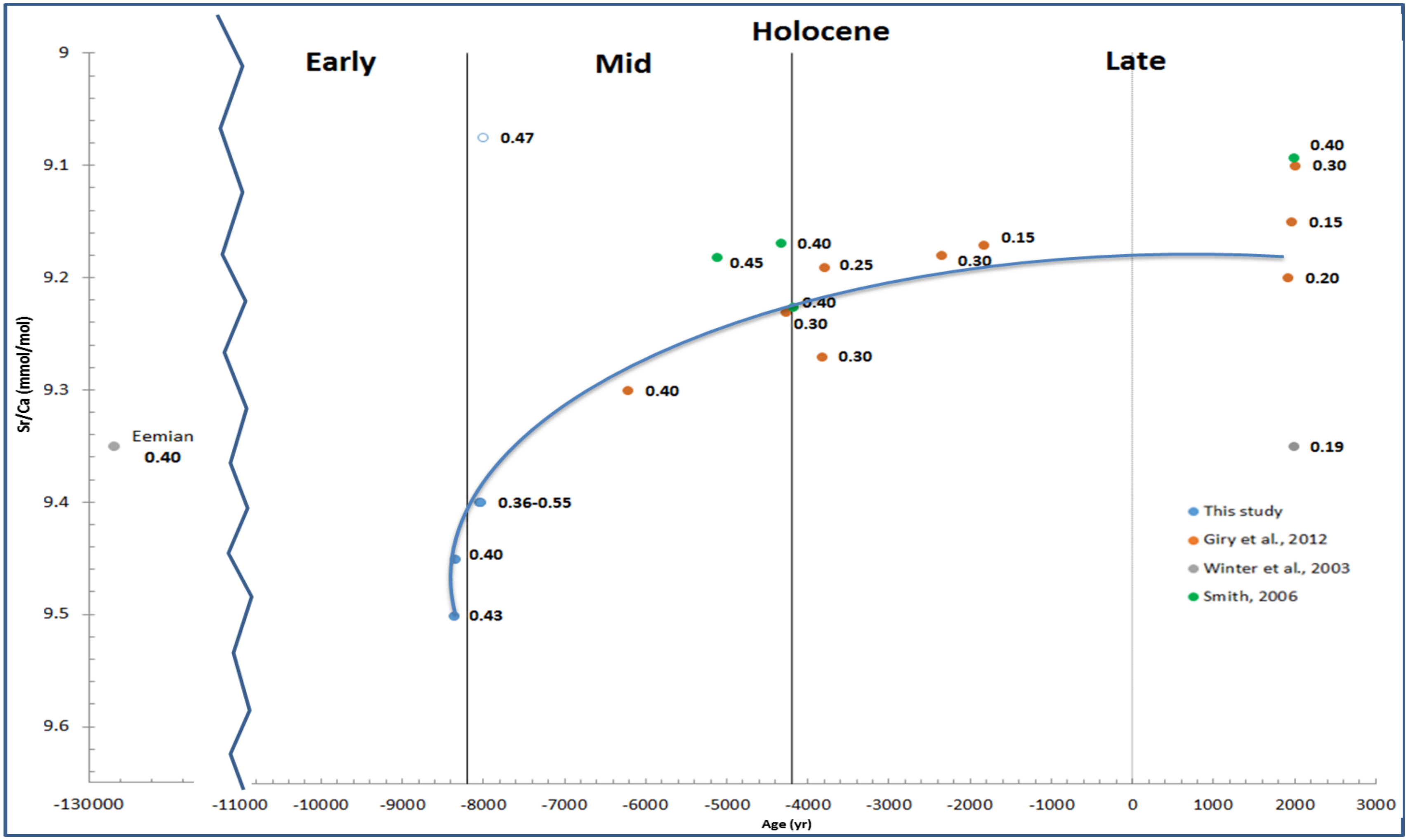

Figure 21: Sr/Ca vs. age in corals from this study and other studies in the Caribbean. Negative ages indicate age B.P.. $\delta^{18}O$ variations are given for each sample and sample M1-1G$_b$ is plotted as a hollowed icon because its age is extrapolated to have been precipitated 8000 yr B.P. Blue line represents a trend, interpreted to be the Holocene Sea Level Curve. Holocene sub-divisions were added as proposed by Walker et al. (2012).

4.7 SST from $\delta^{18}O$

SST-$\delta^{18}O$ derived temperatures calculated for studied samples using the equation derived by Leder et al., (1996) are plotted in (Fig. 23). These temperatures range from 8-15°C which can be considered too cold relative to scleractinean corals in the Caribbean where temperatures vary, in general, from 18-30°C (Felis and Pätzold, 2004). Modern *Monstrastraea sp.* SST-$\delta^{18}O$ derived temperature from Dry Tortugas (Smith, 2006) show temperatures that range from 22.9-30°C and from La Parguera, Puerto Rico (Winter et al., 2000; Winter et al., 2003) temperatures that range from 26-30°C. Fossil *Monstrastrea sp.* temperatures from Dry Tortugas indicate changes in temperatures from -1.9 to +1.5 at 5.1kya B.P. relative to modern samples in the same location. Accounting for these temperature changes, Dry Tortugas show SST no colder than 21°C. Temperatures obtained from coral samples in Enriquillo Valley produced by Greer and Swart (2006) is reported to be ~12.7°C. These values fall within the range obtained in this study and agree that this is inconsistent with temperature changes in the region (Greer and Swart, 2006). Winter et al (2003) sample from the last interglacial period showed temperatures from 22.5-32.0°C, which are temperatures warmer than the ones obtained, this also show increased seasonality relative to modern corals and samples in this study.

According to Leder et al (1996), a change in 1‰ of $\delta^{18}O$ represents a change in temperature of approximately 4°C. That means that variations of $\delta^{18}O$ in this study (-0.69 to -2.41‰) show temperature changes of roughly 7°C in an interval of 8.0-8.4kya. Such a drastic change in temperature has not been recorded during this period (Fensterer et al., 2013), not even during the major 8.2kya cooling event (2-3°C) (Thomas et al., 2007; Wiersma, 2008). This means, that salinity variations have a more prominent impact in $\delta^{18}O$ from these samples than temperature variation in the water (Greet and Swart, 2006). This also implies that salinities in Enriquillo Bay during this period were almost double the amount compared to modern seawater.

4.8 SST from Sr/Ca

With slightly higher Sr/Ca ratios in this study, it is expected that temperatures will be slightly colder (Rosenthal and Linsley, 2006). SST-Sr/Ca derived temperatures were calculated using Sr/Ca calibration equations 6-10 but only SST calculated from calibration equations 7 and 9 were plotted in (Fig. 23). It is understood that temperatures calculated from SST-Sr/Ca are highly dependent on the location (Saenger et al. 2008) and that a calibration from Enriquillo, where this corals formed, is required, however such place no longer exists. Because of this, possible analogues such as the Red Sea (Felis et al., 2004) that may have a similar environment to Enriquillo Bay and Bonaire (Giry et al., 2011) that shared similar SST are compared to other Sr/Ca in open marine waters (Fig. 24). Calculated SST using calibration produced by Swart et al. (2002), Flannery et al. (2013) and Smith (2006) from open marine waters yield colder and more variable temperatures (12-26°C respectively) than those from Giry et al. (2011) (20.0-26.0°C) and Felis et al. 2004 (20.3-27.6°C). Both Bonaire and Red Sea calibration show temperatures appropriate for coral skeletons (18-30°) (Felis and Pätzold, 2004). According to the variation in Sr/Ca, a change of approximately 6-7°C took place and such a change as not been recorded during this time period (8.0-8.4kya B.P.) (Fensterer et al., 2013). This big change could be due to influence of fresh water in this system which has already been stablished by $\delta^{234}U$ (see section 4.4). Decadal to multidecadal pulses of freshwater from storm precipitation (Greer and Swart, 2006) combined with spring water seepage into these waters (Buck et al., 2005), could be responsible for the high variability in Sr/Ca ratio and therefore wide range in temperature.

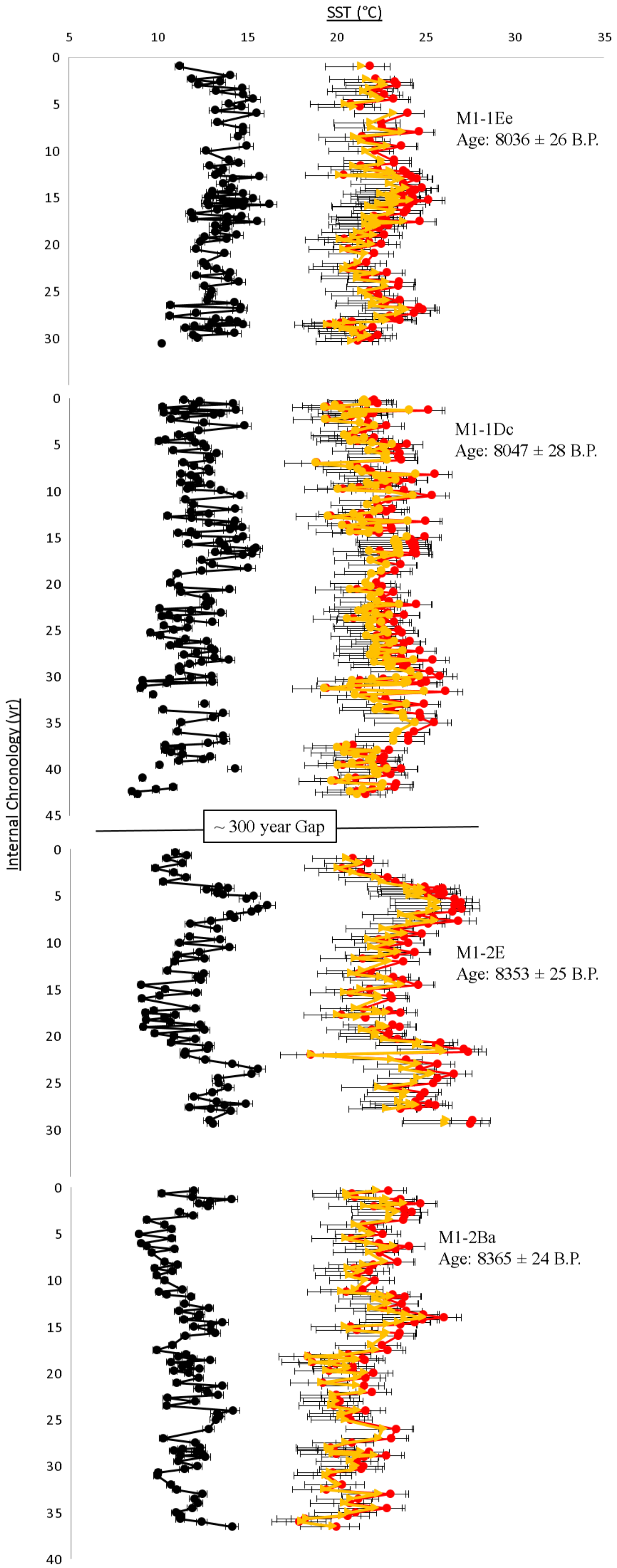

Figure 23: Stacked SST record estimated from $\delta^{18}O$ using Leder et al. (1996) and Sr/Ca using Giry et al. (2011) and Felis et al. (2004) respectively for samples M1-1D$_c$, M1-1E$_e$, M1-2B$_a$ and M1-2E with time. U/Th radiogenic dates are given for each sample. Refer to appendix 12-14 for individual plots.

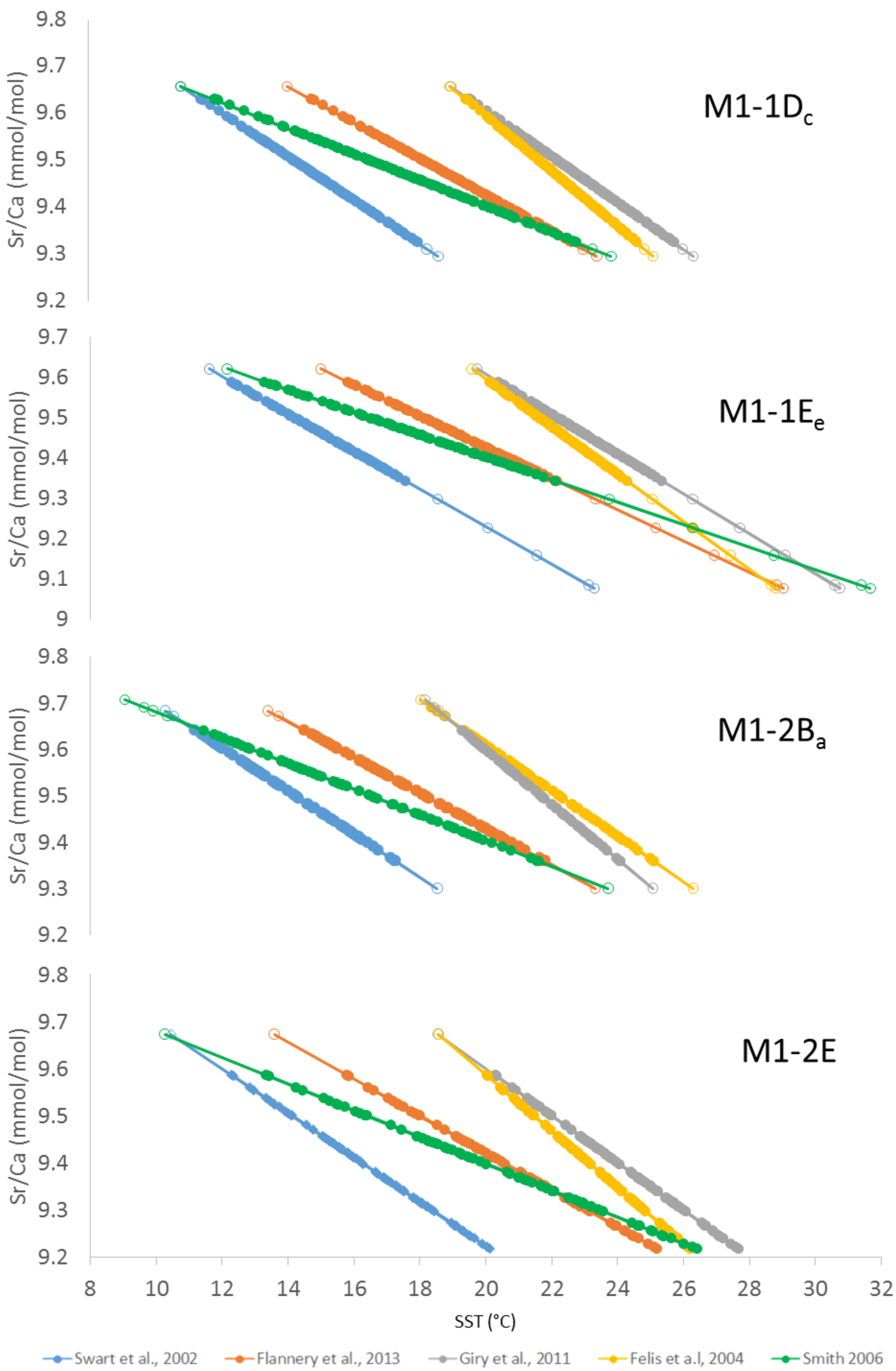

Figure 24: Sr/Ca ratios vs. SST calculated from calibration equations 6-10 in sample M1-2B$_a$ M1-1D$_c$, M1-1E$_e$, M1-2B$_a$ and M1-2E. This graphs shows maximum and minimum temperatures obtained from each curve. Hollowed circles have been identified as outlier values and not considered for interpretations.

4.9 SST correlation between different proxies ($\delta^{18}O$ and Sr/Ca)

Correlation indexes (R) between SST-derived from $\delta^{18}O$ and Sr/Ca for the samples under study vary between (0.02-0.85). The lowest values of 0.02 (M1-1E_e) and 0.20 (M1-2B_a) can be attributed to each variable reacting to a different parameter. A possibility is that specific events of salinity variations (Fig temp) might have drastically altered the chemistry of the $\delta^{18}O$ but not strongly affecting the chemistry of Sr/Ca (Greer and Swart, 2006). Higher correlations of 0.85 (M1-1D_c) and 0.72 (M1-2E) are higher than modern *Monstrastraea sp.* samples in Dry Tortugas (0.56-0.67) by Smith (2006). Smith (2006) attributed the correlation between the variables to a reaction of each to a different forcing other than temperature, which seems to be the case in this samples in this study. Still, it is considered that Sr/Ca is reacting to temperature, even though; variations are influenced by changes in the water chemistry from seawater.

5. Conclusion

The reef developed in Enriquillo Bay during the early to middle Holocene have unique qualities rarely seen in other reef ecosystems. Arid climate combined with high carbonate sediment influx, preserved the pristine composition of the coral skeleton and adapted their morphology for survivability. Corals in the Massive Zone 1 dated from 8.9-8.0 kya B.P. in this study consistent with radiocarbon dates obtained by Hubbard et al. (2004) in the same zone. From the four samples analyzed, two were dated near 8.3kya while the other two dated near 8.0kya which represents a 300yr gap. The samples under study integrity of the coral skeleton of the analyzed samples remains intact as 100% aragonite indicating that these samples suffered little or no alteration therefore discarding diagenesis as an influencing variable in the results obtained.

Calculated growth rates in this were lower compared to open marine settings corroborating Greer and Swart (2006) theory, that high sediment conditions were present at the times these corals were forming and that Cañada Honda fossil reef reflects severe stress conditions due to high sediment influx. Between the 300 year gap, there is a slight increase in growth rate that shows more suitable conditions for aragonite precipitation, possibly to warmer temperatures since the 8.2kya cooling event. The pancake morphology and higher sedimentation rates compared to open marine settings indicate severe stress conditions during reef development. The similarities between sedimentation rates and growth rates may indicate that corals were able to keep up with the sediment influx; however, the veracity of this hypothesis must be tested by calculating sedimentation rates in more than one sample.

Isotopic $\delta^{18}O$ enrichment and high variability of these values related to expected variations for this period, in this bay seems to respond to high salinity environments as pointed by Greer and Swart, (2006). The magnitude of $\delta^{18}O$ variations in this study shows similarities to variations of younger corals from the late Holocene and modern times. It is possible that salinity caused variations in $\delta^{18}O$ combined with temperature caused variations in $\delta^{18}O$, produced seasonalities that are not compatible with the variations expected to be produced by known seasonality records. The temperature variations of 5-7°C suggested by the isotopic data are most likely due to massive events of freshwater influx coming into the small lake from the prominent Sierra the Neiba and Sierra the Bahoruco. Uranium isotopes ($\delta^{234}U$) corroborates that these samples were subject to freshwater influx backed up by evidence of storm deposits such as the Mad Layer.

Measurements of Sr/Ca ratio are enriched relative to all fossil corals from the Eemian and mid-Holocene and also to modern samples. As SST and Sr/Ca ratios are inversely related (Swart et al., 2002), this implies that temperature values relative to the previously mentioned periods are colder, even colder than the sample from the Last Interglacial Period studied by Winter et al (2003). There are various possibilities to the Sr/Ca enrichment: 1) Corals grew in colder waters as expected from the early Holocene therefore incorporating more Sr into their skeleton; 2) Strontium rich sulfurous groundwater from springs associated with Pliocene volcanisms; 3) Slow growth rates due to limitations of photosynthesis and calcification of the coral skeleton; 4) Methodical errors such as sampling an off axis section of the coral and contamination during the sample processing could lead to higher Sr/Ca ratios.

Greer and Swart (2006) made a fair suggestion saying that SST calculations could be resolved using Sr/Ca ratios. However, it is clear that estimated absolute SSTs are not necessarily accurate. While $\delta^{18}O$ is primarily affected by changes in salinity rather than temperature, the temperature driven Sr/Ca shows to be strongly influenced by changes in the water chemistry caused by freshwater inflow. Another problem is that in order to obtain accurate temperatures, a calibration done with modern samples growing in the same environment is required, but since such place does not exist anymore, this is impossible to achieve. Consequently, the only way is to rely on analogue calibrations or calibrate using a coral sample from Barahona Bay southeast of Enriquillo. However trends in temperature variation are consistent with climate variations during the time period. Both proxies follow a trend similar to the Holocene sea level curve when compared from records obtained in other studies, suggesting that they responded to increased temperatures during this time period.

Both $\delta^{18}O$ values and Sr/Ca measurements variations in both suggest temperature variations of approximately 5-7°C. This variation is inconsistent with any record produced during this period (Greer and Swart, 2006), not even during the drastic 8.2kya cooling event (2-3°C) (Thomas et al., 2007; Wiersma, 2008). Yet, these variations are not necessarily unexpected since surface waters combined with ground waters stored in the massive mountain chains surrounding the relative small lake will account for such drastic temperature records. The anomalous variations show the sensitivity to other variables (salinity and freshwater inflow), yet, low correlation index (R) in some samples show that $\delta^{18}O$ values and Sr/Ca are reacting to different mechanisms in some cases. This study was unable to address any cyclicity patterns and a more continuous and longer record of $\delta^{18}O$ values and Sr/Ca is necessary.

References

Alexander, M.A., Bladé, I., Newman, M., Lanzante, J.R., Lau, N.C., Scott, J.D., 2002, The atmospheric bridge: The influence of ENSO teleconnections on air-sea interaction over the global oceans, Journal of Climate, 15, 2205-2231.

Beck, J.W., Edwards, L.R., Ito, E., Taylor, F.W., Recy, J., Rougerie, F., Joannot, P., Henin, C., 1992, Sea-surface temperature from coral skeletal stronrium/calcium rations, Science, 257, 644-647.

Beck, J.W., Récy, J., Taylor, F., Edwards, L.R., Cabioch, G., 1997, Abrupt changes in early Holocene tropical sea surface temperature derived from coral records, Nature, 385, 705-705.

Birgmark, D., 2014, El Niño-Southern Oscillation and North Atlantic Oscillation induced sea surface temperature variability in the Caribbean Sea [M.S. thesis]: University of Gothenburg, 27 p.

Brachert, T. C., M. Reuter, K. F. Kroeger, and J. M. Lough, 2006, Coral growth bands: A new and easy to use paleothermometer in paleoenvironment analysis and paleoceanography (late Miocene, Greece), Paleoceanography, 21, PA4217, doi:10.1029/2006PA001288.

Buck, D.G., Brenner, M., Hodell, D.A., Curtis, J.H., Martin, J.B., Pagani, M., 2005, Physical and chemical properties of hypersaline Lago Enriquillo, Dominican Republic, Verh, Internat, Verein, Limnol., 29, 7p.

Charlery, J., Nurse, L., Whitehall, K., 2006, Exploring the relationship between the North Atlantic Oscillation and rainfall patterns in Barbados, Int. J. Climatol., 26, 819-827, doi: 10.1002/joc.1334.

Cheng, H., Edwards, R.L., Shen, C.C., Polyak, V.J., Asmerom, Y., Woodhead, J., Hellstrom, J., Wang, Y., Kong, X., Spötl, C., Wang., X., Alexander, E.C., 2013, Improvements in ^{230}Th dating, ^{230Th} and ^{234}U half-life values, and U-Th isotopic measurements by a multi-collector inductively coupled plasma mass spectrometry, Earth and Planetary Science Letters, 371-372, 82-91.

Chend, H., Fleitmann, D., Edwards, R.L., Wang, X., Cruz, F.W., Auler, A.S., Mangini, A., Wang, Y., Kong, X., Burns, S.J., Matter, A., 2009, Timing and structure of the 8.2kyr B.P. event inferred from δ^{18}O records of stalagmites from China, Oman and Brazil.

Chollett, I., Müller-Karger, F.E., Heron, S.F., Skirving, W., Mumby, P.J., 2012, Seasonal and spatial heterogeneity of recent seas surface temperature trends in the Caribbean Sea and southeast Gulf of Mexico, Marine Pollution Bulletin, 64, 956-965.

Cobb, K.M., Charles, C.D., Cheng, H., Kastner, M., Edwards, R.L., 2003, U/Th-dating living and young fossil corals form the central tropical Pacific, Earth and Planetary Science Letters, 210, 91-103.

Cobb, K.M., Westphal, N., Sayani, H.R., Watson, J.T., Di Lorenzo, E., Cheng, H., Edwards R.L., Charles, C.D., 2013, Highly variable El Niño-Southern Oscillation throughout the Holocene, Science, 339, 67-70, doi: 10.1126/science.1228246.

Cooke, W., 1989, Geography in: Vaughan, T.W., Cooke, W., Condit, D.D., Ross, C.P., Woodring, W.P., Calkins, F.C., A Geological Reconnaissance of the Dominican Republic, Unites States Geological Survey, Memoirs Vol. 1, p. 26-48.

Cuevas, D., Sherman, C.E., Ramirez, W., Díaz, V., Hubbard, D.K., 2005, Development of Mid-Holocene Cañada Honda fossil reef, Dominican Republic: Preliminary results and implications to modern trends of reef degradation in high sedimentation environments, 17th Caribbean Geological Conference in San Juan, Puerto Rico, 27-36.

Dince, K., 2009, Climate variability and climate change: what is the difference?, Michigan Sea Grant, http://www.miseagrant.umich.edu/downloads/climate/11-703-Climate-Variability-and-Climate-Change.pdf (Accessed December, 2014).

Dokken, Q.R., MacDonald, I.R., Tunnel Jr., J.W., Wade, T., Withers, K., Dilworth, S.J., Bates, T.W., Beaver, C.R., and Rigaud, C.M., 2003, Long-term monitoring at the East and West Flower Garden Banks National Marine Sanctuary, 1998-2001 U.S. Department of the Interior, Minerals Management Service, Gulf of Mexico OCS Region.

Donders, T.H., 2005, Reconstruction of El Niño-Southern Oscillation variability during the Holocene [Ph.D. thesis]: Utrecht University, 176p.

Downs, R.T., 2006, The RRUFF Project: an integrated study of the chemistry, crystallography, Raman and infrared spectroscopy of minerals. Program and Abstracts of the 19th General Meeting of the International Mineralogical Association in Kobe, Japan, O03-13.

Edwards, R.L., 1988, High precision Thorium-230 ages of corals and the timing of sea level fluctuations in the late quaternary, [Ph.D. thesis]: California Institute of Technology, 352p.

Edwards, R.L., Chen, J.H., Wasserburg, G.J., 1985, Precise measurements of $^{234}U/^{238}U$ in Pacific and Atlantic profiles, Geol. Soc. Am., Abst. Prog. 17, 572.

Edwards, R.L., Chen, J.H., Wasserburg, G.J., 1987, ^{238}U-^{234}U-^{230}Th-^{232}Th systematics and the precise measurement of time over the past 500,000 years, Earth and Planetary Science Letters, 81, 175-192.

Enmar R., Stein, M., Bar-Matthews, M., Sass, E., Katz, A., Lazar, B., 2000, Diagenesis in live corals from the Gulf of Aqaba: I. The effect on paleo-oceanography tracers, Geochim. Cosmochim. Acta, 64, 3123–3132.

Escuder Viruete, J., Hernaís Huerta, P.P., Draper, G., Gutiérrez, G., Lewis, J.F., Pérez-Estaún, A., 2002, The metamorphism and structure of the Maimón Formation and Duarte and Rio Verde

Complexes, Dominican Central Cordillera: implications for the structure and evolution of the primitive Caribbean Island Arc, Acta Geologica Hispanica, 37, No. 2-3, p. 123-162.

Faure, G., 1998, Principles and Applications of Geochemistry, 2nd ed., Prentice Hall, New Jersey.

Felis, T. and Pätzold, J., 2004, Climate Reconstruction from annually banded corals, Global Environmental Change in the Ocean and on Land, Eds. M. Shiyomi et al., 205-227.

Felis, T., Lohmann, G., Kuhnert, H., Lorenz, S.J., Scholz, D., Pätzold, J., Al-Rousan S.A., Al-Moghharabi, S.M., 2004, Incresed seasonality in Middle East temperatures during the last interglacial period, Nature, 429, 164-168.

Flannery, J.A., Poore, R.Z., 2013, Sr/Ca proxy sea-surface temperature reconstructions from modern and Holocene *Montastraea faveolata* specimens from the Dry Tortugas National Parl, Florida, U.S.A., Journal of coastal Research, 63, 20-31.

Fensterer, C., Scholz, D., Hoffman, D.L., Spötl, C., Schröder-Ritzrau, A., Horn, C., Pajón, J.M., Mangini, A., Millenial-scale climate variability during the last 12.5 ka recorded in a Caribbean speleothem, Earth and Planetary Science Letters, 361, 143-151.

[a]Giannini A., Cane, M.A., Kushnir, Y., 2001, Interdecadal changes in the ENSO teleconnection to the Caribbean region and the North Atlantic Oscillation, Journal of Climate, 14, 2867-2879.

[b]Giannini, A., Kushnir, Y., Cane, M.A., 2001, Seasonality in the impact of ENSO and the North Atlantic High on Caribbean rainfall, Phys. Chem. Earth (B), 26, No. 2, 143-147.

Gischler, E. and Oschmann, W., 2005, Historical climate variation in Belize (Central America) as recorded in scleractinian coral skeletons, Palaios, 20, No. 2, 159-174.

Giry, C., Felis, T., Kölling, M., Scholz, D., Wei, W., Lohmann, G., Scheffers, S., 2012, Mid- to late Holocene changes in tropical Atlantic temperature seasonality and interannual to muldidecadal variability documented in southern Caribbean corals, Earth and Planetary Science Letters, 331-332, 187-200.

Gonzalez J. and Leon, Y., 2013, Proyecto Lagos de la Española: http://hispaniola-lakes.ccny.cuny.edu/inicio/?lang=1

Greer, L. and Swart, P.K., 2006, Decadal cyclicity of regional mid-Holocene precipitation: Evidence from Dominican coral proxies, Paleoceanography., 21, PA2020, doi:10.1029/2005PA001166.

Grottoli, A.G, 2001, Climate: Past Climate from Corals, in: Encyclopedia of Ocean Sciences [eds. Steele, J., Thorpe, S., Turekian, K.], Academic Press, London p. 2098-2107.

Hagelaars, J., 2013, the two epochs of Marcott, My view on climate change, https://ourchangingclimate.wordpress.com/2013/03/19/the-two-epochs-of-marcott/

(Accessed January, 2015).

Haigh, J., 2011, Solar influences on climate, Grantham Institute for Climate Change, Biefing paper No. 5, 20 p.

Hendy, E.J., Gagan, M.K., Lough, J.M., McCulloch, M., deMenocal, P.D., 2007, Impact of skeletal dissolution and secondary aragonite on trace element and isotopic climate proxies in *Porites* corals, Paleoceanography, 22, PA4101, doi:10.1029/2007PA001462

Hubbard, D.K., 1997, Dynamic processes of coral-reef development, in; Birkeland, C. (ed.), Life and death of coral reefs, Chapman and Hall Publishers, Ed. 1, 43-67.

Hubbard, D.K. and Scaturo, D., 1985, Growth rates of seven species of Scleractinean corals from Cane Bay and Salt River, St. Croix, USVI, Bulletin of Marine Science, 36, No. 2, 325-338.

Hubbard, D.K., Ramirez, W., Cuevas, D., 2004, A preliminary model of Holocene coral-reef development in the Enriquillo Valley, SW Dominican Republic. Abstract. GSA Abstracts with Programs, 36, No. 5, 291 p.

Hubbard, D.K., Ramirez, W., Cuevas D., Erickson, T., Estep, A., 2008, Holocene reef accretion along the north side of Bahia Enriquillo (western Dominican Republic): unique insights into patterns of reef development in response to sea-level rise, Proceedings of the 11th International Coral Reef Symposium, Ft. Lauderdale, Florida, 43-47.

Hughes, T.P., 1994, Catastrophes, phase shifts, and large-scale degradation of a Caribbean coral reef. Science, 265, 1547-1551, doi:10.1126/science.265.5178.1547.

Indermühle, A., Stocker, T.F., Joos, F., Fischer, H., Smith, H.J., Wahlen, M., Deck, B., Mastroianni, D., Tschumi, J., Blunier, T., Meyer, R., Stauffer, B., Holocene carbon-cycle dynamics based on CO_2 trapped in ice at Taylor Dome, Antartica, 1999, Nature, 398, 121-126.

Inoue, M., Suzuki, A., Nohara, M., Hibino, K., Kawahata, H., 2007, Empirical assessment of coral Sr/Ca and Mg/Ca ratios as climate proxies using colonies grown at different temperatures, Geophysical Research Letters, 34, L12611, 4 p, doi:10.1029/2007GL029628.

Jaffey, A.H., Flynn, K.F., Glendenin, L.E., Bentley, W.C., Essling, A.M., 1971, Precision measurement of half-lives and specific activities of ^{235}U and ^{238}U. Phys. Rev. C4, 1889–1906.

Klotzbach, P.J., 2011, The influence of El Niño-Southern Oscillation and the Atlantic Multidecadal Oscillation on Caribbean tropical cyclone activity, Journal of Climate, 24, 721-731, doi:10.1175/2010JCLI3705.1.

Kobashi, T., Severinghaus, J.P., Brook, E.J., Barnola, J.M., Grachev, A.M., 2007, Precise timing and characterization of abrupt climate change 8200 years ago from air trapped in polar ice, Quaternary Science Reviews, 26, 1212-1222.

Lachniet, M.S., 2004. A 1500-year El Niño/Southern Oscillation and rainfall history for the Isthmus of

Panama from speleothem calcite. J. Geophys. Res. 109, 1–8.

Leder., J.J., Swart, P.K., Szmant, A., Dodge, R.E., 1996, The origin of variations in the isotopic record of Scleractinian corals; I Oxygen, Geochim. Cosmochim. Acta, 60, 2857-2870.

Luan, Y., Braconnot, P., Yu, Y., Zheng, W., Marti, O., 2012, Early and mid-Holocene climate in the tropical Pacific: seasonal cycle and interannual variability induced by insolation changes, Clim. Past, 8, 1093-1108.

Mann, P., Taylor F.W., Burke, B., Kulstad, R., 1984, Subaerially exposed Holocene coral reef, Enqiruillo Valley, Dominican Republic: Geological Society of America Bulletin, 95, 1084-1092.

Mann, P., Lawrence, S., 1991, Petroleum potential of Southern Hispaniola: Journal of Petroleum Geology, 14, No. 3, 291-308.

Mann, P., Taylor, F.W., Edwards, R.L., Ku, T., 1995, actively evolving microplate formation by oblique collision and sideways motion along strike-slip faults: An example from the northeastern Caribbean plate margin, Tectonophysics, 246, 1-69.

Mann, P., 1999, Caribbean sedimentary basins: Classification and tectonic setting from Jurassic to present: Sedimentary Basins of the World, 4, 3-90.

Mann, P., McLaughlin P., Van Den Bold, W., Lawrence, S., Lamar M., 1999, Tectonic and Eustatic Controls on Neogene Evaporitic and Siliciclastic Deposition in the Enriquillo Basin, Dominican Republic: Sedimentary Basins of the World, 4, 3287-342.

Mann, P., Hernaiz, P., Ramirez, W., 2008, Stratigraphy, tectonics and subsurface petroleum geology of Ocoa, Azua, and Enriquillo basins, Dominican Republic: 18th Caribbean Geological Conference, 127p.

McLaughlin P. and Van Den Bold, W., 1991, Geology of the Azua and Enriquillo basins, Dominican Republic; 1, Neogene litofacies, biostratigraphy, biofacies, and paleogeography: Geological Society of America Special Paper 262, 337-366.

Marcott, S.A., Shakun, J.D., Clark, P.U., Mix, A.C., 2013, A reconstruction of regional and global temperature for the past 11,300 years, Science, 339, 1198-1201.

Marshall, J.F., and McCulloch, M.T., 2002, An assessment of the Sr/Ca ratio in shallow water hermatypic corals as a proxy for sea surface temperature, Geochimica et Cosmochimica Acta, 66, No. 18, 3263-3280.

Mayewski, P.A., Rohling, E.E., Stager J.C., Karlé, W., Maasch, K.A., Meeker L.D., Meyerson, E.A., Gasse, F., van Kreveld, S., Holmgren, K., Lee-Thorp, J., Rosqvist, G., Rack, F., Staubwasser, M., Schneider R.R., Steig, E.J., 2004, Holocene climate variability, Quaternary Research, 62, 243-255.

Mey, J., Fairbanks, R., Mortlock, R., Bradtmiller, L., 2005, Uranium series diagenesis in corals exposed to freshwater; toward better prospecting for closed system samples for high accuracy dating. American Geophysical Union abstact #PP21C-1572.

Morelock, J., J. Capella, J. R. Garcia, and M. Barreto. 2000. Puerto Rico - Seas at the Millennium. Seas at the Millennium. Ed. C. R. C. Sheppard. London, England: Oxford Press.

Morril, C., Anderson, D.M., Bauer, B.A., Gille, E.P., Gross, W.S., Hartman, M., Shah, A., 2013, Proxy benchmarks for intercomparison of 8.2ka simulations, Clim. Past, 9, p. 423-432.

Nurhati, I.S., Cobb, K.M., Charles, C.D., Dunbar, R.B., 2009, Late 20th century warming and freshening in the central tropical Pacific, Geophys. Res. Lett., 36, L21606, doi:10.1029/2009GL040270.

Pandolfi, J.M., 2002, Coral community dynamics at multiple scales, Coral Reefs, 21, 13-23, doi;10.1007/s00338-001-0204-7.

Pierce, S., 2014, Dominican Republic seeks domestic gas resource, Oil & Gas Journal, http://www.ogj.com/articles/print/volume112/issue4/explorationdevelopment/dominicanrepublicseeksdomesticgasresource.html (Accessed November, 2014)

Riebeek, H., 2005, Paleoclimatology: introduction, NASA earth observatory, https://moodle.up.pt/pluginfile.php/18193/mod_resource/content/1/paleoclimatologia.pdf (Accessed December, 2014).

Robinson, L.F., Belshaw, N.S., Henderson, G.M., 2004, U and Th concentrations in isotope ratios in modern carbonates and waters from the Bahamas, Geochimica et cosmochimica Acta, 68, No. 8, 1777-1789.

Rodbell, D.T., Seltzer, G.O., Anderson, D.E., Abbott, M.B., Enfield, D.B., and Newman, J.H., 1999, A 15,000 year record of El Niño-driven alluviation in southwestern Ecuador: Science, 283, 516-520.

Rogers, C.S., 1990, Response of coral reefs and reef organisms to sedimentation, Mar. Ecol. Prog. Ser., 62, 185-202.

Rohling, E.J., Pälike, H., 2005. Centennial-scale climate cooling with a sudden cold event around 8,200 years ago. Nature, 434, 975–979.

Rosenthal, Y. and Linsley, B., 2006, Mg/Ca and Sr/Ca Paleothermometry from calcareous marine fossils, Encyclopedia of Quaternary Sciences, Elsevier Ltd, 20 p.

Ruddiman, W.F., Kutzbach, J.E., Vavrus, S.J., 2011, Can natural or anthropogenic CO2 and CH4 increases be falsified?, The Holocene, 21, 865–879.

Saenger, C., Cohen, A.L., Oppo D.W., Hubbard, D, 2008, Interpreting sea surface temperature from strontium/calcium ratios in *Monstrastraea* corals: Link with growth rate and implications for proxy reconstructions, Paleoceanography., 23, PA3102, doi:10.1029/2007PA001572

Sallun, A.E.M., Sallun Filho, W., Suguio, K., Babinsky, M., Gioia, S.M.C.L., Harlow, B., Duleba, W., De Oliveira, P.E., Garcia, M.J., Weber, C.Z., Christofoletti, S.R., Santos, C. da S., de Medeiros, V.B., Silva, J.B., Santiago-Hussein, M.C., Fernandes, R.S., 2012, Geochemical evidence of the 8.2 ka event and other Holocene environmental changes recorded in paleolagoon sediments, southeastern Brazil, Quaternary Research, 77, p. 31-43.

Sayani, H.R., Cobb, K.M., Cohen, A.L., Crawford, E.W., Nurhati, I.S., Dunbar, D.B., Rose, K.A., Zaunbrecher, L.K., 2011, Effect of diagenesis on paleoclimate reconstructions from modern and young fossil corals, Geochimica et Cosmochimica Acta, 75, 6361-6373.

Schrag, D.P., 1999, Rapid analysis of high-precision Sr/Ca ratios in corals and the other marine carbonates. Palaeoceanography, 14, 97-102.

Smith, J.M., 2006, Geochemical signatures in the coral Mantastraea: Modern and mid-Holocene perspectives [Ph.D. thesis]: University of South Florida, 125 p.

Swart, P.K. and Grottoli, A., 2003, Proxy indicators of climate in coral skeletons: a perspective, Coral Reefs, 22, 313-315.

Swart, P.K., Elderfield, H., Greaves, M.J., 2002, A high-resolution calibration of Sr/Ca thermometry using the Caribbean coral *Mantastraea annularis*, Geochem. Geophys. Geosyst., 3, 11, 8402.

Tans, P., and Keeling, R., Trends in atmospheric carbon dioxide, Earth System Research Laborarory: Global Monitoring Division, http://www.esrl.noaa.gov/gmd/ccgg/trends/ (Accessed March, 2015).

Taylor, F.W., Mann, P., Valastro, S., Burke, K., 1985, Stratigraphy and radiocarbon chronology of a subaerially exposed Holocene coral reef, Dominican Republic, The Journal of Geology, 93, No. 3, 311-332.

Thomas, E.R., Wolff, E.W., Mulvaney, R., Steffensen, J.P., Johnsen J., Arrowsmith, C., White, J.W.C., Vaughn, B., Popp, T., 2007, The 8.2ka event from Greenland ice cores, Quaternary Science Reviews, 26, 70-81.

Tucker, M.E. and Wright, V.P., 1990, Carbonate Sedimentology, Blackwell Scientific, Oxford, 482p

Walker, M, Johnsen, S, Rasmussen, S.O, *et al.* 2009. Formal definition and dating of the GSSP (Global Stratotype Section and Point) for the base of the Holocene using the Greenland NGRIP ice core, and selected auxiliary records. Journal of Quaternary Science 24: 3–17.

Walker, M.J.C., Berkelhammer, M., Björck, Cwynar, L.C., Fisher, D.A., Long, A.J., Lowe, J.J., Newnham, R.M., Rasmusen, S.O., Weiss, H., 2012, Formal subdivision of the Holocene Series/Epoch; a Discussion Paper by a Working Group of INTIMATE (Integration of ice-core, marine and terrestrial records) and the Subcommission on Quaternary Stratigraphy (International Commission on Stratigraphy), Journal of Quaternary Science, 27 (7), 649-659, doi: 10.1002/jqs.2565.

Wanner, H., Beer, J., Bütikofer, J., Crowley, T.J., Flückiger, J., Cubasch, U., Goosse, H., Grosjea, M., Joos, F., Küttel, M., Kaplan, J.O., Müller, S.A., Prentice, I.C., Solomina, O., Stocker, T.F., Tarasov, P., Wagner, M., Widmann, M., 2008, Mid- to Late Holocene climate change; an overview, Quaternary Science Reviews, 27, 1791-1828.

Wiersma, A.P., 2008, Character and causes of the 8.2ka climate event – Comparing coupled climate model results and palaeoclimate reconstructions, [Ph.D. thesis], Vrije Universiteit Amsterdam.

Winter, A., Ishioroshi, H., Watanabe, T., Oba, T., Christy, J., 2000, Caribbean sea surface temperatures: two-to-thee degrees cooler than present during the Little Ice Age, Geophysical Research Letters, 27, No. 20, 3365-3368.

Winter, A., Paul, A., Nyberg, J., Oba, T., Lundberg, J., Schrag, D., Taggart, B., 2003, Orbital control of low-latitude seasonality during the Eemian, Geophysical Research Letters, 30, No. 4, 1163, doi:10.1029/2002GL016275, 2003

Winter, A., Vieten, R., Miller, T., Mangini, A., Scholz, D., 2013, 8.2ky event associated with high precipitation in the eastern Caribbean, American Geophysical Union, Fall Meeting 2013, abstract #PP31B-1870.

Appendix

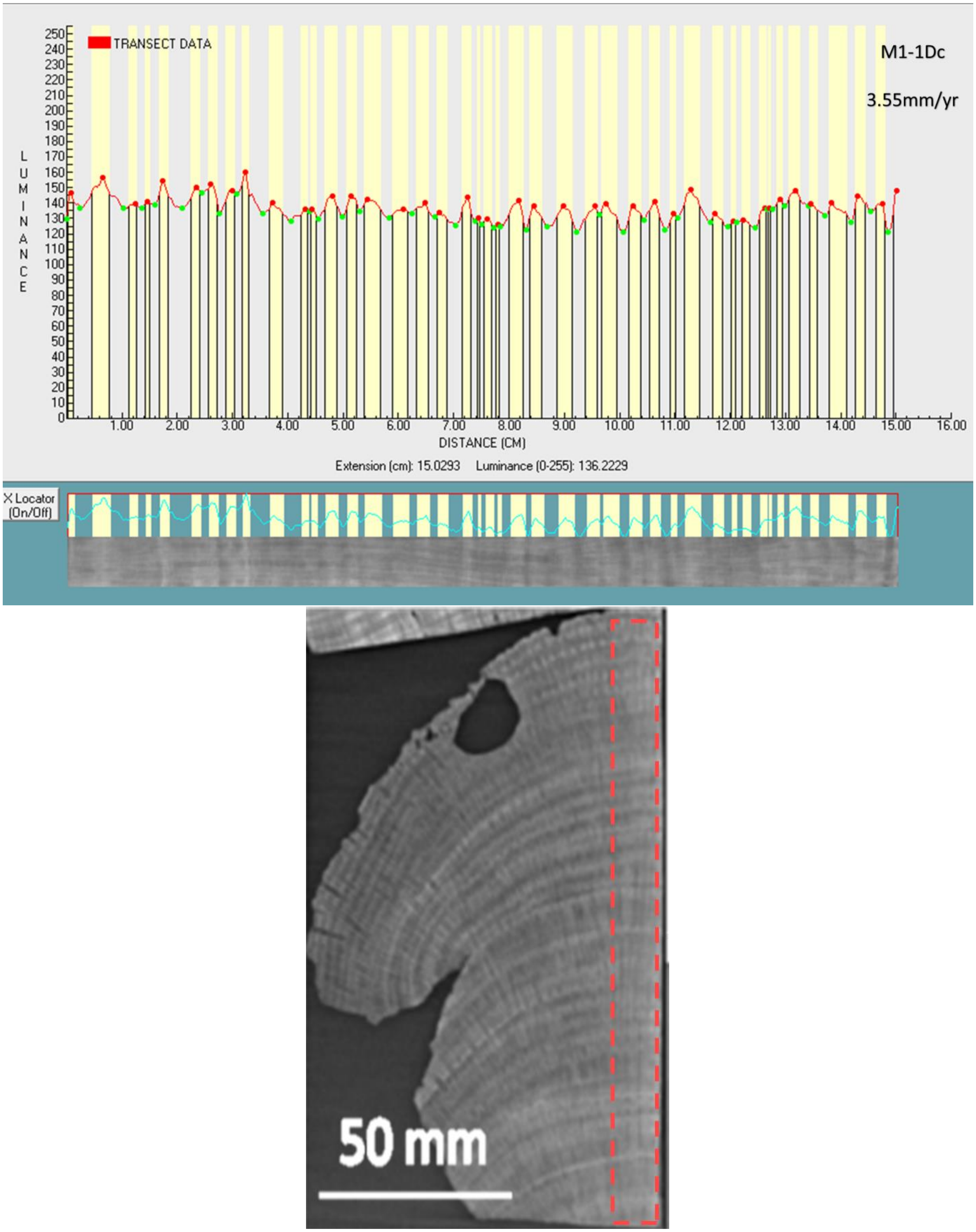

Appendix 1: Drawn transect and densitometry analysis of sample M1-1D$_c$.

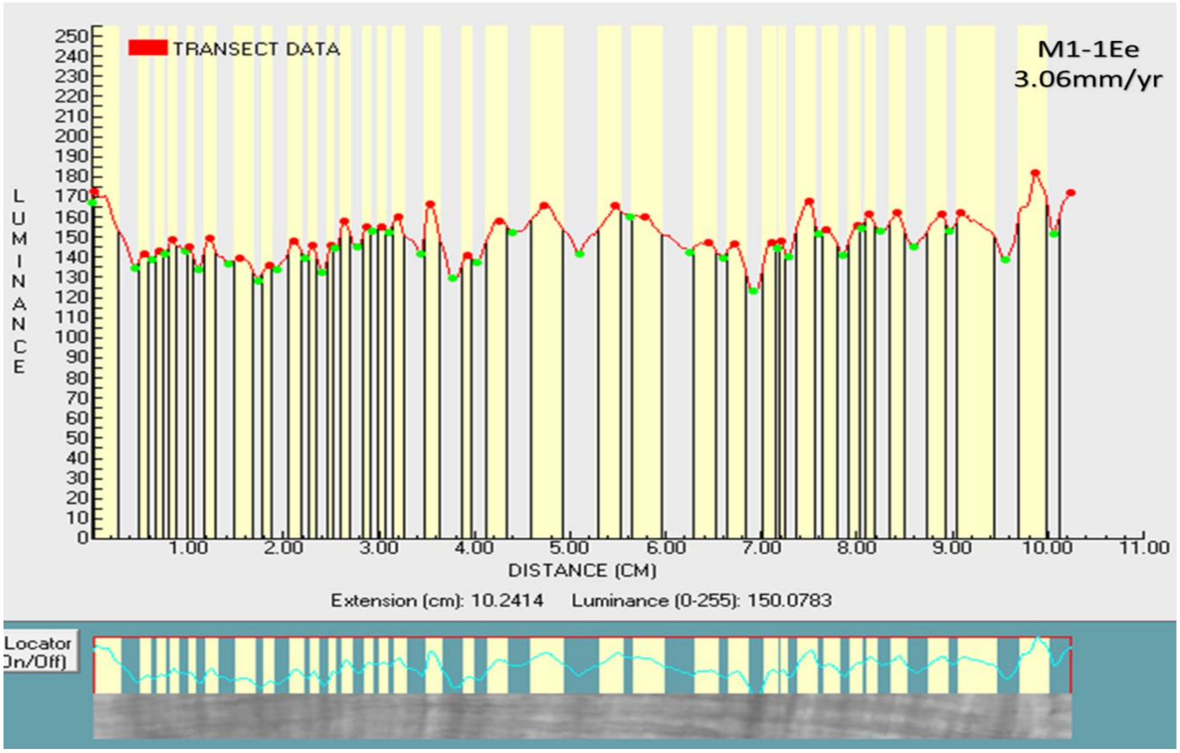

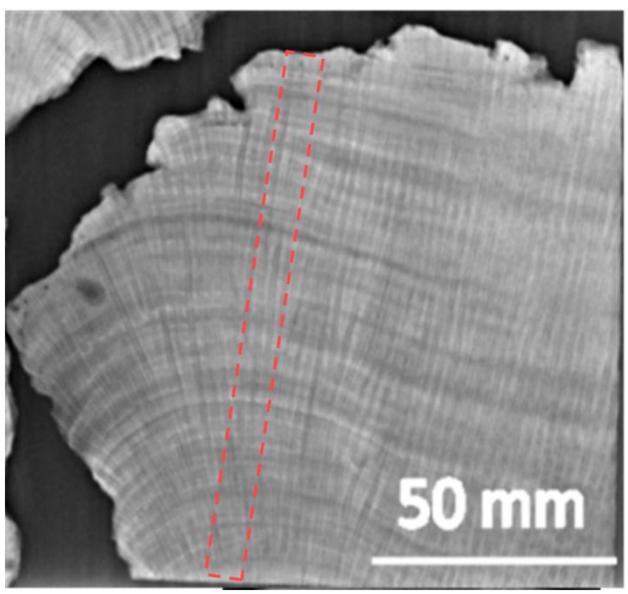

Appendix 2: Drawn transect and densitometry analysis of sample M1-1E$_e$.

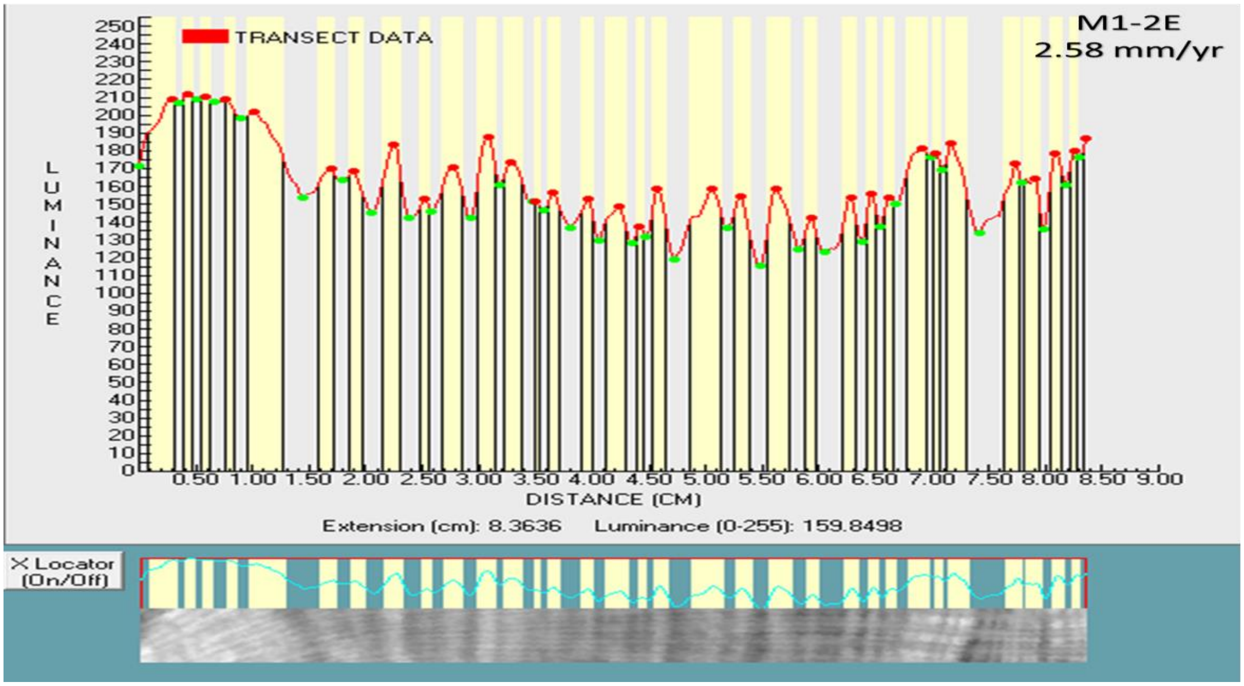

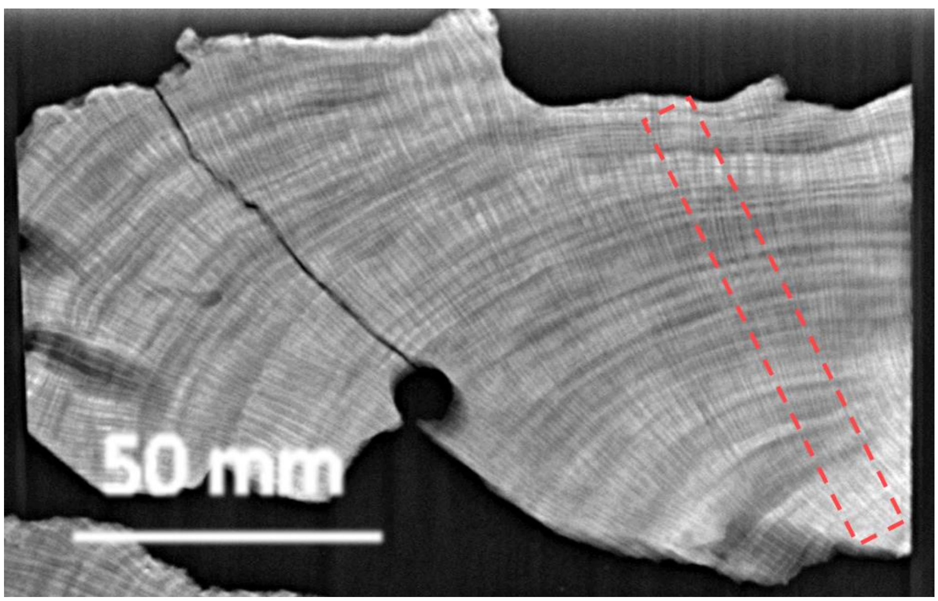

Appendix 3: Drawn transect and densitometry analysis of sample M1-2E.

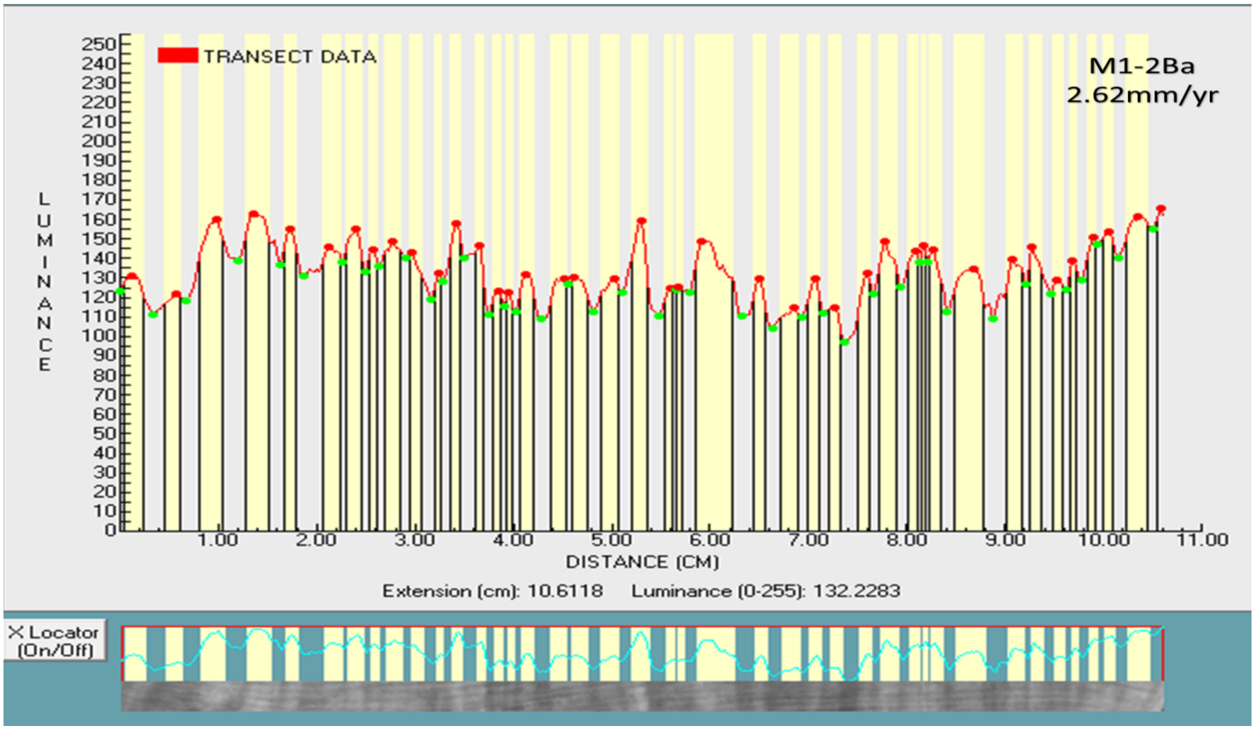

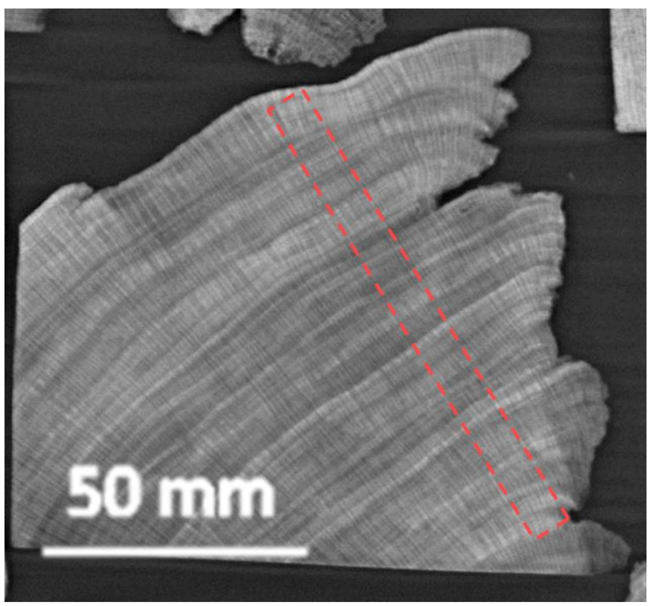

Appendix 4: drawn transect and densitometry analysis of sample M1-2B$_a$.

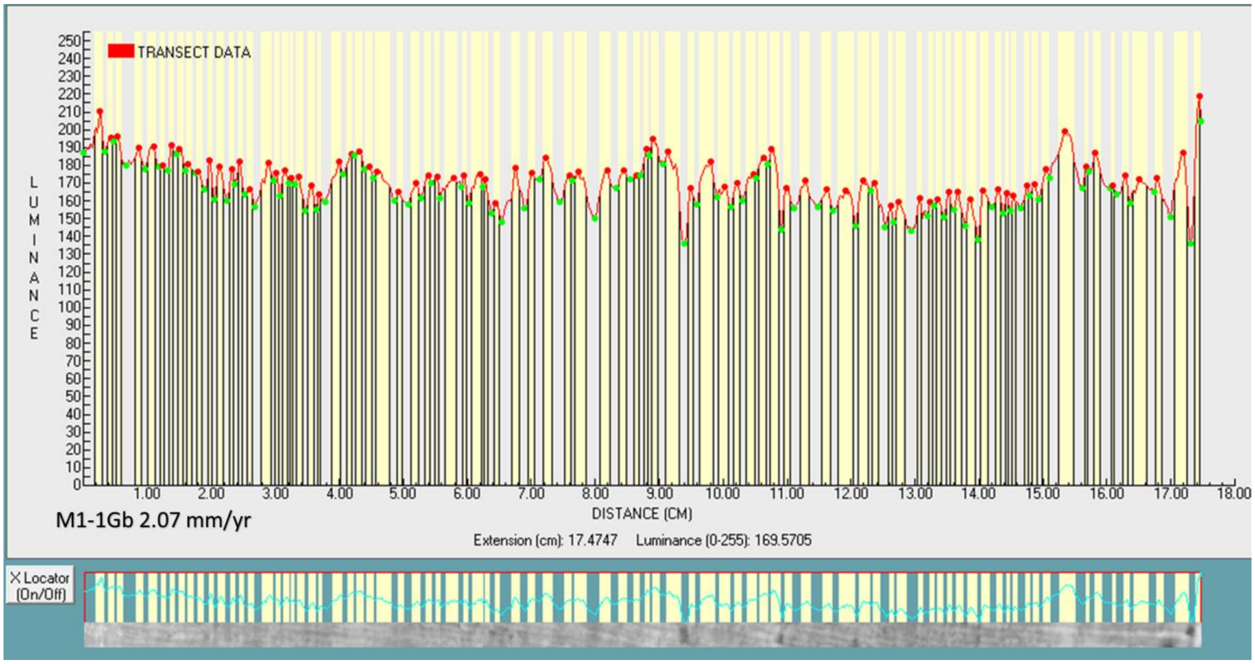

Appendix 5: Densitometry analysis of test sample M1-$1G_b$.

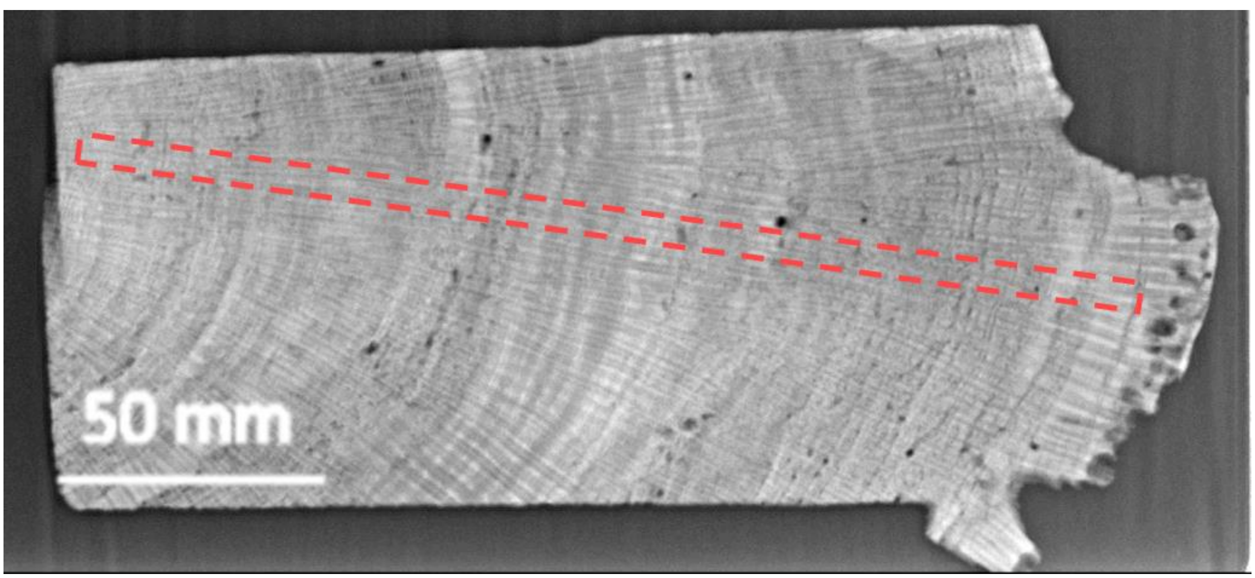

Appendix 5: Drawn transect and densitometry analysis of test sample M1-$1G_b$.

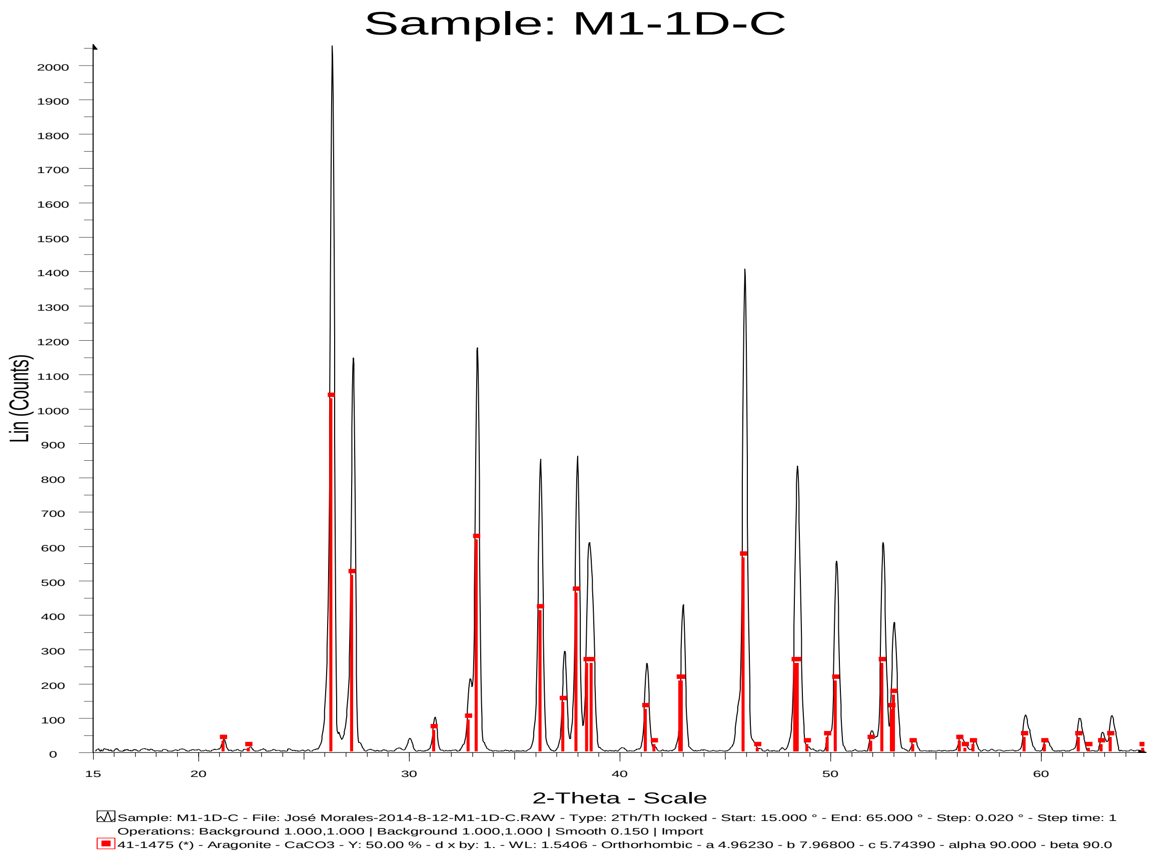

Appendix 6: XRD analysis of sample M1-1D$_c$.

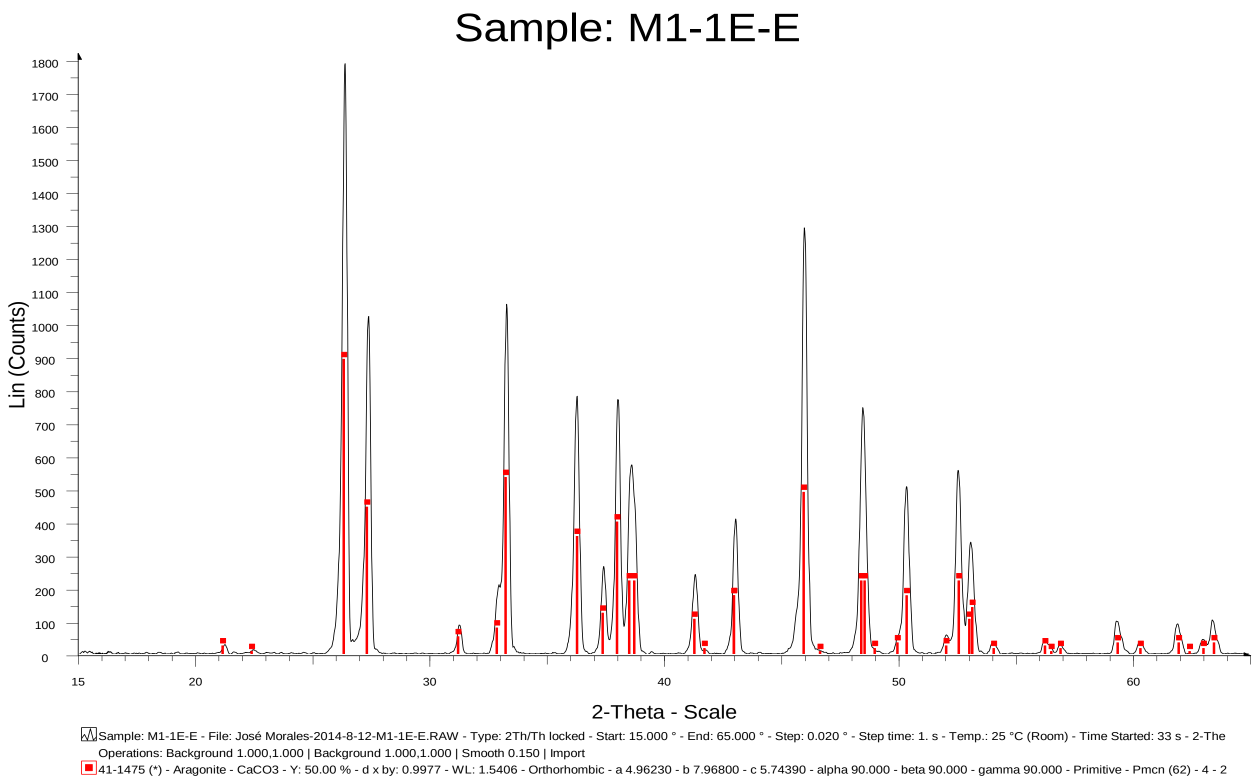

Appendix 7: XRD analysis of sample M1-1E$_e$.

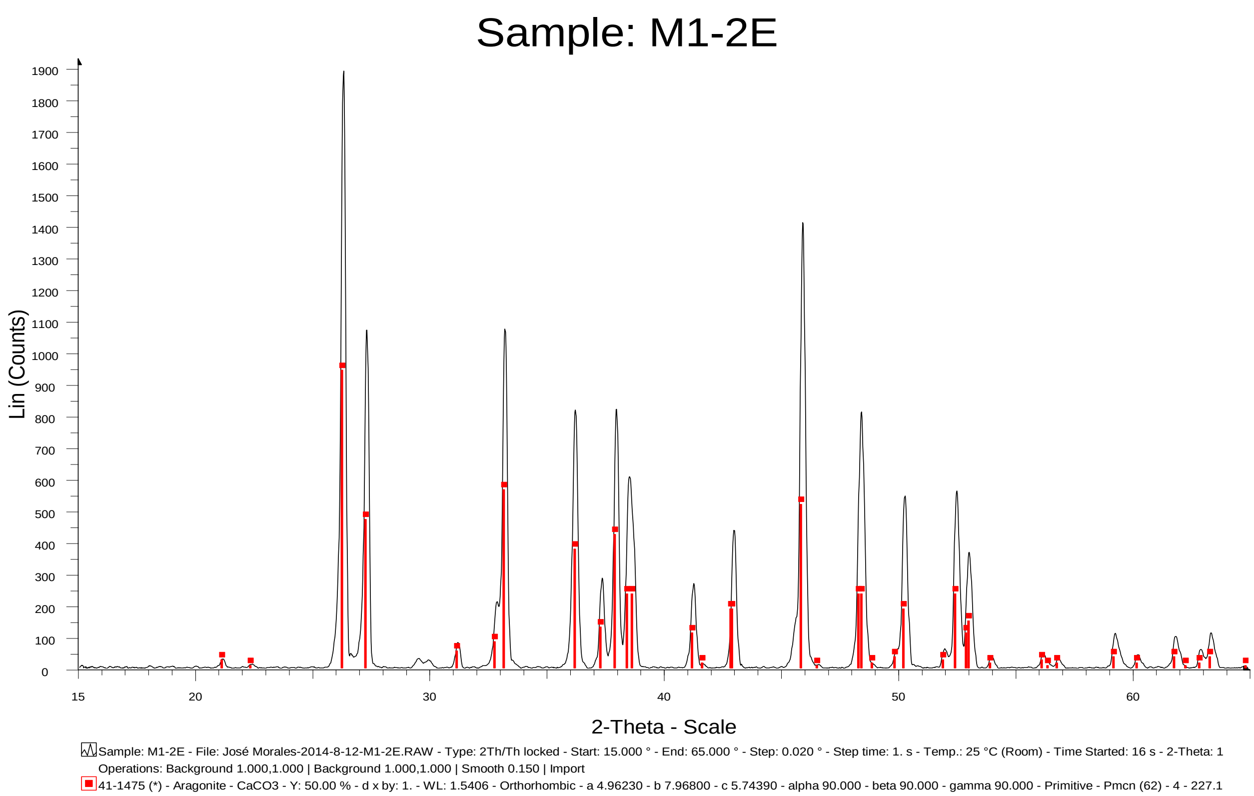

Appendix 8: XRD analysis of sample M1-2E.

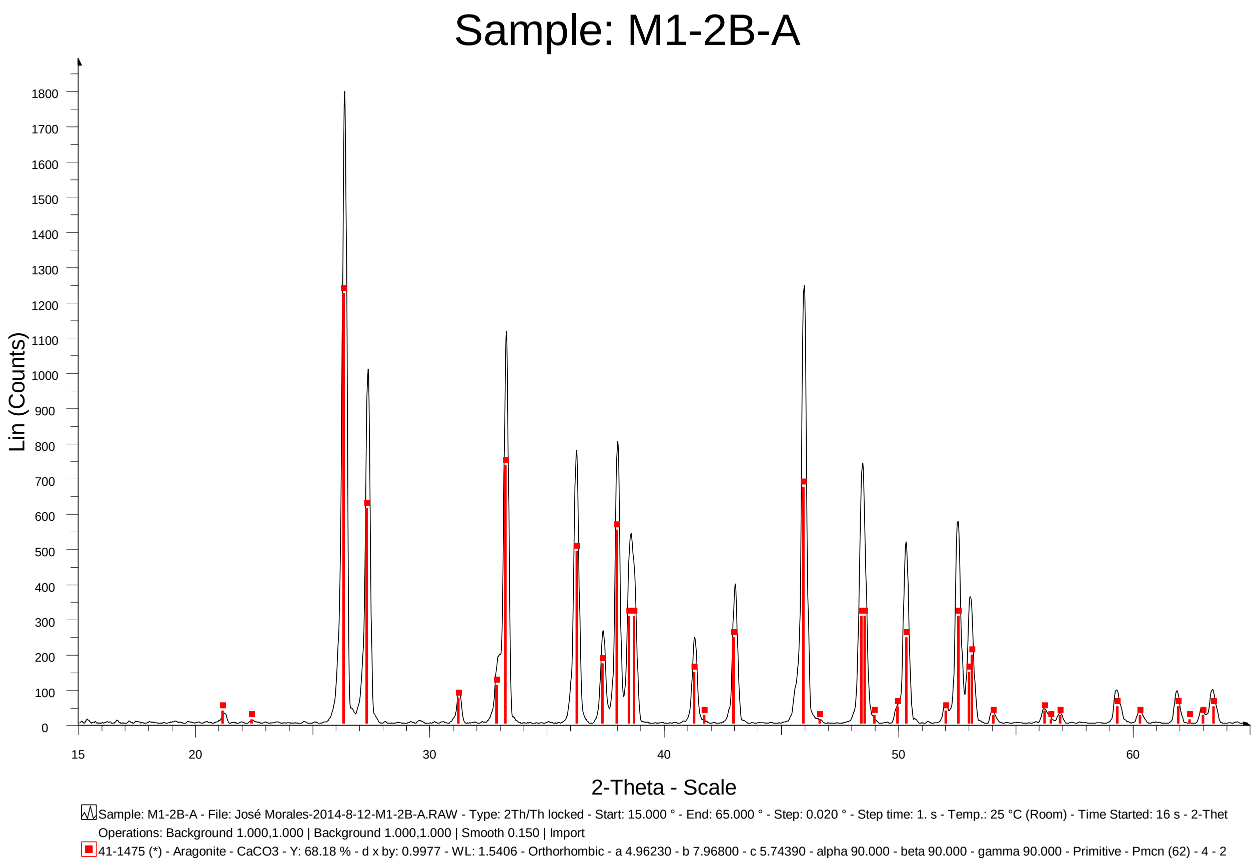

Appendix 9: XRD analysis of sample M1-2B$_a$.

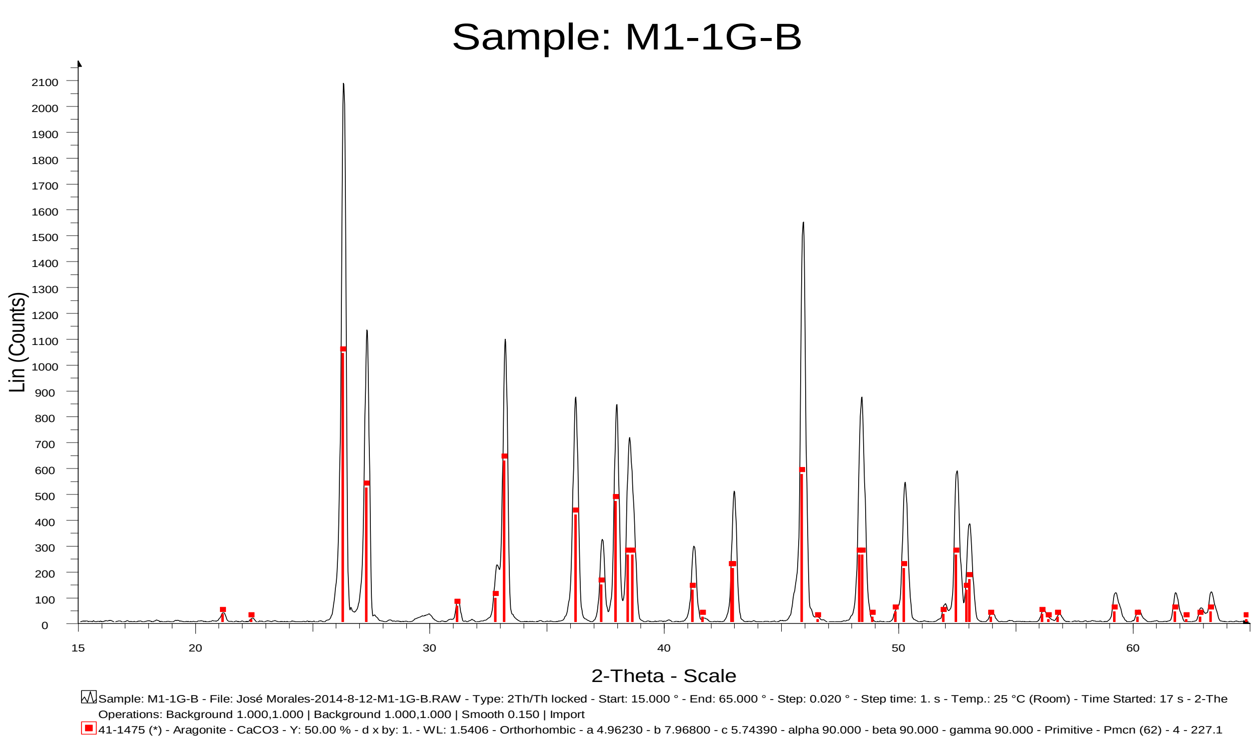

Appendix 10: XRD analysis of sample M1-1G$_b$.

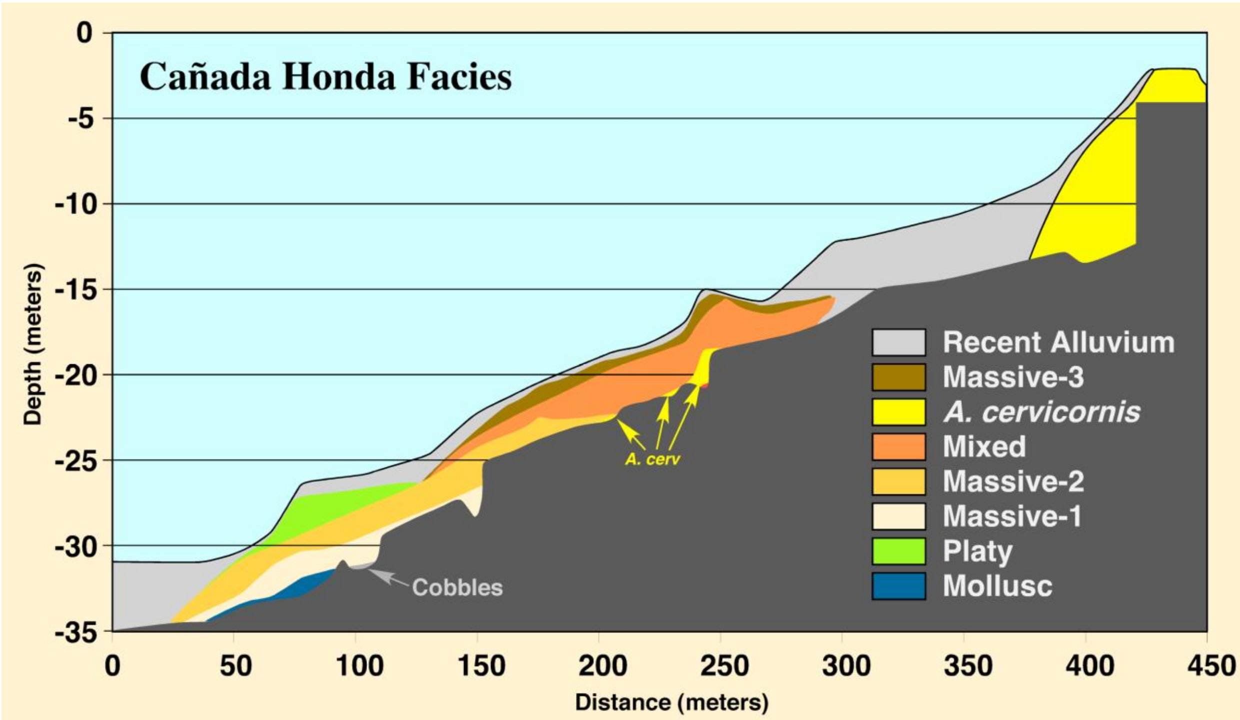

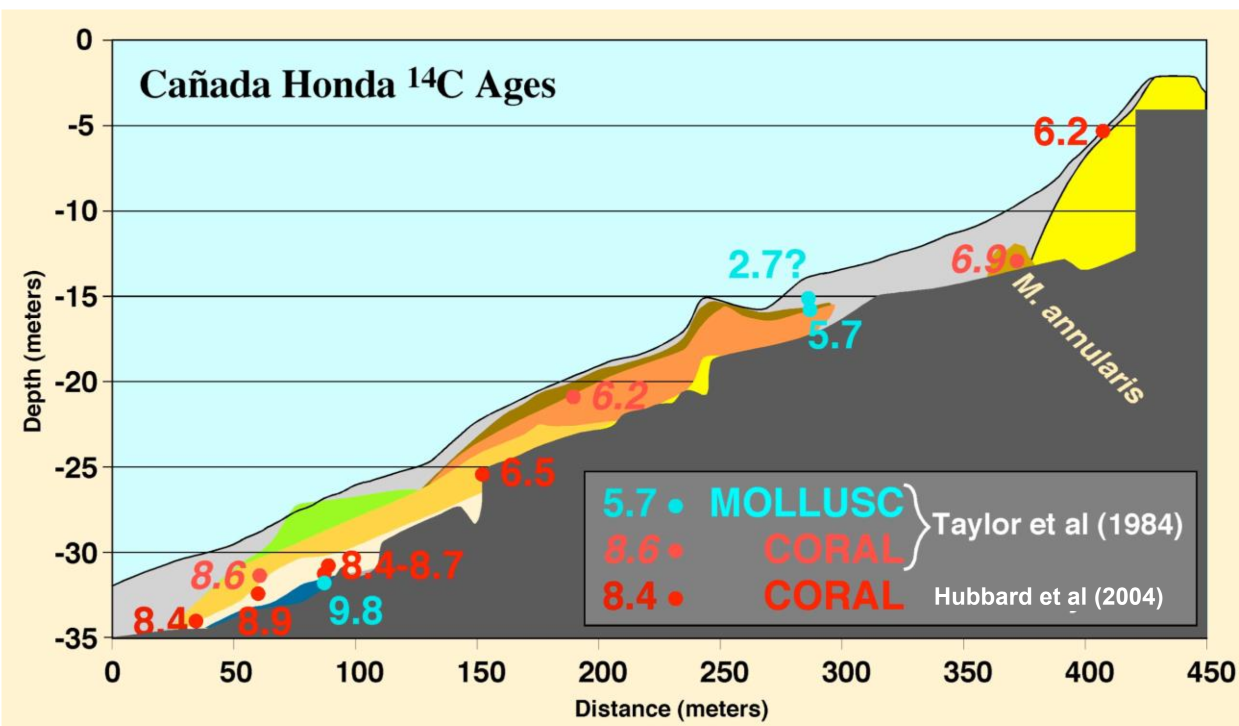

Appendix 11: Cañada Honda facies map from Hubbard et al., 2004 at the top and radiocarbon dating from Taylor et al. (1984) and Hubbard et al., 2004. at the bottom.

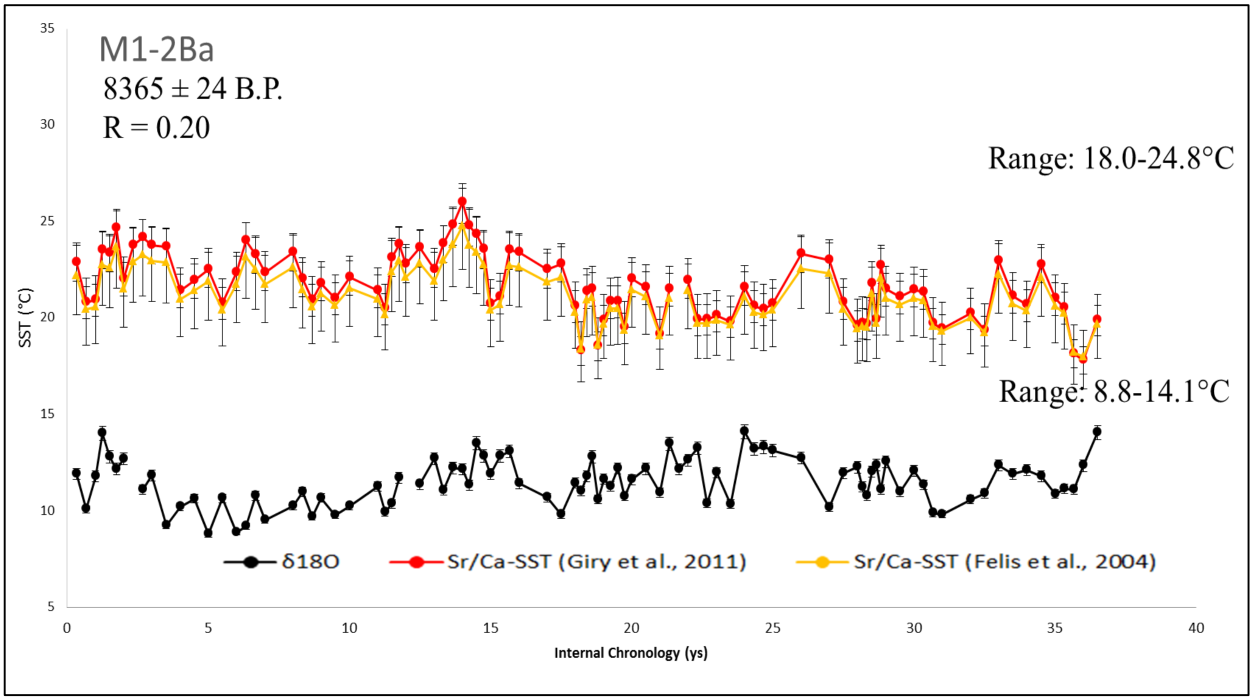

Appendix 12: Sea surface temperature plot for sample M1-2B$_a$.

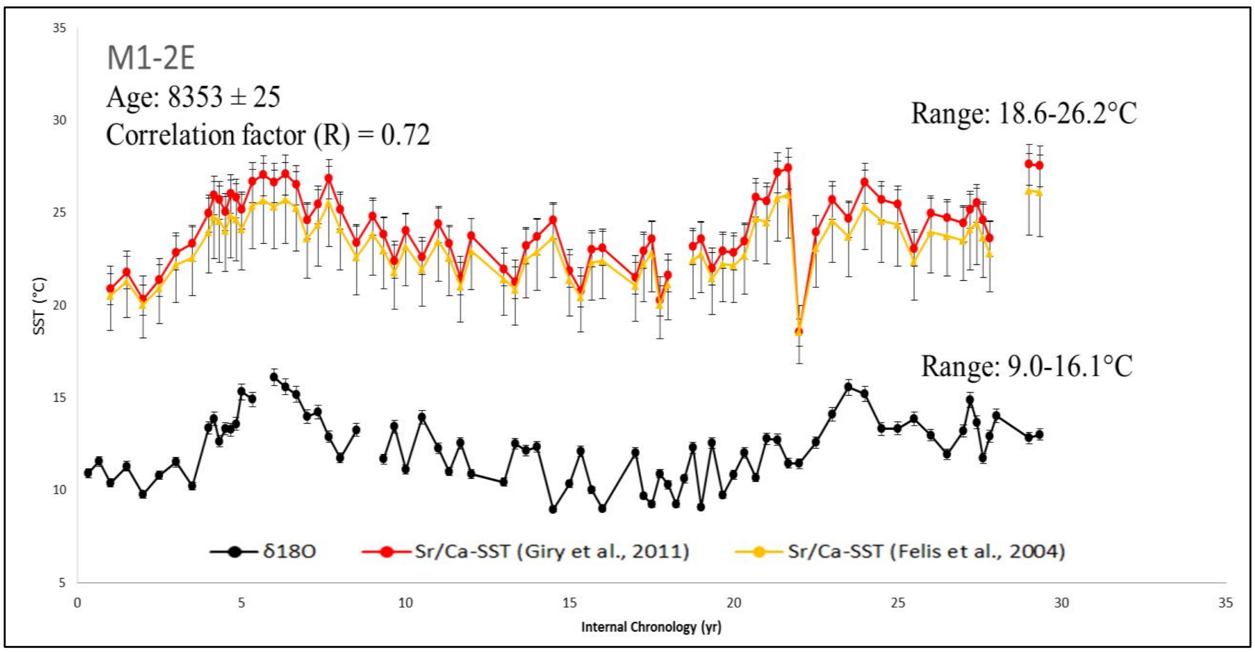

Appendix 13: Sea surface temperature plot for sample M1-2E.

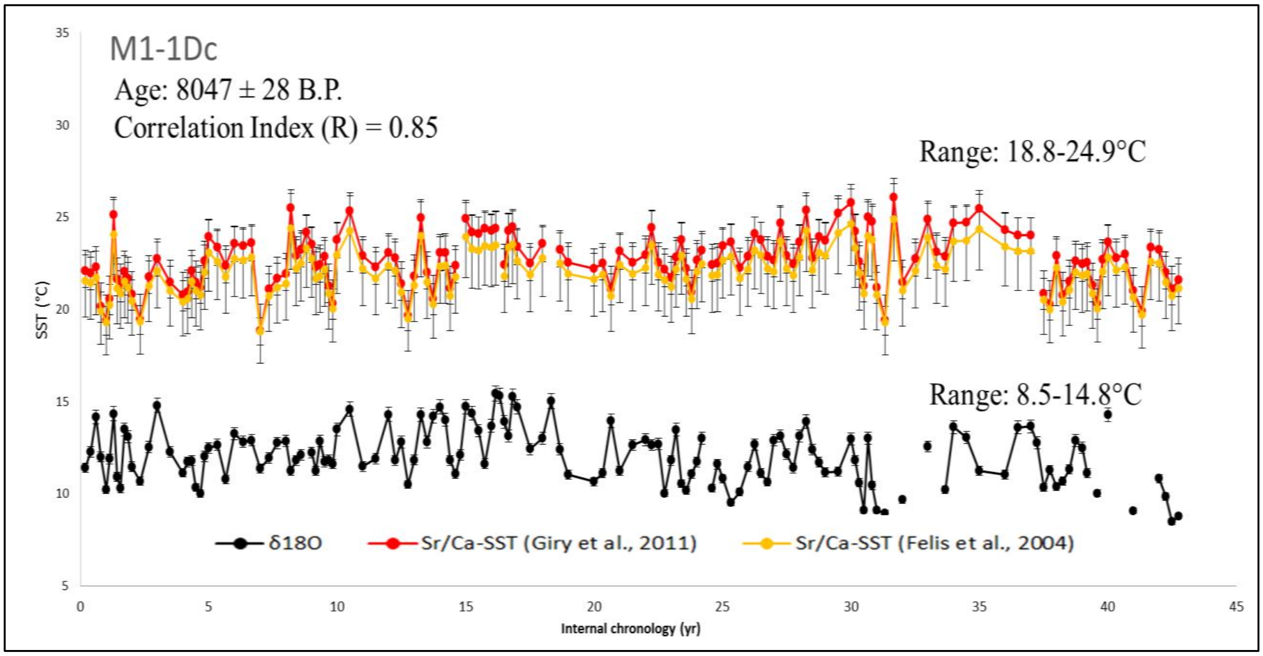

Appendix 14: Sea surface temperature plot for sample M1-1D$_c$.

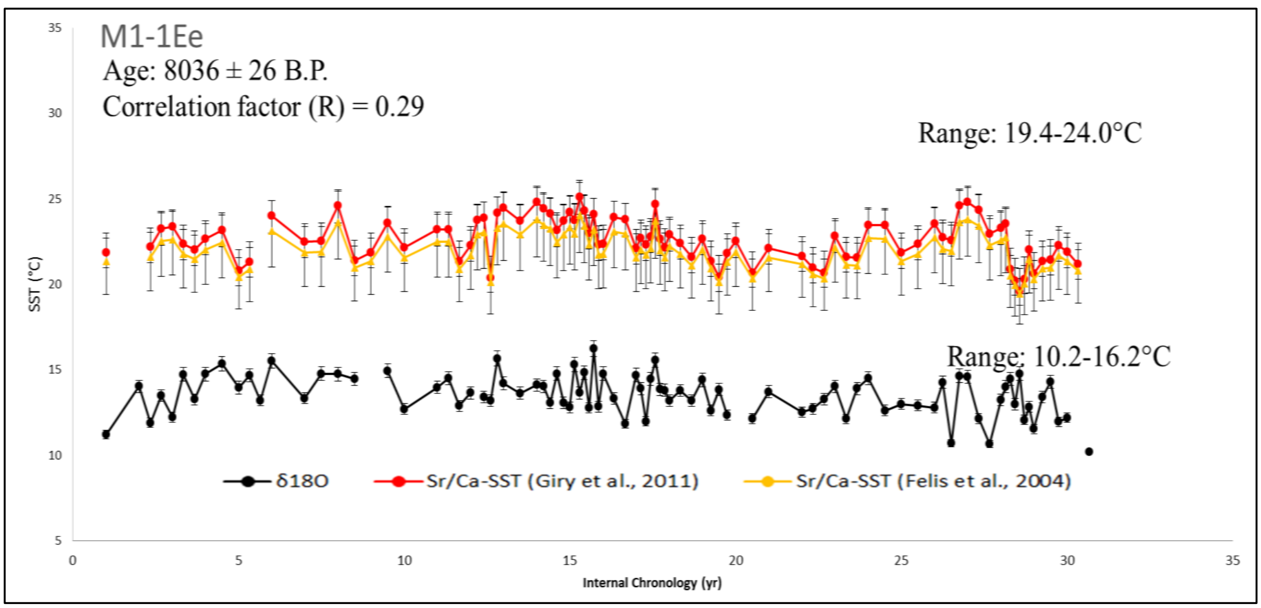

Appendix 15: Sea surface temperature plot for sample M1-1E$_e$.

Appendix 18: Geochemical analysis and calculated SST from simple M1-Ba

Sample M1-2Ba												
Depth (mm)	**Internal Chronology(yr)**	**δ18O**	**STDEV**	**SST (Leder) (^{o}C)**	**δ13C**	**STDEV**	**Sr/Ca (Shrag) (mmol/mol)**	**RSD**	**STDEV**	**SST (Giry) (^{o}C)**	**SST (Felis) (^{o}C)**
0	0.33	-1.457	0.039	11.9142	-4.08286	0.004	9.45609	0.0667	0.0063	22.8782	22.193
1	0.66	-1.053	0.017	10.0885	-4.27986	0.009	9.558533	0.0667	0.0064	20.82934	20.477
2	1	-1.433	0.032	11.8057	-4.61586	0.011	9.55192	0.0667	0.0064	20.96161	20.588
3	1.25	-1.922	0.016	14.0155	-5.20186	0.01	9.422586	0.0667	0.0063	23.54828	22.754
4	1.5	-1.658	0.015	12.8225	-4.31086	0.006	9.431997	0.0667	0.0063	23.36007	22.596
5	1.75	-1.518	0.023	12.1898	-4.82086	0.011	9.365639	0.0667	0.0062	24.68722	23.708
6	2	-1.633	0.02	12.7095	-4.61086	0.009	9.497335	0.0667	0.0063	22.0533	21.502
7	2.33						9.411952	0.0667	0.0063	23.76097	22.932
8	2.66	-1.279	0.007	11.1098	-4.69286	0.007	9.389955	0.0667	0.0063	24.20089	23.301
9	3	-1.442	0.028	11.8464	-4.52586	0.015	9.410635	0.0667	0.0063	23.78731	22.954
10	3.5	-0.87	0.023	9.26153	-4.18186	0.004	9.414237	0.0667	0.0063	23.71527	22.894
11	4	-1.086	0.024	10.2376	-5.07186	0.005	9.527974	0.0667	0.0064	21.44052	20.989
12	4.5	-1.176	0.017	10.6443	-4.28086	0.01	9.502464	0.0667	0.0063	21.95071	21.416
13	5	-0.771	0.007	8.81415	-4.41786	0.011	9.473099	0.0667	0.0063	22.53802	21.908
14	5.5	-1.18	0.024	10.6624	-4.58786	0.011	9.560766	0.0667	0.0064	20.78468	20.439
15	6	-0.792	0.017	8.90905	-4.04886	0.002	9.482728	0.0667	0.0063	22.34544	21.747
16	6.33	-0.864	0.021	9.23442	-4.45586	0.011	9.398491	0.0667	0.0063	24.03018	23.158
17	6.66	-1.21	0.053	10.798	-4.41686	0.007	9.435808	0.0667	0.0063	23.28383	22.533
18	7	-0.931	0.025	9.53719	-4.03686	0.002	9.481433	0.0667	0.0063	22.37135	21.768
19	8	-1.09	0.044	10.2557	-4.30686	0.004	9.429914	0.0667	0.0063	23.40172	22.631
20	8.33	-1.251	0.036	10.9833	-4.50286	0.007	9.498821	0.0667	0.0063	22.02358	21.477
21	8.66	-0.969	0.035	9.70891	-4.64686	0.011	9.552496	0.0667	0.0064	20.95009	20.578
22	9	-1.186	0.034	10.6895	-4.98586	0.008	9.510167	0.0667	0.0063	21.79667	21.287
23	9.5	-0.98729	0.011	9.79154	-4.13429	0.008	9.548018	0.0667	0.0064	21.03964	20.653
24	10	-1.09129	0.01	10.2615	-4.96229	0.008	9.494901	0.0667	0.0063	22.10199	21.543
25	11	-1.31529	0.02	11.2738	-4.54929	0.012	9.529276	0.0667	0.0064	21.41447	20.967

26	11.25	-1.02129	0.007	9.94519	-4.40429	0.006	9.575517	0.0667	0.0064	20.48965	20.192
27	11.5	-1.11629	0.016	10.3745	-4.63529	0.008	9.444261	0.0667	0.0063	23.11479	22.391
28	11.75	-1.41529	0.012	11.7257	-4.25929	0.007	9.410054	0.0667	0.0063	23.79893	22.964
29	12						9.460241	0.0667	0.0063	22.79518	22.123
30	12.5	-1.34029	0.029	11.3868	-4.61529	0.009	9.418169	0.2585	0.0243	23.63663	22.828
31	13	-1.63729	0.028	12.7289	-5.08029	0.005	9.473476	0.2585	0.0245	22.53048	21.902
32	13.33	-1.26929	0.014	11.0659	-4.69529	0.005	9.406341	0.2585	0.0243	23.87317	23.026
33	13.66	-1.52729	0.011	12.2318	-4.17529	0.012	9.359198	0.2585	0.0242	24.81604	23.816
34	14	-1.51029	0.027	12.155	-4.46629	0.01	9.300716	0.2585	0.024	25.98567	24.795
35	14.25	-1.33029	0.011	11.3416	-4.26329	0.008	9.360864	0.2585	0.0242	24.78273	23.788
36	14.5	-1.81329	0.022	13.5242	-4.61829	0.009	9.382903	0.2585	0.0243	24.34193	23.419
37	14.75	-1.66429	0.024	12.8509	-3.90429	0.01	9.421861	0.2585	0.0244	23.56279	22.766
38	15	-1.45729	0.017	11.9155	-3.98229	0.006	9.562834	0.2585	0.0247	20.74332	20.405
39	15.33	-1.66829	0.015	12.869	-5.11529	0.009	9.544518	0.2585	0.0247	21.10965	20.712
40	15.66	-1.71929	0.006	13.0995	-4.17929	0.005	9.424081	0.2585	0.0244	23.51837	22.729
41	16	-1.34829	0.027	11.4229	-3.42929	0.008	9.429296	0.2585	0.0244	23.41407	22.642
42	17	-1.19029	0.01	10.7089	-3.75929	0.011	9.474687	0.2585	0.0245	22.50627	21.881
43	17.5	-0.99229	0.017	9.81414	-3.94429	0.006	9.459477	0.2585	0.0245	22.81046	22.136
44	18	-1.35529	0.017	11.4545	-3.94529	0.009	9.568549	0.2585	0.0247	20.62902	20.309
45	18.2	-1.26029	0.009	11.0252	-4.32629	0.015	9.683468	0.2585	0.025	18.33064	18.384
46	18.4	-1.43329	0.015	11.807	-3.91329	0.011	9.529673	0.2585	0.0246	21.40655	20.96
47	18.6	-1.65529	0.028	12.8102	-3.22629	0.007	9.523771	0.2585	0.0246	21.52458	21.059
48	18.8	-1.16529	0.017	10.5959	-3.56229	0.008	9.671619	0.2585	0.025	18.56761	18.583
49	19	-1.40029	0.014	11.6579	-4.22729	0.007	9.604468	0.2585	0.0248	19.91064	19.707
50	19.25	-1.31529	0.028	11.2738	-4.27129	0.006	9.557247	0.2585	0.0247	20.85506	20.498
51	19.5	-1.52129	0.015	12.2047	-3.65429	0.006	9.556352	0.2585	0.0247	20.87296	20.513
52	19.75	-1.20229	0.02	10.7631	-3.99529	0.006	9.624397	0.2585	0.0249	19.51206	19.374
53	20	-1.39529	0.011	11.6353	-4.52729	0.008	9.498664	0.2585	0.0246	22.02672	21.48
54	20.5	-1.51829	0.02	12.1911	-3.71129	0.013	9.520409	0.2585	0.0246	21.59183	21.115
55	21	-1.24429	0.017	10.9529	-3.96229	0.006	9.640962	0.2585	0.0249	19.18075	19.096
56	21.33	-1.808	0.058	13.5004	-4.874	0.013	9.524973	0.2585	0.0246	21.50055	21.039

57	21.66	-1.514	0.031	12.1718	-4.907	0.024						
58	22	-1.62	0.034	12.6508	-4.367	0.018	9.502335	0.2585	0.0246	21.95331	21.418
59	22.33	-1.757	0.044	13.2699	-3.998	0.013	9.604014	0.2585	0.0248	19.91972	19.715
60	22.66	-1.122	0.048	10.4003	-3.925	0.023	9.602657	0.2585	0.0248	19.94686	19.738
61	23	-1.474	0.047	11.991	-5.172	0.011	9.592931	0.2585	0.0248	20.14138	19.901
62	23.5	-1.115	0.021	10.3687	-4.358	0.021	9.608543	0.2585	0.0248	19.82913	19.639
63	24	-1.945	0.045	14.1195	-4.669	0.031	9.521144	0.2585	0.0246	21.57711	21.103
64	24.33	-1.744	0.032	13.2111	-3.986	0.014	9.568614	0.2585	0.0247	20.62773	20.308
65	24.66	-1.771	0.052	13.3331	-4.041	0.015	9.57612	0.2585	0.0248	20.47759	20.182
66	25	-1.73	0.038	13.1479	-4.136	0.031	9.562615	0.2585	0.0247	20.74769	20.408
67	26	-1.642	0.041	12.7502	-3.963	0.025	9.433875	0.2585	0.0244	23.3225	22.565
68	27	-1.075	0.045	10.1879	-4.131	0.023	9.448744	0.2585	0.0244	23.02512	22.316
69	27.5	-1.472	0.048	11.982	-4.555	0.021	9.55946	0.2585	0.0247	20.8108	20.461
70	28	-1.537	0.064	12.2757	-4.354	0.028	9.618938	0.2585	0.0249	19.62124	19.465
71	28.16	-1.311	0.046	11.2544	-4.095	0.01	9.612426	0.2585	0.0248	19.75148	19.574
72	28.33	-1.205	0.033	10.7754	-4.679	0.028	9.614642	0.2585	0.0249	19.70716	19.537
73	28.5	-1.488	0.077	12.0543	-4.072	0.02	9.5101	0.2585	0.0246	21.79799	21.288
74	28.66	-1.56	0.054	12.3796	-4.631	0.012	9.60274	0.2585	0.0248	19.9452	19.736
75	28.83	-1.283	0.038	11.1279	-4.27	0.019	9.463175	0.2585	0.0245	22.73649	22.074
76	29	-1.59967	0.051	12.5589	-4.271	0.018	9.524981	0.2585	0.0246	21.50038	21.039
77	29.5	-1.25667	0.035	11.0089	-4.652	0.017	9.544732	0.2585	0.0247	21.10536	20.708
78	30	-1.49767	0.03	12.098	-5.289	0.017	9.526269	0.2585	0.0246	21.47462	21.017
79	30.33	-1.33367	0.048	11.3569	-4.248	0.01	9.532412	0.2585	0.0246	21.35176	20.914
80	30.66	-1.01167	0.052	9.90174	-3.875	0.015	9.613676	0.2585	0.0249	19.72647	19.553
81	31	-0.99867	0.06	9.84299	-4.672	0.02	9.628163	0.2585	0.0249	19.43674	19.311
82	32	-1.16767	0.019	10.6067	-3.737	0.022	9.58699	0.2585	0.0248	20.2602	20.000
83	32.5	-1.23767	0.027	10.923	-4.459	0.02	9.632149	0.2585	0.0249	19.35703	19.244
84	33	-1.55967	0.051	12.3781	-5.173	0.038	9.450583	0.2585	0.0244	22.98834	22.285
85	33.5	-1.45967	0.046	11.9262	-4.437	0.02	9.542021	0.2585	0.0247	21.15958	20.753
86	34	-1.50567	0.048	12.1341	-4.762	0.013	9.56549	0.2585	0.0247	20.6902	20.36
87	34.5	-1.43367	0.061	11.8088	-3.868	0.018	9.4613	0.2585	0.0245	22.774	22.106

88	35	-1.23167	0.059	10.8959	-3.891	0.013	9.549549	0.2585	0.0247	21.00901	20.627
89	35.33	-1.29167	0.031	11.1671	-4.156	0.016	9.5723	0.2585	0.0247	20.554	20.246
90	35.66	-1.28367	0.042	11.1309	-4.744	0.014	9.691229	0.2726	0.0264	18.17542	18.254
91	36	-1.55467	0.055	12.3556	-5.246	0.019	9.707466	0.2726	0.0265	17.85067	17.982
92	36.5	-1.93267	0.068	14.0637	-4.953	0.018	9.604266	0.2726	0.0262	19.91469	19.711

Appendix 18: Geochemical analysis and calculated SST from simple M1-2E

Sample M1-2E												
Depth (mm)	**Internal Chronology(yr)**	**δ18O**	**STDEV**	**SST (Leder) (ºC)**	**d13C**	**STDEV**	**Sr/Ca (Shrag) (mmol/mol)**	**RSD**	**STDEV**	**SST (Giry) (ºC)**	**SST (Felis) (ºC)**
1	0.33	-1.23594	0.05	10.9152	-4.00658	0.18					
2	0.66	-1.37744	0.06	11.5547	-4.31448	0.19					
3	1	-1.1236	0.05	10.4075	-4.16369	0.19	9.555074	0.0845	0.0081	20.89851	20.535
4	1.5	-1.32172	0.06	11.3029	-4.25911	0.19	9.510047	0.0845	0.008	21.79906	21.289
5	2	-0.98305	0.04	9.77242	-3.84986	0.17	9.583893	0.0845	0.0081	20.32213	20.052
6	2.5	-1.21072	0.11	10.8013	-4.04648	-0.09	9.53168	0.0845	0.0081	21.3664	20.927
7	3	-1.3683	0.05	11.5134	-4.55921	0.18	9.45631	0.0845	0.008	22.87379	22.189
8	3.5	-1.0794	0.06	10.2078	-3.62178	0.2	9.432754	0.0845	0.008	23.34491	22.584
9	4	-1.77791	0.04	13.3644	-4.37508	0.16	9.35068	0.0845	0.0079	24.98641	23.958
10	4.16	-1.88967	0.08	13.8694	-4.77591	0.2	9.30163	0.0845	0.0079	25.9674	24.78
11	4.33	-1.62086	0.08	12.6546	-3.79006	0.21	9.314765	0.1484	0.0138	25.7047	24.56
12	4.5	-1.77089	0.07	13.3326	-3.98566	0.17	9.346658	0.1484	0.0139	25.06684	24.026
13	4.66	-1.75755	0.08	13.2724	-4.12359	0.18	9.297687	0.1484	0.0138	26.04625	24.846
14	4.83	-1.82701	0.08	13.5863	-3.84297	0.18	9.308689	0.1484	0.0138	25.82622	24.662
15	5	-2.21061	0.08	15.3197	-4.41331	0.17	9.341285	0.1484	0.0139	25.17429	24.116
16	5.33	-2.11869	0.1	14.9044	-4.35586	0.2	9.266196	0.1484	0.0137	26.67608	25.374
17	5.66						9.247604	0.1484	0.0137	27.04791	25.685
18	6	-2.38413	0.11	16.1039	-4.29841	0.19	9.266766	0.1484	0.0137	26.66467	25.364
19	6.33	-2.2686	0.11	15.5818	-4.62265	0.19	9.245633	0.1484	0.0137	27.08735	25.718
20	6.66	-2.18119	0.1	15.1868	-4.52258	0.21	9.272966	0.1484	0.0138	26.54068	25.26
21	7	-1.91732	0.1	13.9944	-4.43659	0.2	9.369748	0.1484	0.0139	24.60505	23.639
22	7.33	-1.96813	0.09	14.224	-3.98705	0.2	9.327097	0.1484	0.0138	25.45806	24.353
23	7.66	-1.67417	0.09	12.8956	-3.92638	0.18	9.25674	0.1484	0.0137	26.86519	25.532
24	8	-1.41947	0.08	11.7446	-4.53504	0.17	9.34131	0.1484	0.0139	25.17379	24.115
25	8.5	-1.75546	0.07	13.2629	-4.17555	0.2	9.430323	0.1484	0.014	23.39355	22.624

26	9						9.358604	0.1484	0.0139	24.82793	23.826
27	9.33	-1.40753	0.07	11.6906	-4.64032	0.21	9.408801	0.1484	0.014	23.82398	22.985
28	9.66	-1.79354	0.08	13.435	-4.26553	0.19	9.479771	0.1484	0.0141	22.40457	21.796
29	10	-1.28554	0.06	11.1393	-4.94072	0.22	9.398085	0.1484	0.0139	24.03829	23.164
30	10.5	-1.90723	0.09	13.9488	-4.8974	0.22	9.4701	0.1484	0.014	22.598	21.958
31	11	-1.53227	0.07	12.2543	-4.03885	0.18	9.380242	0.1484	0.0139	24.39517	23.463
32	11.33	-1.25811	0.06	11.0154	-4.60592	0.2	9.433387	0.1484	0.014	23.33227	22.573
33	11.66	-1.59577	0.08	12.5413	-4.52064	0.2	9.526043	0.1484	0.0141	21.47914	21.021
34	12	-1.227	0.06	10.8748	-4.579	0.2	9.411808	0.1484	0.014	23.76383	22.935
35	13	-1.13217	0.05	10.4463	-4.73578	0.21	9.501541	0.1484	0.0141	21.96918	21.431
36	13.33	-1.5899	0.08	12.5148	-5.21483	0.23	9.537162	0.1484	0.0141	21.25676	20.835
37	13.66	-1.50614	0.07	12.1362	-4.62971	0.2	9.439213	0.1484	0.014	23.21574	22.475
38	14	-1.55479	0.07	12.3561	-4.07806	0.18	9.413372	0.1484	0.014	23.73256	22.908
39	14.5	-0.80589	0.04	8.97183	-3.82143	0.17	9.368827	0.1484	0.0139	24.62347	23.654
40	15	-1.10736	0.05	10.3342	-4.41627	0.2	9.505422	0.1484	0.0141	21.89155	21.366
41	15.33	-1.5023	0.07	12.1189	-3.99009	0.18	9.561072	0.1484	0.0142	20.77856	20.434
42	15.66	-1.03386	0.05	10.002	-4.01841	0.18	9.448507	0.1484	0.014	23.02985	22.32
43	16	-0.81521	0.04	9.01395	-4.13893	0.18	9.444032	0.1484	0.014	23.11935	22.395
44	17	-1.48296	0.07	12.0315	-4.18236	0.19	9.52448	0.1484	0.0141	21.51039	21.047
45	17.25	-0.96539	0.05	9.69258	-3.20361	0.14	9.452608	0.1484	0.014	22.94783	22.251
46	17.5	-0.86306	0.04	9.23016	-3.99291	0.18	9.41974	0.1484	0.014	23.6052	22.802
47	17.75	-1.23101	0.06	10.893	-4.4429	0.2	9.586188	0.1484	0.0142	20.27624	20.014
48	18	-1.09713	0.05	10.2879	-3.49873	0.16	9.518729	0.1484	0.0141	21.62542	21.144
49	18.25	-0.87008	0.04	9.26191	-3.99387	0.18					
50	18.5	-1.17295	0.06	10.6305	-4.28707	0.19					
51	18.75	-1.54009	0.08	12.2897	-3.76038	0.17	9.441903	0.1484	0.014	23.16193	22.43
52	19	-0.83334	0.04	9.09585	-3.40991	0.15	9.420898	0.1484	0.014	23.58205	22.782
53	19.33	-1.59886	0.08	12.5552	-4.02346	0.18	9.500294	0.1484	0.0141	21.99413	21.452
54	19.66	-0.976	0.05	9.74057	-3.173	0.14	9.452503	0.1484	0.014	22.94994	22.253
55	20	-1.21932	0.06	10.8401	-4.01398	0.18	9.456903	0.1484	0.014	22.86194	22.179
56	20.33	-1.48303	0.07	12.0318	-3.62116	0.16	9.426959	0.1077	0.0102	23.46081	22.681

57	20.66	-1.18315	0.06	10.6767	-3.83996	0.17	9.307252	0.1077	0.01	25.85496	24.686
58	21	-1.64868	0.08	12.7804	-4.2601	0.19	9.318546	0.1077	0.01	25.62908	24.497
59	21.33	-1.63772	0.08	12.7309	-3.58769	0.16	9.239863	0.1077	0.01	27.20275	25.815
60	21.66	-1.35641	0.07	11.4596	-3.766	0.17	9.228448	0.1077	0.0099	27.43103	26.006
61	22	-1.35066	0.07	11.4336	-4.37902	0.19	9.672757	0.1077	0.0104	18.54485	18.564
62	22.5	-1.60487	0.08	12.5824	-3.78996	0.17	9.40287	0.1077	0.0101	23.9426	23.084
63	23	-1.94245	0.09	14.1079	-4.65951	0.21	9.314325	0.1077	0.01	25.71349	24.567
64	23.5	-2.26594	0.11	15.5698	-4.96204	0.22	9.36526	0.1077	0.0101	24.6948	23.714
65	24	-2.18709	0.1	15.2135	-4.29768	0.19	9.268054	0.1077	0.01	26.63891	25.342
66	24.5	-1.76615	0.08	13.3112	-3.66711	0.16	9.314936	0.1077	0.01	25.70127	24.557
67	25	-1.77477	0.08	13.3502	-4.21469	0.19	9.326523	0.1077	0.01	25.46954	24.363
68	25.5	-1.88919	0.09	13.8672	-4.04677	0.18	9.447042	0.1077	0.0102	23.05916	22.344
69	26	-1.69255	0.08	12.9787	-3.50934	0.15	9.351585	0.1077	0.0101	24.9683	23.943
70	26.5	-1.46271	0.07	11.94	-4.41269	0.19	9.362399	0.1077	0.0101	24.75201	23.762
71	27	-1.74513	0.08	13.2162	-4.29191	0.19	9.377846	0.1077	0.0101	24.44307	23.503
72	27.2	-2.11647	0.1	14.8943	-4.39551	0.19	9.339976	0.1077	0.0101	25.20048	24.138
73	27.4	-1.84508	0.09	13.6679	-3.52423	0.16	9.321742	0.1077	0.01	25.56516	24.443
74	27.6	-1.41349	0.07	11.7175	-3.79085	0.17	9.368665	0.1077	0.0101	24.6267	23.657
75	27.8	-1.68146	0.08	12.9285	-4.53186	0.2	9.418582	0.1077	0.0101	23.62836	22.821
76	28	-1.92806	0.09	14.0429	-4.58666	0.2					
77	29	-1.65832	0.08	12.824	-3.84831	0.17	9.217343	0.1077	0.0099	27.65313	26.192
78	29.33	-1.7025	0.08	13.0236	-4.68356	0.21	9.221539	0.1077	0.0099	27.56921	26.122

Appendix 19: Geochemical analysis and calculated SST from simple M1-1Dc

Sample M1-1Dc											
Depth (mm)	**Internal Chronology(yr)**	**δ18O**	**STDEV**	**SST (Leder) (°C)**	**d13C**	**STDEV**	**Sr/Ca (Shrag) (mmol/mol)**	**RSD**	**STDEV**	**SST (Giry) (°C)**	**SST (Felis) (°C)**
0	0.2	-1.34367	0.04	11.40204	-4.355	0.022	9.495557	0.2764	0.0262	22.08885	21.532
1	0.4	-1.53267	0.02	12.25614	-4.972	0.023	9.501903	0.2764	0.0263	21.96193	21.425
2	0.6	-1.95367	0.053	14.15863	-4.969	0.019	9.485964	0.2764	0.0262	22.28071	21.692
3	0.8	-1.47167	0.046	11.98048	-4.345	0.01	9.593488	0.2764	0.0265	20.13024	19.891
4	1	-1.07867	0.051	10.20451	-4.098	0.02	9.630799	0.2764	0.0266	19.38402	19.266
5	1.14	-1.44767	0.048	11.87202	-4.758	0.025	9.573221	0.2764	0.0265	20.53558	20.231
6	1.28	-1.98967	0.034	14.32132	-4.867	0.014	9.344835	0.2764	0.0258	25.10331	24.056
7	1.42	-1.23067	0.027	10.8914	-4.094	0.026	9.518597	0.2764	0.0263	21.62807	21.146
8	1.57	-1.09167	0.052	10.26326	-4.56	0.015	9.536254	0.2764	0.0264	21.27491	20.85
9	1.71	-1.80267	0.037	13.47627	-5.141	0.024	9.498005	0.2764	0.0262	22.0399	21.491
10	1.85	-1.71067	0.053	13.06052	-4.422	0.011	9.516025	0.2764	0.0263	21.67951	21.189
11	2	-1.35467	0.045	11.45175	-3.912	0.019	9.5608	0.2764	0.0264	20.78399	20.439
12	2.33	-1.17967	0.041	10.66093	-4.42	0.03	9.627502	0.2764	0.0266	19.44996	19.322
13	2.66	-1.58967	0.047	12.51372	-4.675	0.031	9.511936	0.2764	0.0263	21.76128	21.257
14	3	-2.09067	0.068	14.77774	-5.1	0.027	9.462401	0.2764	0.0262	22.75198	22.087
15	3.5	-1.53067	0.066	12.2471	-4.036	0.018	9.526234	0.2764	0.0263	21.47532	21.018
16	4	-1.28167	0.054	11.12187	-4.005	0.029	9.562877	0.2764	0.0264	20.74245	20.404
17	4.16	-1.41267	0.058	11.71386	-4.836	0.024	9.554793	0.2764	0.0264	20.90413	20.539
18	4.33	-1.42667	0.058	11.77712	-4.509	0.022	9.496886	0.2764	0.0262	22.06227	21.509
19	4.5	-1.107	0.057	10.33253	-3.919	0.013	9.527756	0.2764	0.0263	21.44487	20.992
20	4.66	-1.031	0.038	9.989089	-3.724	0.01	9.541438	0.2764	0.0264	21.17124	20.763
21	4.83	-1.478	0.049	12.00908	-5.175	0.026	9.468948	0.2764	0.0262	22.62103	21.977
22	5	-1.578	0.054	12.46098	-4.651	0.026	9.404058	0.2764	0.026	23.91885	23.064
23	5.33	-1.617	0.029	12.63722	-4.885	0.021	9.432497	0.2764	0.0261	23.35005	22.588

24	5.66	-1.203	0.052	10.76636	-4.706	0.015	9.482158	0.2764	0.0262	22.35685	21.756
25	6	-1.75	0.029	13.23825	-5.362	0.009	9.423298	0.2764	0.026	23.53404	22.742
26	6.33	-1.654	0.038	12.80443	-5.485	0.019	9.427632	0.2764	0.0261	23.44737	22.669
27	6.66	-1.671	0.055	12.88125	-4.816	0.025	9.41948	0.2764	0.026	23.6104	22.806
28	7	-1.333	0.031	11.35383	-4.272	0.034	9.65883	0.2764	0.0267	18.8234	18.797
29	7.33	-1.46	0.04	11.92774	-4.295	0.016	9.544969	0.2764	0.0264	21.10062	20.704
30	7.66	-1.639	0.045	12.73664	-5.455	0.033	9.517378	0.2764	0.0263	21.65244	21.166
31	8	-1.662	0.034	12.84058	-4.702	0.023	9.504574	0.2764	0.0263	21.90853	21.381
32	8.2	-1.308	0.051	11.24085	-4.487	0.01	9.325286	0.2764	0.0258	25.49428	24.384
33	8.4	-1.431	0.051	11.79669	-5.243	0.022	9.455332	0.2764	0.0261	22.89337	22.205
34	8.6	-1.495	0.049	12.08591	-5.354	0.029	9.437977	0.2764	0.0261	23.24046	22.496
35	8.8						9.390732	0.2764	0.026	24.18536	23.288
36	9	-1.523	0.049	12.21244	-4.44	0.035	9.425086	0.2764	0.026	23.49828	22.712
37	9.16	-1.303	0.023	11.21826	-4.497	0.034	9.4869	0.2764	0.0262	22.262	21.677
38	9.33	-1.664	0.033	12.84962	-5.518	0.03	9.480045	0.2764	0.0262	22.3991	21.792
39	9.5	-1.414	0.061	11.71987	-4.818	0.028	9.457693	0.2764	0.0261	22.84615	22.166
40	9.66	-1.432	0.048	11.80121	-4.744	0.019	9.537693	0.2764	0.0264	21.24615	20.826
41	9.83	-1.387	0.03	11.59785	-5.571	0.018	9.584788	0.2764	0.0265	20.30423	20.037
42	10	-1.801	0.059	13.46872	-5.163	0.031	9.411887	0.2764	0.026	23.76226	22.933
43	10.5	-2.042	0.04	14.5578	-5.051	0.023	9.333233	0.2764	0.0258	25.33535	24.251
44	11	-1.356	0.047	11.45776	-4.465	0.022	9.455605	0.2764	0.0261	22.88789	22.201
45	11.5	-1.452	0.046	11.89159	-4.918	0.03	9.48676	0.2764	0.0262	22.2648	21.679
46	12	-1.981	0.043	14.28214	-5.628	0.016	9.446357	0.2764	0.0261	23.07287	22.356
47	12.25	-1.431	0.036	11.79669	-4.184	0.021	9.462292	0.2764	0.0262	22.75416	22.089
48	12.5	-1.65	0.021	12.78635	-4.484	0.018	9.531435	0.2764	0.0263	21.3713	20.931
49	12.75	-1.14	0.042	10.48166	-4.876	0.018	9.617246	0.2764	0.0266	19.65508	19.493
50	13	-1.436	0.072	11.81928	-5.388	0.025	9.510122	0.2764	0.0263	21.79756	21.288
51	13.25	-1.978	0.049	14.26858	-5.961	0.031	9.351512	0.2764	0.0258	24.96977	23.945
52	13.5	-1.651	0.051	12.79087	-4.498	0.017	9.500388	0.2764	0.0263	21.99224	21.451
53	13.75	-1.958	0.04	14.1782	-5.355	0.036	9.571722	0.2764	0.0265	20.56555	20.256
54	14	-2.071	0.038	14.68885	-5.187	0.027	9.447484	0.2764	0.0261	23.05031	22.337

55	14.2	-1.91822	0.033	13.99845	-4.51244	0.025	9.446504	0.2764	0.0261	23.06992	22.353
56	14.4	-1.43022	0.036	11.79317	-4.21544	0.018	9.543273	0.2764	0.0264	21.13453	20.732
57	14.6	-1.26622	0.046	11.05206	-4.45644	0.02	9.482288	0.0564	0.0053	22.35424	21.754
58	14.8	-1.49622	0.022	12.09143	-4.96844	0.034					
59	15	-2.07522	0.046	14.70793	-5.49344	0.014	9.353492	0.0564	0.0053	24.93017	23.911
60	15.25	-1.99822	0.06	14.35997	-4.62944	0.032	9.391195	0.0564	0.0053	24.17609	23.28
61	15.5	-1.78722	0.028	13.40646	-3.83944	0.019	9.396211	0.0564	0.0053	24.07579	23.196
62	15.75	-1.39122	0.032	11.61693	-4.76544	0.011	9.381607	0.0564	0.0053	24.36787	23.44
63	16	-1.84422	0.038	13.66404	-5.12844	0.016	9.388219	0.0564	0.0053	24.23562	23.33
64	16.16	-2.23322	0.031	15.42193	-5.34844	0.024	9.380481	0.0564	0.0053	24.39039	23.459
65	16.33	-2.20622	0.039	15.29992	-4.55244	0.022					
66	16.5	-1.89222	0.023	13.88095	-5.14644	0.007	9.479102	0.0564	0.0053	22.41797	21.807
67	16.66	-1.72722	0.051	13.13532	-5.25144	0.009	9.386445	0.0564	0.0053	24.27111	23.359
68	16.83	-2.19322	0.027	15.24117	-5.33644	0.036	9.37708	0.0564	0.0053	24.45841	23.516
69	17	-2.07322	0.053	14.69889	-5.08444	0.035	9.430496	0.0564	0.0053	23.39009	22.622
70	17.5	-1.56422	0.058	12.39872	-5.00144	0.028	9.475324	0.0564	0.0053	22.49353	21.871
71	18	-1.69422	0.065	12.98619	-5.01644	0.007	9.421902	0.0564	0.0053	23.56197	22.765
72	18.33	-2.14122	0.072	15.00618	-5.02244	0.021					
73	18.66	-1.56222	0.049	12.38968	-4.27044	0.031	9.437965	0.0564	0.0053	23.24071	22.496
74	19	-1.25822	0.062	11.01591	-4.30344	0.031	9.473491	0.0564	0.0053	22.53019	21.901
75	20	-1.17622	0.047	10.64535	-4.39644	0.022	9.491055	0.0564	0.0054	22.17889	21.607
76	20.33	-1.27622	0.055	11.09725	-4.48644	0.011	9.474971	0.0564	0.0053	22.50057	21.877
77	20.66	-1.90522	0.038	13.9397	-5.65844	0.011	9.545142	0.0564	0.0054	21.09715	20.701
78	21	-1.30322	0.055	11.21926	-4.26744	0.027	9.442936	0.0564	0.0053	23.14128	22.413
79	21.5	-1.61422	0.051	12.62467	-5.15844	0.01	9.473962	0.0564	0.0053	22.52077	21.893
80	22	-1.67922	0.054	12.91841	-5.18844	0.021	9.453889	0.0564	0.0053	22.92223	22.23
81	22.25	-1.61422	0.047	12.62467	-5.23044	0.016	9.378695	0.0564	0.0053	24.42609	23.489
82	22.5	-1.62622	0.043	12.6789	-4.29044	0.015	9.474281	0.0564	0.0053	22.51437	21.888
83	22.75	-1.03622	0.054	10.01269	-4.28144	0.008	9.492715	0.0564	0.0054	22.14571	21.579
84	23	-1.43022	0.056	11.79317	-4.95444	0.032	9.514961	0.0564	0.0054	21.70079	21.207
85	23.2	-1.79989	0.037	13.4637	-4.759	0.02	9.458587	0.0564	0.0053	22.82825	22.151

86	23.4	-1.15189	0.045	10.53539	-3.888	0.012	9.412984	0.0564	0.0053	23.74031	22.915
87	23.6	-1.06689	0.041	10.15128	-4.392	0.022	9.490968	0.0564	0.0054	22.18065	21.609
88	23.8	-1.26489	0.042	11.04604	-5.075	0.015	9.554728	0.0564	0.0054	20.90544	20.541
89	24	-1.41189	0.021	11.71033	-4.733	0.02	9.466609	0.0564	0.0053	22.66782	22.017
90	24.2	-1.69889	0.019	13.00728	-4.338	0.012	9.439924	0.0564	0.0053	23.20152	22.464
91	24.4										
92	24.6	-1.09289	0.052	10.26877	-5.044	0.016	9.478972	0.0564	0.0053	22.42056	21.81
93	24.8	-1.38489	0.038	11.58832	-5.191	0.016	9.474965	0.0564	0.0053	22.50071	21.877
94	25	-1.21189	0.051	10.80653	-4.194	0.027	9.428441	0.0564	0.0053	23.43119	22.656
95	25.33	-0.92689	0.06	9.518616	-3.528	0.019	9.417184	0.0564	0.0053	23.65631	22.844
96	25.66	-1.04989	0.068	10.07445	-4.541	0.021	9.488628	0.0564	0.0053	22.22744	21.648
97	26	-1.35389	0.028	11.44823	-4.905	0.012	9.457377	0.0564	0.0053	22.85246	22.171
98	26.25	-1.62189	0.06	12.65932	-4.496	0.018	9.396394	0.0564	0.0053	24.07212	23.193
99	26.5	-1.27889	0.027	11.1093	-3.79	0.025	9.411081	0.0564	0.0053	23.77839	22.947
100	26.75	-1.16789	0.015	10.60769	-4.462	0.012	9.45649	0.0564	0.0053	22.87021	22.186
101	27	-1.67289	0.045	12.88979	-5.352	0.017	9.46648	0.0564	0.0053	22.67039	22.019
102	27.25	-1.72489	0.043	13.12478	-4.278	0.026	9.367336	0.0564	0.0053	24.65327	23.679
103	27.5	-1.50289	0.03	12.12156	-4.085	0.017	9.455578	0.0564	0.0053	22.88845	22.201
104	27.75	-1.33689	0.046	11.37141	-4.233	0.009	9.478325	0.0564	0.0053	22.4335	21.82
105	28	-1.72489	0.045	13.12478	-4.872	0.037	9.419203	0.0564	0.0053	23.61594	22.811
106	28.25	-1.89789	0.033	13.90656	-4.932	0.024	9.332587	0.0564	0.0053	25.34826	24.262
107	28.5	-1.55989	0.028	12.37914	-3.948	0.023	9.461861	0.0564	0.0053	22.76278	22.096
108	28.75	-1.40789	0.03	11.69225	-4.486	0.012	9.403861	0.0564	0.0053	23.92278	23.068
109	29	-1.29089	0.062	11.16353	-4.932	0.023	9.413125	0.0564	0.0053	23.73751	22.912
110	29.5	-1.29789	0.027	11.19516	-5.164	0.028	9.340513	0.0564	0.0053	25.18974	24.129
111	30	-1.68789	0.052	12.95757	-5.22	0.035	9.311947	0.0564	0.0052	25.76107	24.607
112	30.16	-1.42989	0.044	11.79167	-4.234	0.027	9.389747	0.0564	0.0053	24.20507	23.304
113	30.33	-1.16389	0.056	10.58962	-4.215	0.016	9.470958	0.0564	0.0053	22.58083	21.944
114	30.5	-0.82989	0.035	9.080273	-4.522	0.018	9.536849	0.0564	0.0054	21.26303	20.84
115	30.66	-1.69589	0.044	12.99373	-4.768	0.019	9.350446	0.0564	0.0053	24.99108	23.962
116	30.83	-1.12889	0.037	10.43145	-4.094	0.024	9.363392	0.0564	0.0053	24.73215	23.746

117	31	-0.83289	0.03	9.09383	-4.534	0.029	9.540848	0.0594	0.0057	21.18305	20.773
118	31.33	-0.79889	0.044	8.940184	-4.338	0.019	9.630146	0.0594	0.0057	19.39707	19.277
119	31.66						9.296091	0.0594	0.0055	26.07817	24.873
120	32	-0.95489	0.04	9.645148	-4.269	0.012	9.526578	0.0594	0.0057	21.46844	21.012
121	32.5						9.463225	0.0594	0.0056	22.73551	22.073
122	33	-1.59489	0.059	12.53731	-4.892	0.019	9.356072	0.0594	0.0056	24.87855	23.868
123	33.33						9.445131	0.0594	0.0056	23.09739	22.376
124	33.66	-1.07889	0.042	10.2055	-4.665	0.016	9.457323	0.0594	0.0056	22.85354	22.172
125	34	-1.82789	0.008	13.59023	-5.454	0.01	9.367034	0.0594	0.0056	24.65931	23.685
126	34.5	-1.70589	0.033	13.03892	-4.734	0.017	9.365284	0.0594	0.0056	24.69433	23.714
127	35	-1.30389	0.035	11.22228	-4.53	0.031	9.327599	0.0594	0.0055	25.44803	24.345
128	36	-1.26189	0.049	11.03248	-4.863	0.028	9.3845	0.0594	0.0056	24.31001	23.392
129	36.5	-1.82689	0.031	13.58572	-5.483	0.02	9.399437	0.0594	0.0056	24.01125	23.142
130	37	-1.83889	0.039	13.63994	-5.04	0.015	9.399426	0.0594	0.0056	24.01148	23.142
131	37.25	-1.64189	0.057	12.7497	-4.437	0.012					
132	37.5	-1.10689	0.046	10.33204	-4.22	0.038	9.557093	0.0594	0.0057	20.85815	20.501
133	37.75	-1.31289	0.022	11.26295	-4.979	0.013	9.587652	0.0594	0.0057	20.24696	19.989
134	38	-1.11189	0.048	10.35463	-3.508	0.021	9.454294	0.0594	0.0056	22.91412	22.223
135	38.25	-1.18089	0.027	10.66644	-4.537	0.014	9.562492	0.0594	0.0057	20.75017	20.411
136	38.5	-1.32189	0.037	11.30362	-4.951	0.018	9.525447	0.0594	0.0057	21.49105	21.031
137	38.75	-1.66689	0.03	12.86268	-5.243	0.012	9.468563	0.0594	0.0056	22.62874	21.984
138	39	-1.58189	0.048	12.47856	-4.464	0.015	9.478787	0.0594	0.0056	22.42426	21.813
139	39.2	-1.27989	0.021	11.11382	-4.244	0.022	9.473033	0.0594	0.0056	22.53934	21.909
140	39.4						9.535943	0.0594	0.0057	21.28114	20.855
141	39.6	-1.03489	0.03	10.00667	-4.358	0.026	9.585103	0.0594	0.0057	20.29794	20.032
142	39.8						9.464611	0.0594	0.0056	22.70779	22.05
143	40	-1.97489	0.04	14.25453	-5.264	0.022	9.419121	0.0594	0.0056	23.61759	22.812
144	40.33						9.461189	0.0594	0.0056	22.77621	22.107
145	40.66						9.450299	0.0594	0.0056	22.99402	22.29
146	41	-0.82689	0.022	9.066716	-4.286	0.039	9.548957	0.0594	0.0057	21.02086	20.637
147	41.33						9.605307	0.0594	0.0057	19.89385	19.693

148	41.66						9.433322	0.0594	0.0056	23.33356	22.574
149	42	-1.21089	0.018	10.80201	-4.393	0.022	9.437965	0.0594	0.0056	23.24069	22.496
150	42.25	-0.99589	0.031	9.830427	-4.069	0.012	9.500053	0.0594	0.0056	21.99893	21.456
151	42.5	-0.69289	0.033	8.46117	-4.168	0.022	9.544752	0.0594	0.0057	21.10496	20.708
152	42.75	-0.76189	0.055	8.772981	-4.421	0.014	9.520159	0.0594	0.0057	21.59683	21.12

Appendix 20: Geochemical analysis and calculated SST from simple M1-1Ee

Sample M1-1Ee											
Depth (mm)	Internal Chronology(yr)	δ18O	STDEV	SST (Leder) (°C)	d13C	STDEV	Sr/Ca (Shrag) (mmol/mol)	RSD	STDEV	SST (Giry) (°C)	SST (Felis) (°C)
0	0.16						9.085231	0.0594	0.0054	30.29538	28.405
1	0.33	-1.55289	0.046		-3.813	0.023	9.158833	0.0594	0.0054	28.82335	27.172
2	0.5	-1.20989	0.035		-3.779	0.016	9.298074	0.0594	0.0055	26.03851	24.84
3	0.66	-1.64089	0.052		-4.661	0.015	9.077548	0.0594	0.0054	30.44904	28.534
4	0.83	-0.83589	0.036		-4.125	0.023	9.353861	0.0594	0.0056	24.92278	23.905
5	1	-1.81689	0.046		-3.973	0.03	9.373672	0.0594	0.0056	24.52655	23.573
6	2	-1.92989	0.049		-3.846	0.011	9.456994	0.0594	0.0056	22.86012	22.178
7	2.5	-1.60789	0.019		-3.67	0.012	9.438997	0.0594	0.0056	23.22005	22.479
8	3	-1.74689	0.013		-4.897	0.014	9.456725	0.0594	0.0056	22.86549	22.182
9	3.5	-1.73889	0.052		-4.453	0.024	9.227437	0.0594	0.0055	27.45126	26.023
10	4	-1.37789	0.015		-3.901	0.015					
11	1	-1.30089	0.043		-3.966	0.028	9.506289	0.0594	0.0056	21.87422	21.352
12	2	-1.92389	0.054		-4.273	0.014					
13	2.33	-1.45389	0.019		-4.105	0.031	9.491293	0.0594	0.0056	22.17414	21.603
14	2.66	-1.80189	0.04		-4.59	0.013	9.436793	0.0594	0.0056	23.26415	22.516
15	3	-1.52489	0.032		-3.372	0.007	9.431723	0.0594	0.0056	23.36554	22.601
16	3.33	-2.07789	0.043		-4.456	0.021	9.48169	0.0594	0.0056	22.3662	21.764
17	3.66	-1.75389	0.047		-3.692	0.022	9.498721	0.0594	0.0056	22.02558	21.479
18	4	-2.08389	0.048		-5.033	0.018	9.46634	0.0594	0.0056	22.67319	22.021
19	4.5	-2.21289	0.033		-4.089	0.019	9.441558	0.0594	0.0056	23.16885	22.436
20	5	-1.90789	0.044		-4.228	0.013	9.561078	0.0594	0.0057	20.77844	20.434
21	5.33	-2.06789	0.036		-4.66	0.021	9.533989	0.0594	0.0057	21.32022	20.888
22	5.66	-1.743	0.057		-4.62133	0.026		0.0594	0		

23	6	-2.252	0.04	-4.52133	0.027	9.400232	0.0594	0.0056	23.99536	23.128
24	7	-1.772	0.042	-4.03633	0.026	9.475446	0.1008	0.0096	22.49108	21.869
25	7.5	-2.089	0.033	-5.08133	0.014	9.473869	0.1008	0.0096	22.52261	21.895
26	8	-2.084	0.057	-4.19533	0.014	9.369925	0.1008	0.0094	24.6015	23.636
27	8.5	-2.021	0.026	-3.99433	0.021	9.529771	0.1008	0.0096	21.40457	20.959
28	9					9.506393	0.1008	0.0096	21.87213	21.35
29	9.5	-2.127	0.058	-4.35633	0.012	9.420033	0.1008	0.0095	23.59934	22.797
30	10	-1.63	0.027	-4.19733	0.019	9.493332	0.1008	0.0096	22.13336	21.569
31	11	-1.912	0.035	-4.74233	0.022	9.439454	0.1008	0.0095	23.21093	22.471
32	11.33	-2.03	0.037	-4.16533	0.027	9.439631	0.1008	0.0095	23.20738	22.468
33	11.66	-1.672	0.036	-4.48533	0.03	9.533522	0.1008	0.0096	21.32956	20.896
34	12	-1.839	0.031	-4.27633	0.01	9.485142	0.1008	0.0096	22.29716	21.706
35	12.2	-1.699	0.037	-3.71733	0.03	9.412418	0.1008	0.0095	23.75163	22.924
36	12.4	-1.786	0.034	-5.31633	0.031	9.405481	0.1008	0.0095	23.89039	23.041
37	12.6	-1.738	0.034	-4.54433	0.016	9.580939	0.1008	0.0097	20.38121	20.102
38	12.8	-2.286	0.029	-4.46433	0.018	9.390676	0.1008	0.0095	24.18648	23.289
39	13	-1.961	0.054	-4.06933	0.022	9.375868	0.1008	0.0095	24.48264	23.537
40	13.5	-1.836	0.04	-3.90333	0.012	9.413626	0.1008	0.0095	23.72748	22.904
41	14	-1.942	0.066	-4.56033	0.027	9.360227	0.1008	0.0094	24.79545	23.799
42	14.2	-1.922	0.034	-3.44433	0.029	9.379265	0.1008	0.0095	24.4147	23.48
43	14.4	-1.707	0.043	-3.60533	0.027	9.394003	0.1008	0.0095	24.11994	23.233
44	14.6	-2.089	0.029	-4.44033	0.031	9.441934	0.1008	0.0095	23.16132	22.43
45	14.8	-1.71	0.057	-4.03933	0.023	9.413689	0.1008	0.0095	23.72622	22.903
46	15	-1.654	0.065	-3.61133	0.038	9.387916	0.1008	0.0095	24.24169	23.335
47	15.14	-2.205	0.046	-4.57333	0.032	9.411185	0.1008	0.0095	23.77629	22.945
48	15.28	-1.839	0.042	-4.05833	0.028	9.343944	0.1008	0.0094	25.12113	24.071
49	15.42	-2.101	0.041	-4.17633	0.036	9.38403	0.1008	0.0095	24.31941	23.4
50	15.57	-1.645	0.057	-3.68433	0.012	9.449358	0.1008	0.0095	23.01284	22.306
51	15.71	-2.412	0.064	-4.62733	0.009	9.394811	0.1008	0.0095	24.10377	23.219
52	15.85	-1.664	0.035	-3.708	0.021	9.483604	0.1008	0.0096	22.32792	21.732
53	16	-2.087	0.055	-4.102	0.026	9.481896	0.1008	0.0096	22.36207	21.761

54	16.33	-1.767	0.069	-4.467	0.023	9.402891	0.1008	0.0095	23.94219	23.084
55	16.66	-1.44	0.03	-3.678	0.019	9.410085	0.1008	0.0095	23.7983	22.963
56	17	-2.07	0.063	-4.615	0.011	9.4949	0.1008	0.0096	22.10199	21.543
57	17.14	-1.894	0.034	-3.962	0.035	9.465072	0.1008	0.0095	22.69856	22.042
58	17.28	-1.471	0.034	-4.264	0.021	9.483055	0.1008	0.0096	22.33889	21.741
59	17.42	-2.022	0.052	-5.471	0.018	9.460763	0.1008	0.0095	22.78475	22.115
60	17.57	-2.265	0.05	-4.659	0.024	9.366473	0.1008	0.0094	24.67055	23.694
61	17.71	-1.888	0.028	-3.827	0.022	9.467658	0.1008	0.0095	22.64683	21.999
62	17.85	-1.875	0.031	-4.729	0.017	9.492994	0.1008	0.0096	22.14011	21.575
63	18	-1.74	0.064	-3.887	0.017	9.45474	0.1008	0.0095	22.9052	22.215
64	18.33	-1.871	0.042	-3.773	0.021	9.480103	0.1008	0.0096	22.39794	21.791
65	18.66	-1.74	0.063	-3.776	0.031	9.5207	0.1008	0.0096	21.58599	21.111
66	19	-2.006	0.062	-5.313	0.012	9.467053	0.1008	0.0095	22.65893	22.009
67	19.25	-1.613	0.056	-3.378	0.022	9.531917	0.1008	0.0096	21.36166	20.923
68	19.5	-1.884	0.053	-4.857	0.021	9.579433	0.1008	0.0097	20.41135	20.127
69	19.75	-1.556	0.048	-3.866	0.017	9.5097	0.0845	0.008	21.80601	21.295
70	20					9.474099	0.0845	0.008	22.51801	21.891
71	20.5	-1.507	0.05	-4.396	0.016	9.566529	0.0845	0.0081	20.66941	20.343
72	21	-1.855	0.043	-3.528	0.029	9.494636	0.0845	0.008	22.10728	21.547
73	22	-1.592	0.031	-3.438	0.023	9.517595	0.0845	0.008	21.6481	21.163
74	22.33	-1.634	0.039	-4.147	0.017	9.552614	0.0845	0.0081	20.94771	20.576
75	22.66	-1.76	0.022	-4.069	0.014	9.56618	0.0845	0.0081	20.67639	20.349
76	23	-1.925	0.023	-3.995	0.033	9.458794	0.0845	0.008	22.82411	22.147
77	23.33	-1.501	0.034	-4.179	0.029	9.519763	0.0845	0.008	21.60474	21.126
78	23.66	-1.898	0.047	-5.022	0.015	9.521672	0.0845	0.008	21.56656	21.094
79	24	-2.032	0.044	-4.284	0.019	9.42593	0.0845	0.008	23.4814	22.698
80	24.5	-1.612	0.029	-3.971	0.021	9.427423	0.0845	0.008	23.45154	22.673
81	25	-1.694	0.045	-3.874	0.013	9.507741	0.0845	0.008	21.84517	21.328
82	25.5	-1.67675	0.074	-4.468	0.021	9.482214	0.0845	0.008	22.35573	21.755
83	26	-1.648	0.038	-4.0353	0.031	9.422469	0.0845	0.008	23.55062	22.756
84	26.25	-1.977	0.054	-4.2643	0.03	9.463847	0.0845	0.008	22.72305	22.063

85	26.5	-1.186	0.026	-4.3563	0.007	9.471208	0.0845	0.008	22.57585	21.94
86	26.75	-2.061	0.052	-4.9693	0.018	9.369313	0.0845	0.0079	24.61373	23.646
87	27	-2.047	0.043	-4.6723	0.018	9.359622	0.0845	0.0079	24.80756	23.809
88	27.33	-1.505	0.049	-3.8473	0.019	9.382464	0.0845	0.0079	24.35072	23.426
89	27.66	-1.18	0.037	-4.0513	0.023	9.451442	0.0845	0.008	22.97116	22.271
90	28	-1.749	0.045	-4.8613	0.018	9.434472	0.0845	0.008	23.31057	22.555
91	28.14	-1.921	0.047	-3.7363	0.02	9.423422	0.0845	0.008	23.53156	22.74
92	28.28	-2.019	0.036	-4.6523	0.026	9.556279	0.0845	0.0081	20.87442	20.515
93	28.42	-1.693	0.037	-4.4673	0.019	9.589625	0.0845	0.0081	20.2075	19.956
94	28.57	-2.088	0.016	-4.355	0.02	9.620777	0.0845	0.0081	19.58447	19.434
95	28.71	-1.489	0.044	-4.3913	0.029	9.584924	0.0845	0.0081	20.30153	20.035
96	28.85	-1.659	0.017	-4.163	0.02	9.499307	0.0845	0.008	22.01387	21.469
97	29	-1.371	0.033	-4.25	0.02	9.569098	0.0845	0.0081	20.61804	20.3
98	29.25	-1.786	0.054	-5.002	0.016	9.531993	0.0845	0.0081	21.36014	20.921
99	29.5	-1.981	0.048	-3.971	0.009	9.528643	0.0845	0.0081	21.42714	20.978
100	29.75	-1.465	0.057	-3.55	0.011	9.485591	0.0845	0.008	22.28818	21.699
101	30	-1.519	0.039	-4.457	0.02	9.505846	0.0845	0.008	21.88308	21.359
102	30.33		0.05		0.027	9.540379	0.0845	0.0081	21.19243	20.781
103	30.66	-1.075	0.041	-3.901	0.014					